Universidad Autónoma de Madrid

Escuela Politécnica Superior

Programa de Doctorado de Ingeniería Informática y de Telecomunicación
Universidad Autónoma de Madrid
Escuela Politécnica Superior
Departamento de Ingeniería Informática

Doctoral Thesis

Understanding the balance between coordination and flexibility in central pattern generators: an experimental and computational study

Author:

Irene Elices Ocón

Supervisor:

Dr. Pablo Varona Martínez

June 2019

Nothing in life is to be feared, it is only to be understood.
Now is the time to understand more, so that we may fear less.

-Marie Curie

Acknowledgments

First of all, I would like to thank my director Pablo Varona Martínez for the opportunity to work on this project, his invaluable help, and dedication during these years. I would also like to thank Rafael Levi for sharing his knowledge in experimental neuroscience, without which part of this work would have been impossible. To Francisco de Borja for his help, his ideas and advice. Thank you very much to all three for all those meetings negotiating the ”negotiation”.

To my teammates Manu and Roy, creators of RT-Hybrid, for their patience in the experiments and in our fight against Murphy. To my fellow GNB labmates Carlos, Angel L, Aaron, Alex, Vinicio, Angel F., Guille, Jessica, Víctor and Miguel for all the great moments lived inside and outside the laboratory, for those meals in psychology, karaoke nights and escape-rooms.

I want to thank my mother Carmen and my brother Jorge for all the love and support and for always being there all the way, especially in the most difficult moments. I would also like to thank my family and friends for their encouragement and support over the years.

Finally, this work would not have been possible without financing from the predoctoral grant MINECO BES-2013-064742 and the projects MINECO TIN2012-30883, DPI2015-65833-P, PGC2018-095895-B-I00 (http://www.mineco.gob.es/) and ONRG Grant N62909-14-1-N279.

Agradecimientos

En primer lugar, me gustaría agradecer a mi director Pablo Varona Martínez por la oportunidad de trabajar en este proyecto, su inestimable ayuda y dedicación durante estos años. Quiero agradecer también a Rafael Levi por compartir su conocimiento en neurociencia experimental, sin el que parte de este trabajo habría sido imposible. A Francisco de Borja por su ayuda, sus ideas y consejos. Muchas gracias a los tres por todas esas reuniones negociando la "negociación".

A mis compañeros Manu y Roy, creadores de RT-Hybrid, por su paciencia en los experimentos y en nuestra lucha contra Murphy. A mis compañeros del GNB Carlos, Ángel L, Aaron, Alex, Vinicio, Ángel F., Guille, Jessica, Víctor y Miguel por todos los grandes momentos vividos dentro y fuera del laboratorio, por esas comidas en psicología, las noches de karaoke y escape-rooms.

Quiero agradecer a mi madre Carmen y a mi hermano Jorge todo el cariño y apoyo y por estar siempre ahí durante todo el camino, especialmente en los momentos más difíciles. Quiero dar las gracias también a mi familia y amigos por sus ánimos y su apoyo en estos años.

Finalmente, este trabajo no habría sido posible sin la financiación de la beca predoctoral MINECO BES-2013-064742 y de los proyectos MINECO TIN2012-30883, DPI2015-65833-P, PGC2018-095895-B-I00 (http://www.mineco.gob.es/) y ONRG Grant N62909-14-1-N279.

Abstract

Robust sequences of neural activations can be found in any nervous system, from simple invertebrate circuits to almost any vertebrate system. Unveiling general principles in the generation and coordination of neural sequences, particularly in transient regimes, is an important step in relating neural activity to function. *Central Pattern Generator (CPG)* circuits are neural networks that generate rhythmic motor patterns. CPGs are convenient neural circuits to study sequential neural activations due to their remarkable rich dynamics generating coordinated rhythms.

In this thesis, we study different sources of temporal variability in CPG circuits, and we unveil fundamental aspects of the instantaneous balance between flexibility and robustness in sequential dynamics. Our analysis of the triphasic rhythm of the pyloric CPG (*Carcinus maenas*) demonstrates robust dynamics that preserves not only the activation sequence but also specific cycle-by-cycle temporal relationships, i.e., *dynamical invariants* in the form of linear correlations between pivotal time intervals. Out of the many possible combinations of time intervals studied, only two cycle-by-cycle dynamical invariants were identified, existing even outside steady states. These dynamical invariants contribute to bound adaptability balancing flexibility and robustness in sequential dynamics. Our experimental results indicate that such boundaries arise from the interaction between the rich dynamics of neurons and connections.

We also study the connectivity of CPGs from a computational point of view. Many CPGs are built on a basic subcircuit of reciprocally connected inhibitory neurons (the so-called *half-center oscillator*), the minimal configuration that can produce distinct rhythmic patterns for controlling antagonistic muscles. Here we use a closed-loop protocol to control the rhythm of a half-center oscillator, adapting the maximum conductance of the inhibition to achieve regular activity. Our results show that the closed-loop control can rapidly find the best connectivity that leads to the regularization goal. In the model, we assess the role of asymmetric maximal synaptic conductances, time constants, and gap-junction connectivity to establish the regularity of the half-center oscillator. The analysis shows that asymmetry both in the maximal conductances and in the temporal dynamics of mutually inhibitory neurons can synergistically contribute to shape wide regimes of regular spiking-bursting activity. Then, departing from a simplified model of the pyloric CPG, we study how the triphasic rhythm is generated by means of the connectivity and the presence or absence of the dynamical invariants found in our experimental work. The results show that both asymmetric maximal conductances and inhibitory synaptic time scales contribute to the shaping of wide regimes of regular and irregular triphasic spiking-bursting activity. The models did not reproduce the invariants found in the experiments despite the intrinsic variability introduced by setting the individual neuron dynamics in a chaotic bursting regime. This suggests that a key dynamical element is still missing in the theoretical paradigms.

Finally, to further study the origin and relevance of the unveiled dynamical invariants and how the actual intervals build the sequence, we have also designed and implemented *hybrid circuits* by connecting neuron models to a living pyloric CPG neuron. We show that as a function of the connectivity parameters dynamical invariants arise between living and model neurons. Our results indicate that dynamical invariants can be propagated through

artificial synapses but only under certain configurations.

Resumen

Las secuencias de activación neuronal robustas se pueden encontrar en cualquier sistema nervioso, desde los circuitos simples en invertebrados hasta los sistemas más complejos en vertebrados. Un paso muy importante para conseguir relacionar la actividad neuronal con la función que desempeña es desvelar principios generales que rigen la generación y coordinación de secuencias neuronales. Los circuitos *Generadores Centrales de Patrones* (CPGs en inglés) son redes neuronales que producen patrones motores rítmicos. Estos circuitos son sistemas ideales para estudiar la activación neuronal secuencial.

En esta tesis estudiamos las diferentes fuentes de variabilidad temporal en circuitos CPG para desvelar aspectos fundamentales del equilibrio entre flexibilidad y robustez en la dinámica secuencial. Nuestros análisis del ritmo trifásico del CPG pilórico (*Carcinus maenas*) muestran la fuerte robustez de las dinámicas transitorias para mantener, además de la secuencia, relaciones temporales específicas ciclo-a-ciclo que toman forma de correlaciones lineales entre intervalos de tiempo claves. A estas correlaciones robustas las denominamos *invariantes dinámicos*. De todas las posibles combinaciones de intervalos de tiempo que se han analizado en este estudio, solo se han identificado dos invariantes dinámicos que se mantienen incluso fuera del estado estacionario de la dinámica del CPG. Nuestros resultados experimentales indican que estas reglas para la limitación en la adaptabilidad surgen de la interacción entre la riqueza dinámica de las neuronas y su conectividad.

También hemos llevado a cabo un estudio de la conectividad en los CPGs desde el punto de vista computacional. Muchos CPGs están construidos a partir de subcircuitos básicos basados en la inhibición mutua entre neuronas (los llamados *half-center oscillators* en inglés), que es la configuración mínima capaz de producir patrones rítmicos para controlar músculos antagónicos. Usando un protocolo de ciclo cerrado para controlar la actividad de un circuito *half-center oscillator*, hemos adaptado la conductancia máxima en la inhibición hasta conseguir un ritmo regular. Nuestros resultados muestran que el control en ciclo cerrado puede encontrar rápidamente la mejor conectividad que lleva a la regularidad del ritmo. También hemos estudiado el papel que juegan la asimetría de la conductancia máxima de las sinapsis, las constantes de tiempo y las conexiones eléctricas para establecer la actividad regular en este circuito. El análisis muestra que la asimetría tanto en la conductancia máxima como en la escala temporal de la inhibición mutua contribuye a dar forma a extensos regímenes de actividad regular. Hemos empleado además un modelo simplificado del CPG pilórico para estudiar cómo se genera el ritmo trifásico en función de la conectividad y analizar la presencia de invariantes dinámicos. Los resultados muestran que la asimetría en la conductancia máxima y en la escala temporal de la inhibición sináptica contribuyen en la generación de las características de los ritmos trifásicos regulares e irregulares. Sin embargo, los modelos no han podido reproducir los invariantes dinámicos encontrados en los experimentos a pesar del uso de modelos neuronales con variabilidad intrínseca, configurados para producir actividad en ráfagas en modo caótico. Ésto indica que puede haber elementos dinámicos fundamentales que no han sido considerados en los modelos teóricos.

Finalmente, para estudiar con mayor detalle el origen y relevancia de los invariantes dinámicos y cómo se moldean los intervalos temporales con los que se construye la secuen-

cia del ritmo, hemos diseñado e implementado *circuitos híbridos* conectando un modelo de neurona a una neurona viva del CPG pilórico. Mostramos también que, dependiendo de los parámetros de la conectividad, los invariantes dinámicos pueden surgir entre la neurona viva y el modelo. Nuestros resultados indican, por tanto, que los invariantes dinámicos se pueden propagar a través de sinapsis artificiales en determinadas circunstancias.

Contents

List of Figures

List of Tables

Part I

Introduction and State of the Art

Chapter 1

Introduction

Living neural systems constitute the most complex and highest efficient devices to encode, to process and learn information, even when compared to the latest developments of human technology. This has awoken an increased interest in the last decades in studying neural systems in detail, ranging from the properties of individual neurons to the emergent phenomena of complex large neural networks. In most cases, a full study of neural systems, either experimental, theoretical or computational, is a hard task mainly due to the many complex biophysical processes involved at the neuron, synapse and network levels, which endows these systems with high dimensionality.

Neuroscience studies the nervous system from different points of view and covers a wide range of levels of description, from interactions at the molecular level to the cognitive functions of complex networks. This multidisciplinary science combines physiology, morphology, molecular biology, cytology, mathematical modeling and psychology to study the properties of neurons and neural networks. The study of nervous systems can be approached from a theoretical or an experimental point of view.

Experimental neuroscience comprises a wide range of techniques such as genetics, imaging, electrophysiology, optogenetics, EEG, fMRI..., which allow scientists to extract data from neural systems. The posterior analysis provides fundamental knowledge and insight into the functioning of neurons and neural networks at different levels. The data provided by experimentalists are the basis for theoretical studies and modeling. Computational neuroscientists study the nervous system from the point of view of its functionality by means of theoretical models of individual neurons and neural networks, and their subsequent simulation in a computer. Models allow us to analyze and manipulate variables and parameters that otherwise are not accessible in experiments and thus, help to understand and identify their role in the system (such as the functional relevance of cells and synapses). However, modeling presents constraints derived from the need for simplification due to limited observability or restricted computational power. Thus, many features and physiological aspects of the living system must be omitted when designing models. Computational modeling generates predictions and insights into the functioning of the nervous system and inspires further experimentation to validate and refine the models. However, all hypotheses and insight developed in theoretical studies must be validated in subsequent experiments. Therefore, there is a continuous flux of information between experiments and theoretical work, intertwining both branches of neuroscience. This mixed approach will be used throughout this thesis.

1.1 Aims

The general aim of this thesis is the study of robust sequential activations in the rhythm generation and coordination in Central Pattern Generators (CPGs). CPGs are neural circuits that produce rhythmic output for muscle function control in repetitive movements (Marder and Bucher, 2001; Selverston, 2010). They are present in most animals, vertebrates or invertebrates. Since these circuits contain usually a small number of neurons and produce a relatively simple pattern output, they are convenient systems to understand rhythm generation and coordination. In particular, this work is focused on the study of the crustacean pyloric CPG (Selverston and Moulins, 1987; Harris-Warrick et al., 1992; Marder and Calabrese, 1996; Selverston et al., 2000).

This thesis combines two perspectives of study in the context of neural sequences: experimental and computational. Both works have been carried out simultaneously and have influenced each other. The combination of experimental and computational studies have provided further insight to design experiments and models, and also to interpret the results. The specific aims of this work are:

1. The characterization of the rhythm variability in the crustacean pyloric CPG by means of intracellular and extracellular electrophysiological recordings. The analysis of the circuit activity through pivotal time references and time intervals in regular and irregular regimes. The identification and analysis of dynamical invariants in the sequences that define the CPG rhythm.
2. The design and implementation of CPG circuit models with distinct levels of complexity in network elements and connectivity. The analysis of the role of the asymmetric connectivity in the generation of regular rhythms.
3. The characterization and tuning of the models to reproduce the triphasic rhythm generated by the pyloric CPG. The analysis of the presence or absence of the experimentally found dynamical invariants in computational models.
4. The design and implementation of hybrid circuits between living neurons of the pyloric CPG and neuron models bidirectionally connected to study and reproduce the dynamical invariants.

1.2 Thesis structure

The aims described in the section above have been structured and presented as follows:

- Part I: Here we present the state of the art in the field and introduce the biological basis of CPGs used in this work. We also introduce models of neurons and synapses and techniques relevant to this work.
- Part II: includes the results obtained in the experimental work. In particular, we characterize regular and irregular pyloric CPG activity and study the dynamical principles shaping the associated rhythms, which can underlay the optimal functioning of the motor system. We present a cycle-by-cycle analysis of dynamical invariants in transient regimes, which allowed demonstrating the adaptation between key intervals that build the sequence.

- Part III: includes the results of the computational work. By means of closed-loop protocols, we explore regions of regular and irregular regimes in a minimal network architecture based on half-center oscillators. We also make use of CPG models to study the role of asymmetry in synaptic strength and temporal scale to generate regular and irregular rhythms, and also to sustain a certain sequence, in particular, a triphasic rhythm.
- Part IV: includes the results of the study with hybrid circuits. Hybrid circuits were designed and implemented by connecting neuron models to living CPG circuits. Here we explore the connectivity parameters that allow dynamical invariants to arise between living and model neurons. We use models of fast and slow graded chemical synapses to connect the living LP neuron to different neuron models.
- Part V: we discuss the results of our analyses and present the conclusions of this work. We also introduce future lines of work to continue this study.
- Appendices: finally, in the last part of this thesis, we provide all parameters and variables values used in the models for the computational study, additional analysis justifications, and the scripts for the characterization of time intervals from the spike timings of the experimental or computational time series.

Chapter 2

Biological basis

The results presented in this thesis have been obtained from a combination of experimental and computational work. In this chapter, we introduce the biological context on which this thesis is based. In particular, we introduce the basic elements of neural circuits: *neurons* and *synapses*, and explain the fundamental mechanisms derived from their electrical properties, as well as the different processes affecting the transmission of information at the synapses. We introduce a special type of neural circuits, the so-called *CPGs* (Central Pattern Generators), known for their role in motor control and their robust sequential activity. We also present a specific CPG used in our study, the *pyloric circuit* of the crustacean *stomatogastric system*.

2.1 Introduction

The *nervous system* is in charge of acquiring and processing sensory information and transmitting associated signals to activate a motor response. In *vertebrates*, the nervous system is considered to be organized in two parts: the *central nervous system* (CNS), formed by the brain and the spinal cord; and the *peripheral nervous system* (PNS), formed by nerves and ganglia that do not belong to the CNS (Kandel et al., 2012). Nevertheless, in *invertebrates*, the nervous system is usually much simpler than in vertebrates, although the level of complexity depends greatly on the type of invertebrate. CNS in invertebrates such as insects, mollusks, crustaceans, etc., is organized in clusters of neuron cell bodies called *ganglia* (see ***Figure 2.1***). The peripheral part of their nervous system is formed by the extensions of the cells in these ganglia; some carry sensory information from the environment, while others carry signals from the ganglia to produce a response (e.g. movement). This organization in clusters of neurons allows segmentation so that each ganglion responds to and controls a part of the body.

The *motor system* is the part of the nervous system that controls and coordinates movement. It also consists of two parts: the *central motor system*, formed by elements from the central nervous system, which coordinate and control the movement; and the *peripheral motor system* formed by the motor nerves and the muscles, which perform the movement. Many of the most common movements in animals are repetitive in cycles and are called *rhythmic movements*. The muscles involved in this type of movements activate in *sequences* or *patterns* maintaining the coordination among them, which is crucial for an effective performance. The mechanisms that generate and control such sequences can be originated in

complex neural networks such as the cortex or the hippocampus (Yuste et al., 2005; Buzsáki and Tingley, 2018), but also in simpler neural circuits like central pattern generators (Selverston and Moulins, 1987). In this thesis, we focus our study on the rhythm generation and coordination in CPGs.

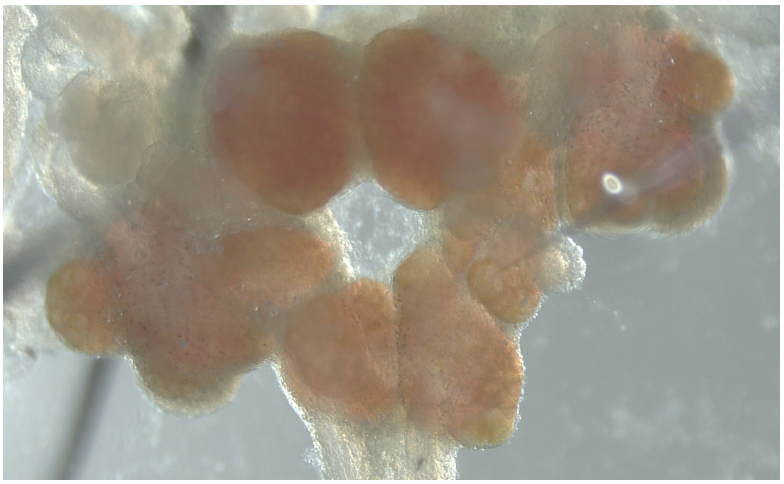

Figure 2.1: Example of the ganglia organization in the mollusk *Lymnaea* stagnalis. This group of ganglia forms the central ring and is composed of nine ganglia: left and right cerebral ganglia, left and right pedal ganglia, left and right pleural ganglia, left and right parietal ganglia, and the visceral ganglion. Specific motor control functions are implemented in different ganglia.

2.2 Neurons

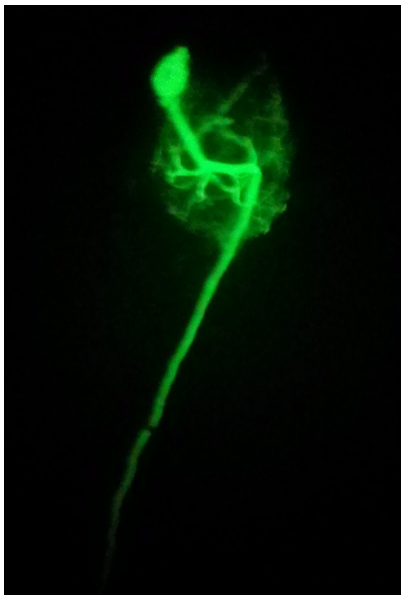

Figure 2.2: Crustacean pyloric neuron as seen with a calcium-sensitive dye. Crustacean CPG neurons are highly robust for long intracellular recordings. They are also suitable for hybrid circuit experiments in which living and model neurons interact bidirectionally.

The cells that build the nervous system are *neurons* and *glial cells* (Cajal, 1888; Virchow, 1846). Neurons are cells that present a high level of specialization and process and transmit information by means of electrical and/or chemical signaling (see ***Figure 2.2***). A typical neuron has three defined fundamental structures: *soma*, *axon*, and *dendrites*. The *soma*, is the cell body of the neuron and contains the main organelles such as cellular nucleus, mitochondria, and other important organelles, and realizes the main metabolic processes. The *axon* is a single long structure that extends away from the soma and acts as the main conductor of the output signals to other neurons. *Dendrites*, on the other hand, are tree-like structures that grow from the soma. They receive signals from sensory receptors or other neurons and can participate in triggering the action potential (Herreras, 1990). The information is transmitted by means of action potentials or *spikes*. These electrical transient signals take the form of a peak of electrical activity that moves along the axon to reach other neurons. Between the terminals portions of one neuron and the receptors of another neuron, specialized connections are established, which are known as *synapses*.

Depending on their functionality, neurons can be classified as *sensory neurons*, *interneurons*, and *motoneurons*. Sensory neurons receive external stimuli and transform that information into action potentials. The interneurons process information of the inputs they receive from other neurons and propagate it to other cells. Finally, motoneurons receive information from sensory neurons or interneurons and innervate muscles directly.

The generation and propagation of an action potential is based on changes in flow of ions through *channels*, which are specialized proteins located in the neuron membrane whose opening and closing are typically voltage-dependent (Kandel et al., 2012). In the absence of stimuli from other neurons, there is a difference of electrical potential across the cell membrane produced by an excess of negative charges inside the cell, and of positive charges on the extracellular medium. This difference of potential between the exterior and interior in the absence of stimulus is defined as *resting potential*. The value typically chosen as reference potential in the extracellular medium is $0\ mV$, thus the resting potential is always negative. Outside the membrane, in the extracellular medium, the most abundant ions are Na^+ and Cl^-, while in the intracellular medium the most common ions are K^+ and other organic anions (Hille, 2001). Whenever an external input signal from other neurons arrives, some of the channels in the membrane start to open, causing an influx of ions into the cell and thus, disturbing the equilibrium of the membrane potential. If the net influx of charges into the neuron is positive, the membrane potential becomes less negative (*depolarization*), whereas if the net influx is negative, the difference of potential across the membrane increases, leading to a more negative membrane potential (*hyperpolarization*).

After the stimulus arrives disturbing the equilibrium, the neuron can react in two possible ways. If the stimulus is small enough, the neuron is able to recover its equilibrium once it has finished. On the other hand, if the depolarization is sufficiently strong and the membrane potential reaches a certain threshold value, the neuron becomes active and responds to the stimulus. Then, several voltage-dependent channels of Na^+ open, causing a net influx of positive charge into the neuron and a further depolarization. The increase in depolarization causes the opening of more Na^+ voltage-channels, which amplifies, even more, the depolarization to reach the Na^+ equilibrium potential. Before the membrane potential reaches this value, two parallel processes activate to repolarize the membrane potential to its resting value. One process is the closing of the majority of Na^+ voltage-dependent channels, and the other is the opening of K^+ voltage-dependent channels that produces an increasing flux of K^+ out of the neuron. The combination of these processes results in the fast hyperpolarization of the membrane potential until it reaches the resting potential again. This process is known as the generation of a *spike* or *action potential*.

The membrane potential fluctuates all the time. Small depolarizations or/and hyperpolarizations around the resting value are known as *sub-threshold activity*. If the depolarizations are strong enough to trigger the generation of spikes then, the neuron present *spiking activity* (see ***Figure 2.3*** left panel). However, some neurons can generate spikes in groups, forming bursts of two or more spikes in a short interval of time, and alternating silent periods with only sub-threshold activity, and bursts. This is the case of *bursting activity*, which present a richer dynamics since it combines two temporal scales (see ***Figure 2.3*** right panel). The fast mechanisms are responsible for exciting the neuron and generating spikes, while the slow dynamics depolarizes the cell to start the burst and then reduces the neuron's excitability after a short time, ending the burst. A wide variety of ionic channels can be involved in the onset and termination of neuronal bursting activity.

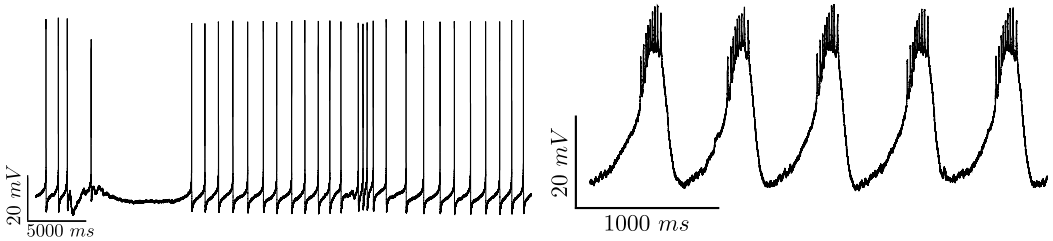

Figure 2.3: Examples of different types of neuronal membrane potential waveforms. Left panel: An example of spiking activity. The trace corresponds to a neuron of the feeding CPG in *Lymnaea* stagnalis. Right panel: An example of bursting activity. The trace corresponds to a PD neuron of the pyloric CPG in crustacean.

2.3 Synapses

A synapse is a connection established between two neurons (Kandel et al., 2012). The neuron that sends electrical signals in the form of action potentials is called the *presynaptic* neuron, and the one that receives them is called the *postsynaptic* neuron. Depending on the mechanism that the cell uses for the transmission of the signal, synapses can be classified as *electrical* or *chemical*.

Electrical synapse

In an electrical synapse, the presynaptic and postsynaptic neurons are very close, with a separation between their membranes of approximately a few nanometers (Connors and Long, 2004). Thus, the transmission of information is very fast and almost immediate. Both subthreshold and spiking activity can be transmitted through this type of synapses. In most of the cases, the electrical synapses are bidirectional and symmetric, that is, current flows in both ways and approximately with the same intensity. In this type of synapse, the neurons are joined by specific protein structures called *gap-junctions*, which are specialized ionic channels that connect the cytoplasm of both cells. However, in some electrical synapses, there is a preferential direction in the current flow or even current can flow only in one direction. These synapses are known as *rectifying synapses* (Selverston and Moulins, 1987).

Chemical synapse

In a chemical synapse, the separation among neurons is larger than in gap-junctions, about 20-40 nm, therefore there is no physical contact among the cells (Cowen et al., 2001). In chemical synapses, the transmission of the signal is mediated by *neurotransmitters*, which are chemical messengers generated at the end of the axon of the presynaptic neuron. When a presynaptic action potential arrives at the synapse, it induces the release of neurotransmitters near the membrane. The released neurotransmitters can bind to some specific molecular receptors located in the postsynaptic membrane, which induces the opening of ionic channels. This produces the depolarization or hyperpolarization of the postsynaptic membrane. Since the action potential arrives at the synapse in the presynaptic neuron, there is a delay of 1 to 5 ms until an effect is induced in the postsynaptic membrane. Some common neurotransmitters are dopamine, serotonin, acetylcholine or glutamate. In this type of synapses, the transmission of the signal is intrinsically asymmetric, thus, informa-

tion is transmitted from the presynaptic neuron to the postsynaptic neuron. In some cases, the release of neurotransmitters is gradual and they are delivered before the presynaptic action potential, which can play an important role in certain oscillator networks (Graubard et al., 1983). These connections are known as *graded synapses*.

2.4 Central Pattern Generators

Central pattern generators (CPGs) are neural circuits that produce flexible rhythmic motor patterns (Marder and Bucher, 2001; Selverston, 2010), which control repetitive movements. The robust and highly coordinated neuron activation sequences underlying their rhythms arise from the combination of intrinsic membrane currents and properties of the synaptic connections (Selverston et al., 2000; Gjorgjieva et al., 2016). They are present in most animals, vertebrates and invertebrates. In invertebrates, many neurons have individual characteristics that can be recognized repeatedly across animals and from one experiment to the next. These circuits also have a reasonably small number of neurons, produce a relatively simple pattern output and are easily manipulated *in vitro*. Thus, invertebrate CPGs are key neural circuits to understand rhythm generation and coordination, as their cells and connections have been identified and mapped, like in the crustacean pyloric CPG that we use in this study (Selverston and Moulins, 1987; Harris-Warrick et al., 1992; Marder and Calabrese, 1996; Selverston et al., 2000).

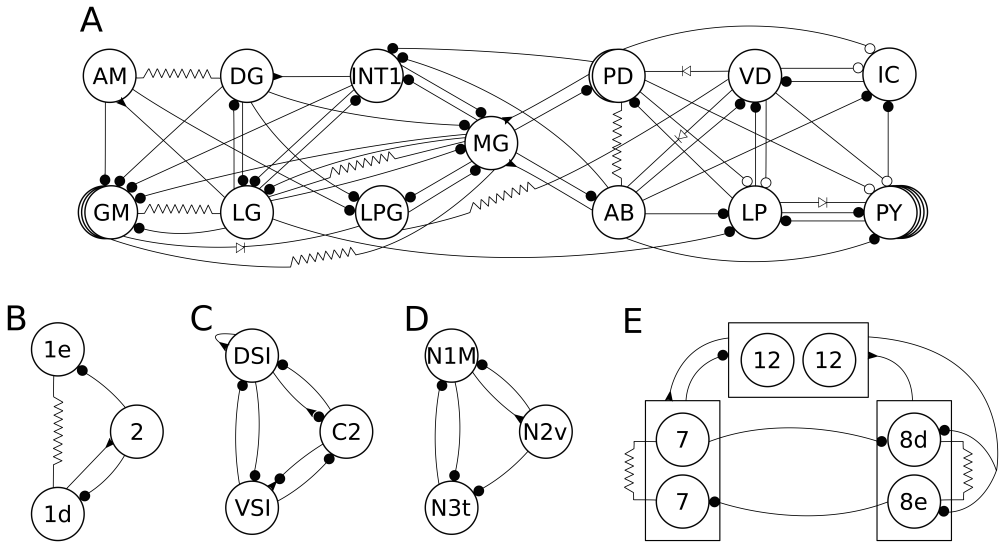

Figure 2.4: Examples of non-open topologies in CPGs of invertebrates. Panel A: Gastric and pyloric circuits in crustaceans. Panel B: Feeding CPG in Planorbis. Panel C: Swimming CPG in Tritonia. Panel D: Feeding CPG in *Lymnaea* stagnalis. Panel E: Swimming CPG in *clione* limacina. Note that all these examples present non-open topologies, in which all neurons in the circuit receive input from other cells. Mutual inhibition is also an essential property that is present in most CPGs (examples A, C, D and E in the figure). Black filled circles represent fast chemical inhibitory synapses, empty circles represent slow chemical inhibitory synapses, black triangles represent excitatory synapses, white triangles represent rectifying synapses and resistors represent gap-junctions.

Most CPGs have what is called a non-open topology (Huerta et al., 2001; Stiesberg et al., 2007), i.e., all neurons in the CPG receive input from other cells in the circuit for transient closed-loop computation. An essential component of these sequence generator networks is reciprocal inhibition between pairs of neurons. Mutual inhibition together with electrical

coupling and other non-reciprocal interactions (Huerta et al., 2001; Benjamin et al., 2001) underlie the timing of neuron activations that shape each cycle (Weaver and Hooper, 2003b; Hooper et al., 2009; Selverston, 2010; Sakurai et al., 2014). Some examples of CPGs topologies are shown in ***Figure 2.4***. Another highly relevant property in these neural networks is the presence of intrinsically irregular/chaotic neurons, which typically display rich slow-fast dynamics able to generate bursts with different duration, phases, and spike temporal structures (Abarbanel et al., 1996; Elson et al., 1998). The reciprocal inhibitory connections between neurons lead to the regularization of the chaotic behavior when the neurons interact with each other in the circuit. The rich intrinsic dynamics provide flexibility and robustness for negotiating rhythms as a function of external inputs, producing the characteristic regular spiking-bursting activity that allows the CPG to control motor movements (Selverston et al., 2000).

Most CPGs are typically studied in regular regimes, however, irregular rhythms can also be observed in control or induced conditions, e.g. see (Bartos et al., 1999; Thuma and Hooper, 2003; Nadim et al., 2011; Elices and Varona, 2015; Hooper et al., 2015). In fact, central and sensory feedback continuously alter the CPG rhythm, resulting in transient regimes, which underlay the adaptability of these circuits. CPGs activate the muscles that produce motor rhythms related to specific functions, such as walking, breathing, chewing, etc. (in the case of the pylorus, a triphasic rhythm) and their flawless function is crucial for the animal survival (Selverston and Moulins, 1987; Harris-Warrick et al., 1992).

2.5 Stomatogastric system

Probably one of the most studied circuits in neuroscience is the *stomatogastric* nervous system (STN) in crustacean (crabs, lobsters. etc.). One of the reasons why this system is so well known is that it is relatively easy to isolate and manipulate both in *in vivo* and *in vitro* conditions. All modulatory inputs arrive at the ganglion through only one nerve containing 130 axons at the most, which is a very small number as compared to other systems.

The stomatogastric system, located in the foregut (see ***Figure 2.5***), comprises a short esophagus and a large stomach. The stomach is divided in two parts: the *cardiac sac*, which is the anterior large chamber, and a posterior chamber called the *pylorus* (Selverston and Moulins, 1987). The cardiac sac stores coarsely shredded food after entering through the mouth, while the pylorus filters the food particles going to the midgut. The foregut wall is covered with a soft cuticle in which there are calcified regions called ossicles. Two lateral and one central modified ossicles or teeth, which are located in the posterior dorsolateral region of the cardiac sac, form a system called the *gastric mill*. The gastric mill macerates the food passing from the lower portion of the cardiac sac. Then food is transferred to the pylorus through the *cardio-pyloric valve* where is reduced to small particles by the hepatopancreas gland secretions located into the lateral wall of the pyloric chamber. There, food particles are filtered before exiting the stomach. Rhythmic movements of the whole system: esophagus, the cardiac sac, gastric mill, and the pyloric chamber, are produced by striated muscles, which are innervated by the stomatogastric nervous system. There are four different rhythms, generated in different parts of the system: esophageal, cardiac sac, gastric and pyloric and control the contractions of different groups of muscles. The esophageal rhythm produces a peristaltic movement of the esophagus allowing the food to travel from the mouth to the stomach. The cardiac sac rhythm function is to drive the food to the gastric mill. Then, the gastric rhythm controls the stomach muscles that grind the food. Finally, the pyloric rhythm controls the opening and closing of the cardio-pyloric valve. The different circuits generating these four rhythms, share information and adapt their activity as a function of inputs arriving from the other circuits in a coordinated way

that ensures the correct and optimal functioning of the whole system.

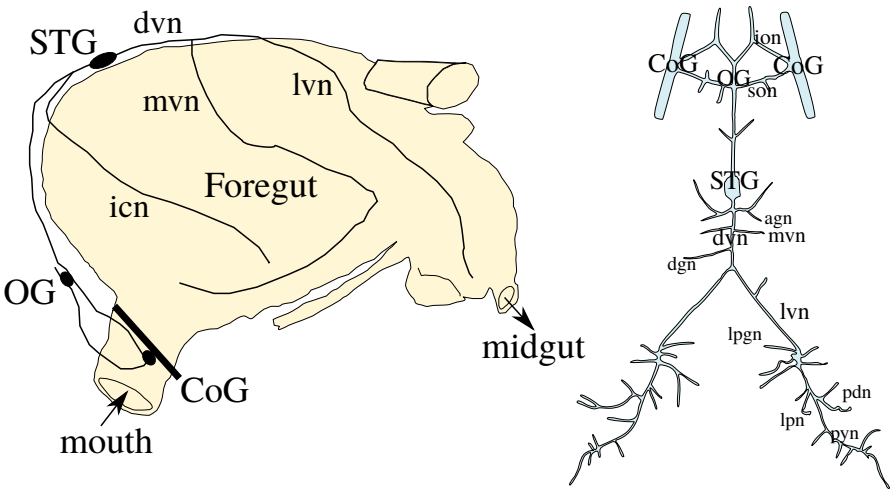

Figure 2.5: Scheme of the crustacean foregut and the stomatogastric nervous system. The stomatogastric nervous system is located in the foregut as it is shown in the left panel. It comprises four ganglia: *Commissural Ganglia* (COGs), *Oesophageal Ganglion* (OG) and *Stomatogastric Ganglion*. The main nerves: ion, son, dvn, lvn, etc. are also indicated in the figure. The whole nervous system as shown in the right panel can be dissected off the stomach and kept alive in an experimental dish for many hours or even days. Modified from (http://www.scholarpedia.org/article/Stomatogastric_ganglion).

Figure 2.6: The stomatogastric ganglion of the crab *Carcinus maenas*. The nervous system is dissected and extracted from the stomach. Then, the remaining tissue is cleaned off all the nerves and ganglia. The STG is exposed after desheathing. In this ganglion, around 25 somas can be seen. The membrane potential of individual neurons can be recorded using sharp glass electrodes.

All neurons comprising the stomatogastric system are located in four ganglia: *Commissural Ganglia* (COGs), *Oesophageal Ganglion* (OG) and *Stomatogastric Ganglion* (see ***Figure 2.5***). The OG is connected directly to the brain and contains around 10 to 15 cell bodies. Each COG contains several hundreds neurons, of which all the identified ones are interneurons that are involved with both the pyloric and gastric rhythms. These ganglia are connected to the STG through the *stomatogastric nerve* (STn).

The dissection of the stomatogastric system is a complex and long procedure, see (Mulloney and Selverston, 1974a). After removing part of the top carapace, the whole stomach is extracted. Once the excess of tissue around the stomach is cleaned off, the stomach is cut open from below and put in a Sylgard dish with the dorsal side on top. Then the nerves and ganglia are cleaned exposing the stomatogastric system (***Figure 2.5***). The stomatogastric ganglion is located inside an artery that runs dorsally on top of the stomach from the heart to the brain underneath two layers of muscles. Once they are removed, the tissue below the ganglion is cut to improve visibility later on. The final and most delicate step is desheathing the thin membrane covering the ganglion to expose the neurons. The whole procedure takes approximately 3 hours.

The ganglion contains about 30 cell bodies of which 24 are motoneurons and 6 interneurons (see ***Figure 2.6***). Of the identified motoneurons, two innervate the cardiac sac muscles, 9 innervate the musculature of the gastric mill, two innervate the cardio-pyloric valve and 11 innervate the pyloric muscles. These neurons can be grouped into two circuits: the *gastric CPG* and the *pyloric CPG* (see ***Figure 2.7***).

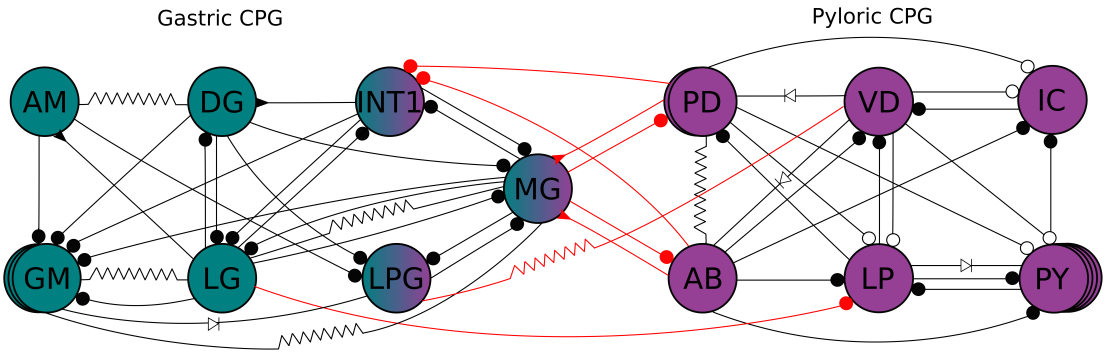

Figure 2.7: Scheme of the pyloric and gastric circuit in crabs. Both circuits are part of the STG and contain about 30 cell bodies. The gastric CPG is build up with 11 neurons (green color) while the pyloric CPG with 14 neurons (purple color). Both circuits are connected among them (see connections colored in red) by means of the neurons LG-MG, LPG and Int1 (gastric circuit) and the neurons PD, AB, VD and LP (pyloric circuit). Int1, MG, LPG neurons receive pyloric modulation; hence they are represented with mixed colors in the scheme. Black filled circles represent fast chemical inhibitory synapses, empty circles represent slow chemical inhibitory synapses, filled triangles represent excitatory synapses, white triangles represent rectifying synapses and resistors represent gap-junctions.

2.5.1 Gastric CPG

The gastric CPG is build up with 11 neurons, of which one is an interneuron (Int1) and the rest are motoneurons (LG, MG, DG, AM, two LPGs and four GMs), see a scheme of the circuit in ***Figure 2.7*** (Mulloney and Selverston, 1974a,b; Selverston and Mulloney, 1974). The LG-MG and DG-AM, which are not spontaneously active, innervate intrinsic muscles in the stomach and when they are silent these muscles are relaxed. On the contrary, Int1, LPGs and GMs fire on their own, in the absence of synaptic inputs. They innervate extrinsic muscles supporting the stomach.

The gastric rhythm is intermittently active and, depending on how is activated, can change the phase relations among the participating muscles and the neurons that innervate them. The kernel of the gastric system is the reciprocal inhibition between LG-MG and Int1-DG-AM that forces these two groups of neurons to fire in alternating bursts. The lateral teeth are controlled by LG, MG y LPGs neurons while DG y GMs control medial tooth movements. This pattern of activation results in a coordinated movement of the tooth-system and the correct grinding of the food.

The gastric CPG is connected to the pyloric CPG through neurons LG-MG, LPG, and Int1 (see a scheme of the circuits in ***Figure 2.7***). Consequently, the activities of both circuits are interdependent.

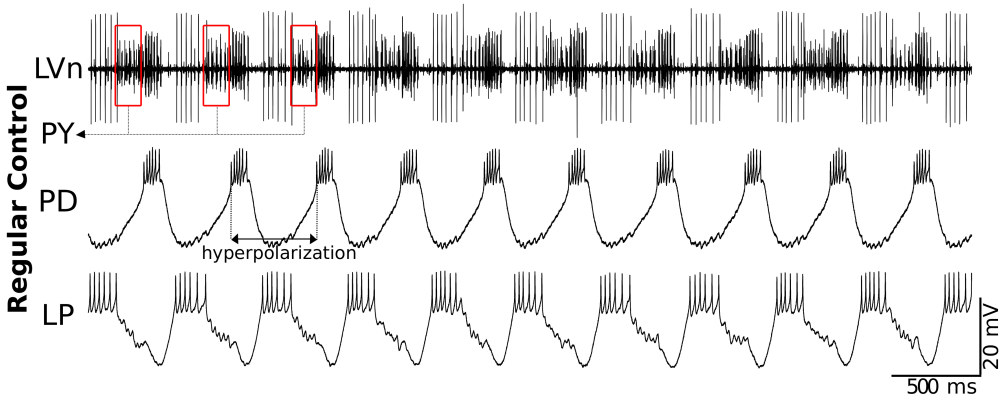

Figure 2.8: An example of the characteristic regular triphasic spiking-bursting activity of the pyloric CPG in the crab *Carcinus maenas*. The traces correspond to simultaneous extracellular recordings of the LVn nerve (upper trace) and intracellular recordings of PD and LP neurons in the intact CPG. Large spikes in the LVn trace correspond to the LP neuron. Note that LP spikes occur in anti-phase with PD spikes and the respective IPSPs can be observed in the PD neuron trace. PY spikes can be observed in the extracellular recording after the LP and before the PD spikes (red boxes in the upper trace). PD and LP burst durations and hyperpolarization intervals are nearly constant in the recordings.

2.5.2 Pyloric CPG

The pylorus filters food particles as they come through the stomach due to the rhythmic activation of muscles that open and close the pylorus. The pyloric rhythm is coordinated by the pyloric CPG. This circuit consists of 14 neurons, of which one, the AB, is an interneuron and the rest are motoneurons (two PDs, LP, eight PYs, VD and IC) (Selverston and Moulins, 1987; Marder and Bucher, 2001; Selverston, 2005). These neurons are connected by means of electrical and chemical synapses (see a scheme of the circuit in ***Figure 2.7***). The electrical synapses are bidirectional and in one case rectifying (from LP to PYs). The chemical synapses are all graded and inhibitory of two types, glutamatergic (fast synapse) and cholinergic (slow synapse).

Figure 2.9: Picture of the crab *Carcinus maenas*, used for experiments in this thesis. It is a common littoral crab, generally referred to as the shore crab, or green shore crab. It has a carapace up to 90 mm long and 210 mm wide approximately.

The kernel of the pyloric circuit is built on reciprocal inhibition among three groups of neurons AB-PDs, LP and PYs, which gives rise to a *triphasic rhythm* (LP-PY-PD sequence). ***Figure 2.8*** shows an example of extracellular recording of the LVn nerve in which these three components can be clearly distinguished, along with intracellular recordings from PD and LP neurons. When the LP and IC are activated, they inhibit the rest of the neurons forcing them to remain silent. Then, as the burst of the LP ends, the PYs are liberated and start to fire. Finally, when the PDs and AB, which are electrically coupled, activate they inhibit the LP and the PYs. In control conditions, this circuit typically produces a regular and robust rhythm with nearly constant burst durations and hyperpolarization intervals (***Figure 2.8***). The period of the pyloric rhythm is approximately ten times faster than the gastric, ranging from 1 to 5 s. The sequence, LP-PY-PD, produces the coordinated contraction and relaxation of the muscles that these neurons innervate. In the first stage, as the anterior intrinsic constrictor muscles contract, the anterior region of the chamber constricts and the cardio-

pyloric valve closes. Then, the posterior region of the pyloric chamber constricts. Finally, the extrinsic dilator muscles contract simultaneously, dilating the pyloric chamber and opening the cardio-pyloric valve (Hartline and Maynard, 1975; Rezer and Moulins, 1983).

In this thesis, we will analyze and study pyloric CPG rhythms from a novel perspective, paying special attention to sequential activations in regular and irregular regimes. All the recordings of the pyloric CPG, presented in this thesis have been performed in the crab *Carcinus maenas* (see ***Figure 2.9***).

2.5.3 Transients, irregular rhythms and approximate phase maintenance

Experimental and computational studies of pyloric CPG traditionally examine their rhythmic output from periodic spiking-bursting regimes. Recordings of pyloric neurons in the semi-intact network typically show regular sequential behavior of the circuit, e.g. (Selverston et al., 2000; Soofi et al., 2014). On the other hand, *in vivo* recordings of CPG activity display further temporal characteristics and a larger degree of irregularity than *in vitro* recordings (Rezer and Moulins, 1983; Clemens et al., 1998; Soofi et al., 2014). Furthermore, recordings of isolated cells show that most of them are highly irregular (Bal et al., 1988; Abarbanel et al., 1996; Elson et al., 1999; Varona et al., 2001a), see ***Figure 2.10***. Rich intrinsic cell and synaptic dynamics, arising from different time scales (Gjorgjieva et al., 2016), enable neurons comprising the CPG to establish readily a network rhythm in concert (Selverston et al., 2000). However, external and intrinsic factors continuously affect the system inducing transients and therefore making them an important element of the system functionality, which can only be observed in recordings of irregular activity. Inputs from the gastric CPG constantly affect the pyloric rhythm since both circuits have to exchange information in order to coordinate the movements they control (Selverston et al., 1976; Mulloney, 1977; Selverston and Moulins, 1987; Clemens et al., 1998; Bartos et al., 1999; Thuma and Hooper, 2003).

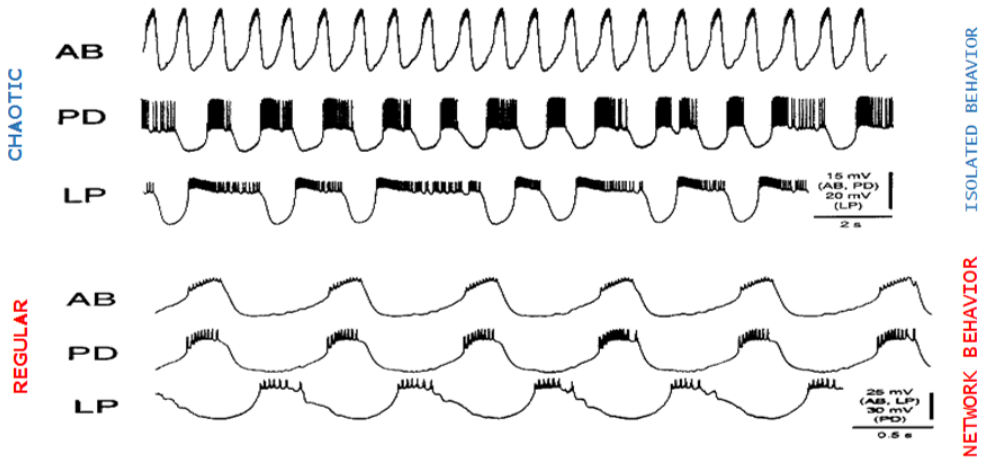

Figure 2.10: Examples of recordings of the pyloric neurons AB, PD and LP in control conditions and in isolation. Typically, recordings of pyloric neurons in the semi-intact network show regular sequential behavior of the circuit. However, most of the pyloric neurons in isolation show highly irregular activity (Bal et al., 1988; Abarbanel et al., 1996; Elson et al., 1999; Varona et al., 2001a). Figure kindly provided by Dr. Al Selverston.

Early on, the CPG research community identified the importance of phase maintenance for motor function (Grillner and Kashin, 1976; Dicaprio et al., 1997; Fischer et al., 2001). Previous studies in the pyloric CPG have reported approximate maintenance of phase-frequency relationships when altering the rhythm speed by current injection (Hooper, 1997a,b; Weaver and Hooper, 2003a; Hooper et al., 2009) or by temperature changes (Tang et al., 2010; Soofi et al., 2014). By quantifying average delays and periods and comparing across preparations, authors could show that certain elements of the rhythm maintain relative timing with changes in frequency (Hooper, 1997a,b; Soofi et al., 2014). In this context, most works discard irregular activity, as well as, transient changes. Information regarding variability can be addressed through the characterization of the instantaneous generation and coordination of neural sequences.

While there is a vast list of efforts that address the generation and function of brain rhythms, the dynamical origin of the balance between robustness and flexibility in building sequential activations, which underlie many of such rhythms, has not been investigated in detail. Finding dynamical principles that shape neuronal sequences in each cycle of the rhythm can lead to a closer link between neural activity and function at all levels of description of the nervous system. In the following chapters, we will address this challenge using a dual theoretical and experimental approach in the context of the neural sequences generated in the pyloric CPG.

Chapter 3

Computational Models

In this chapter, we present several mathematical models that are often used in the study of neural systems and synaptic transmission. These models vary in complexity attending to the level of realistic biophysical features included in their description. We also introduce examples of CPG models and, in particular, models of the crustacean pyloric CPG. Finally, we briefly describe the integration methods generally used in computational studies.

3.1 Introduction

Models in Computational Neuroscience are usually designed following two strategies: bottom-up approaches, in which detailed biophysical models are developed departing from data obtained in experimental studies with the aim of validating theoretically experimental hypothesis; and top-down approaches, in which models aim to reproduce certain dynamical features or behaviors of neural systems and find general mechanisms that cause them in simplified paradigms. Both types of models allow to propose novel hypotheses and suggest new experiments. Ideally, these two approaches can be combined.

The level of description of the mathematical model chosen to describe a network, neuron and/or synapses chosen in all studies is crucial. A very detailed and realistic model entails typically a high computational cost and a wide parametric space to explore and analyze. On the other hand, an oversimplified model may not include the precise biological properties needed to reproduce the key phenomena under study. Therefore, depending on the aim of the research, the model must be chosen carefully to reach a compromise between accuracy and efficiency.

3.2 Neuron models

In order to understand and simulate neuronal behavior, several mathematical descriptions have been developed in the last few decades (Koch, 1999; Torres and Varona, 2012). The level of detail in the description varies among the different phenomenological models used in computational neuroscience. Thus, they can be classified in two main categories:

biophysical models and simplified models. However, neural models built on simplified paradigms may lead to more detailed biophysical models, keeping the same dynamical principles but implemented with more biophysically realistic mechanisms. The other way around is also possible, that is, a realistic model can be simplified as well by keeping only those features that allow to reproduce the behavior characterizing the phenomena under study. Below we describe the different approaches for the theoretical description of the models employed in this work.

3.2.1 Biophysical models

Hodgkin-Huxley conductance-based model

The generation of action potentials is a consequence of the competition of different ionic currents across the membrane. There are several types of voltage-dependent ionic channels, such as sodium, potassium and calcium channels that control the flux of ions through the membrane, which generates the ionic currents responsible for the neuron excitability. These currents have complex voltage-dependent nonlinear dynamics, including in some cases a dependency on the concentration of specific ions. Other ion channels, whose proportion in the membrane is not too high, can also contribute to the excitability of the membrane and usually are considered in the biological models as part of the so-called *leakage current*. The flow of all these ionic currents generates voltage changes that propagate across the membrane. The opening probability of a type of ionic channel depends nonlinearly on the membrane voltage and the current state of the channel.

Hodgkin and Huxley were the first to model these processes assuming that the membrane potential of the neuron could be described by the following set of nonlinear differential equations (Hodgkin and Huxley, 1952):

$$
\begin{aligned}
C_m \frac{dV(t)}{dt} &= g_L(V_L - V(t)) + g_{Na}\, m(t)^3\, h(t)(V_{Na} - V(t)) + g_K\, n(t)^4\, (V_K - V(t)) + I; \\
\frac{dm(t)}{dt} &= \frac{m_\infty(V(t)) - m(t)}{\tau_m(V(t))}; \\
\frac{dh(t)}{dt} &= \frac{h_\infty(V(t)) - h(t)}{\tau_h(V(t))}; \\
\frac{dn(t)}{dt} &= \frac{n_\infty(V(t)) - n(t)}{\tau_n(V(t))};
\end{aligned}
\tag{3.2.1}
$$

where $m(t)$, $h(t)$, $n(t)$ are conductance variables that describe the activation and deactivation of the ionic conductances through the channels and $V(t)$ is the membrane potential. This model considers two active channels: a Na^+ channel and a K^+ channel, and a passive leakage channel L. The parameters g_{Na}, g_K and g_L are the maximal conductances of these ionic channels and V_{Na}, V_K and V_L are the corresponding reversal potentials; I is the external current arriving at the neuron that acts as a stimulus to the model and C_m is the *capacitance* of the membrane. Finally, the steady state values of the active conductance

variables m_∞, h_∞, n_∞ and the time constants τ_m, τ_h, τ_n for channel activation and inactivation present a nonlinear voltage dependence, usually by means of *sigmoid* or exponential functions, whose parameters can be fitted from experimental data.

The conductance-based description of Hodgkin-Huxley neuron models, particularly with further ionic channel descriptions, can account for a wide range of phenomenology observed dynamics in living neurons, such as subthreshold oscillations, chaotic dynamics, and bursting behavior among others (Izhikevich, 2003). Multicompartment approaches can also provide further realism and precise reproduction of waveforms and intracellular action potential propagation (Gouwens et al., 2018).

Komendantov-Kononenko model

The Komendantov-Kononenko model is a Hodgkin-Huxley type model that considers only one compartment. This model was based on experimental data and tuned to simulate the behavior of CPG bursting neurons of the snails *Helix Pomatia*, see (Komendantov and Kononenko, 1996).

The equation describing the membrane potential in the model is:

$$-C_m dV(t)/dt = I_{Na(TTX)} + I_{K(TEA)} + I_K + I_{Na} + I_{Na}(V) + I_B + I_{Ca} + I_{Ca-Ca}, \tag{3.2.2}$$

where C_m is the capacitance of the membrane and V the membrane potential in mV. The model describes the conductances of eight membrane currents, which define four components:

- A slow-wave generating mechanism, given by sodium, potassium and chemosensitive currents:

$$I_{Na}(V) = g^*_{Na}(V)(1/(1 + exp(-0.2(V(t) + 45))))(V(t) - V_{Na}); \tag{3.2.3}$$
$$I_{Na} = g^*_{Na}(V(t) - V_{Na}); \tag{3.2.4}$$
$$I_K = g^*_K(V(t) - V_K); \tag{3.2.5}$$
$$I_B = g^*_B m_B(t) h_B(t)(V(t) - V_B); \tag{3.2.6}$$
$$dm_B(t)/dt = (1/(1 + exp(0.4(V(t) + 34))) - m_B(t))/0.05; \tag{3.2.7}$$
$$dh_B(t)/dt = (1/(1 + exp(-0.55(V(t) + 43))) - h_B(t))/1.5; \tag{3.2.8}$$

- A spike-generating mechanism, which is described by TTX-sensitive sodium and TEA-sensitive potassium Hodgkin-Huxley type currents:

$$I_{Na(TTX)} = g^*_{Na(TTX)} m(t)^3 h(t)(V(t) - V_{Na}); \tag{3.2.9}$$
$$I_{K(TEA)} = g^*_{K(TEA)} n(t)^4 (V(t) - V_K); \tag{3.2.10}$$
$$dm(t)/dt = (1/(1 + exp(-0.4(V(t) + 31))) - m(t))/0.0005; \tag{3.2.11}$$
$$dh(t)/dt = (1/(1 + exp(0.25(V(t) + 45))) - h(t))/0.01; \tag{3.2.12}$$
$$dn(t)/dt = (1/(1 + exp(-0.18(V(t) + 25))) - n(t))/0.015; \tag{3.2.13}$$

- A calcium transient voltage-dependent current, described by:

$$I_{Ca} = g^*_{Ca} m^2_{Ca}(V(t) - V_{Ca}); \tag{3.2.14}$$
$$dm_{Ca}(t)/dt = (1/(1 + exp(-0.2V(t))) - m_{Ca}(t))/0.01; \tag{3.2.15}$$

- A calcium stationary $[Ca^{2+}]_{in}$ inhibited current given by:

$$I_{Ca-Ca} = g^*_{Ca-Ca} \frac{1}{1 + exp(-0.06(V(t) + 45))} \tag{3.2.16}$$
$$\frac{1}{1 + exp(K_\beta([Ca](t) - \beta))}(V(t) - V_{Ca}); \tag{3.2.17}$$
$$d[Ca](t)/dt = \rho - I_{Ca}/2Fv - K_s[Ca](t); \tag{3.2.18}$$

where $v = 4\pi R^3/3$ is the volume of the cell; $[Ca]$ is $[Ca^{2+}]_{in}$ (mM), F is Faraday number (F=96,485 $Cmol^{-1}$), K_s is the intracellular Ca-uptake rate constant and ρ is the endogenous Ca buffer capacity.

This conductance based model displays a very rich dynamics as a function of the parameters. It can be tuned in four main modes: beating-mode (tonic spiking activity), chaotic-mode (irregular spiking activity), regular bursting activity and chaotic bursting activity (see ***Figure 3.1***).

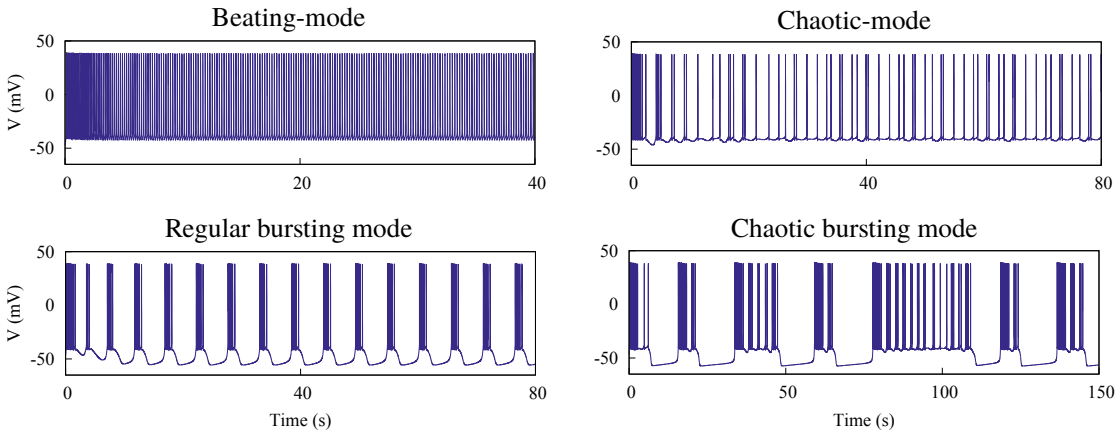

Figure 3.1: Activity examples of the Komendantov-Kononenko model. Each panel corresponds to one of the four regimes in which it can be tuned: beating-mode (tonic spiking activity), chaotic-mode (irregular spiking activity), regular bursting activity and chaotic bursting activity. Parameters used for each mode are included in appendix A.1, see also (Komendantov and Kononenko, 1996).

3.2.2 Simplified models

Izhikevich model

Due to the high number of variables involved in biophysical models and their nonlinear character, obtaining a theoretical solution is not possible, and computing them numerically

implies a high cost. These reasons had led to the development of a large number of simplified models, which despite losing some realistic features, allow faster computation and theoretical analysis.

One of these approaches is the Izhikevich model which is not based upon biophysical parameters and combines the computational efficiency of the integrate-and-fire neurons with the biological plausibility of Hodgkin-Huxley-type dynamics (Izhikevich, 2003). This simple model reproduces faithfully many of the neurocomputational dynamical features of several neuron types. It consists of a two-dimensional system of ordinary differential equations. One variable corresponds to a fast voltage variable v and the other to a slower recovery variable u, which describes the activation of the K+ current and the inactivation of the Na+ current.

$$\begin{aligned} \frac{dv(t)}{dt} &= 0.04v^2 + 5v + 140 - u + I; \\ \frac{du(t)}{dt} &= a(bv - u); \\ if\ v \geq 30mV, then &\begin{cases} v \leftarrow c \\ u \leftarrow u + d; \end{cases} \end{aligned} \tag{3.2.19}$$

where a represents the time scale of the recovery variable u, and parameter b describes how sensitive is u the subthreshold fluctuation of the membrane potential v. The sign of b determines whether u is an amplifying (b < 0) or a resonant (b > 0) variable. Parameter c describes the after-spike reset value of v. The parameters c and d take into account the action of high-threshold voltage-gated currents activated during the spike, and affect only the after-spike transient behavior.

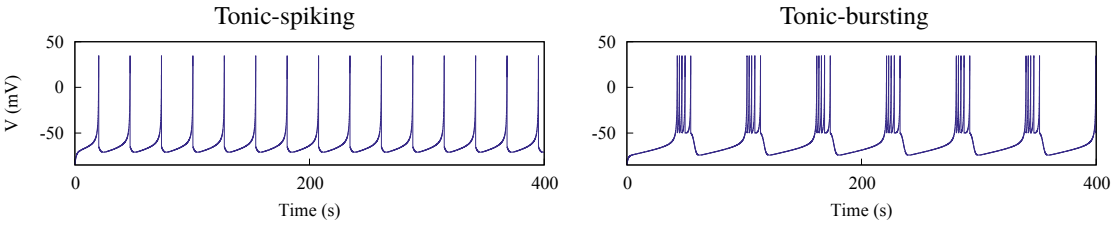

Figure 3.2: Activity examples of the Izhikevich model in two different modes: tonic spiking and tonic bursting. Parameters used in these simulations are included in appendix A.2.

3.3 Synapse models

Synapses can be classified depending on the mechanism that the cell uses for the transmission of the signal. Here, we briefly introduce the mathematical models for electrical and chemical synapses that will be used later in this work.

3.3.1 Gap junctions

In electrical synapses, the presynaptic and postsynaptic membranes are joined by gap junctions, which connect the cytoplasm of both neurons, allowing a direct flux of ions between them. Using the Ohm's law is a simple way of modeling electrical synapses, so that, the synaptic current received by the postsynaptic neuron from the presynaptic neuron would have the form:

$$I_{post}^{gj} = g_{prepost}^{gj}(V_{post} - V_{pre}), \tag{3.3.1}$$

where $g_{prepost}^{gj}$ is the maximal synaptic conductance, considered constant, and $V_{pre,post}$ is the membrane potential of the presynaptic and postsynaptic and neurons, respectively. Thus, the synaptic current I_{post}^{gj} is directly proportional to the difference of membrane potential between the two neurons. This expression takes into a count the passive diffusion of ions through the gap junctions, that is, the bidirectional nature of electric synapses. These interactions are responsible for several properties such as synchrony and pattern formation (Connors and Long, 2004; Latorre et al., 2013a). It is important to note than in a non-rectified electrical synapse model, the same current flows in both neurons with opposite sign, which causes the synchronization if the conductance is high enough. In a rectified electrical synapse, the current only flows in one direction.

3.3.2 Fast chemical graded synapses

As it was explained in the previous section, in chemical synapses there is no real physical contact among the presynaptic and postsynaptic neurons due to the larger separation between them. As a consequence, the transmission of the signal is mediated by specialized molecules called neurotransmitters that can be released and diffused in such space. The chemical synapses of the pyloric CPG are all graded, either fast or slow. The effect of the binding of the neurotransmitters to the neuroreceptors of the postsynaptic cell results in a postsynaptic current that in a fast graded synapse can be simulated as (Golowasch et al., 1999; Latorre et al., 2002, 2006):

$$I_{post}^{f} = \frac{g_{prepost}^{f}\,(V_{post} - E_{Syn})}{1.0 + exp(s^{f}(V^{f} - V_{pre}))}, \tag{3.3.2}$$

where $g_{prepost}^{f}$ is the maximal synaptic conductance of the postsynaptic neuron. V_{post} is the membrane potential of the postsynaptic neuron, E_{Syn} is the synaptic reversal potential, i.e. the voltage value at which the synaptic current cancels out. V^{f} determines the threshold of the graded synapse, and V_{pre} is the membrane potential of the presynaptic neuron.

3.3.3 Slow chemical graded synapses

The slow synaptic current can also be described by a similar approach (Golowasch et al., 1999; Latorre et al., 2002, 2006):

$$I^s_{post} = g^s_{prepost} m^s_{post} (V_{post} - E_{Syn}), \tag{3.3.3}$$

where

$$\frac{dm^s_{post}}{dt} = \frac{k_1(1.0 - m^s_{post})}{1.0 + exp(s^s(V^s - V_{pre}))} - k_2 m^s_{post}. \tag{3.3.4}$$

Here $g^s_{prepost}$ is the maximal synaptic conductance of the postsynaptic neuron, k_1 and k_2 are time constants, which control the speed and duration of the synaptic current, and V^s determines the threshold of the graded slow synapse. Note that in this case, there is a dynamical variable that has to be integrated with the rest of the neuron model equations.

3.4 CPG models

There have been several previous efforts to model CPGs and reproduce their rhythmic patterns and properties. In particular, the pyloric CPG has been widely modeled since the system is well known and all neurons and connections have been identified, e.g. see (Golowasch et al., 1999; Latorre et al., 2002; Prinz et al., 2004b; Greenberg and Manor, 2005; Nowotny et al., 2007; Selverston, 2010; Nadim et al., 2011; Soofi et al., 2012). At the level of topology, most computational models include only the so-called core of the CPG, built up of AB, PDs, LP and PYs neurons, since they produce the characteristic triphasic rhythm. Furthermore, as a simplification, PYs neurons are frequently represented as a single neuron as well as PDs neurons, and even PDs together with AB neuron. Depending on the aim of the study, the models used in these studies include different realistic features. Some of them focus on the shape of the bursts of each neuron and make use of multicompartimental models to reproduce some details (Golowasch et al., 1999; Greenberg and Manor, 2005). Other studies focus on the dynamics of neurons and the circuit seeking to reproduce temporal properties, e.g. the temporal distribution of the spikes within the burst, the so-called neural signatures of the neurons (Latorre et al., 2002; Szücs et al., 2003).

However, there are constraints in those models derived from the need for simplification and many features and physiological aspects of the living system (e.g. neuron and synapse heterogeneity or modulation) are typically omitted when designing theoretical paradigms. As a result, crucial properties present in the living system are missing in models. For instance, variability in the rhythm, which can be essential to reveal rhythmic properties (Elices et al., 2019), is not often addressed in models. Fortunately, there are techniques that allow to combine the best features of computational modeling and experimental electrophysiology by using *dynamic-clamp* (see chapter 4).

3.5 Integration methods

Most of the models described above contain ordinary differential equations. There are many integration methods to find numerical approximations to the solutions, which can be classified in two categories: *linear multistep methods*, and *Runge-Kutta methods*. Linear multistep methods start from an initial point and then take a short step forward in time to find the next solution point, repeating the process with subsequent steps to map out

the solution. In particular, these methods use a linear combination of the previous points and derivative values. On the other hand, Runge-Kutta methods take intermediate steps to obtain a higher order approximation before taking a second step. Integration methods can also be classified in explicit or implicit methods. Explicit methods calculate the state of the system at a later time *(t_{k+1}=t_k + Δt)*, while implicit methods find a solution by solving an equation involving both the current state $y(t_k)$ of the system and the later one $y(t_{k+1})$.

3.5.1 Linear multistep methods

Given the initial value problem:

$$y'(t) = f(t, y(t)), y(t_0) = y_0$$

A linear k-step method is defined as:

$$sum_{i=0}^{k} a_i y_{n+i} = h \sum_{i=0}^{k} b_i f(y_{n+i}), \tag{3.5.1}$$

where h is the time step (Δt) $a_k \neq 0$, $a_0 \neq 0$ and $b_0 \neq 0$. If $b_k = 0$ then the method is explicit, otherwise the method is implicit since $y(t_{n+k})$ depends on $f(t_{n+k}, y_{n+k})$. If k=1, then the method is known as the *Euler method* and is the most basic method for numerical integration of ordinary differential equations. However, Euler method is usually inefficient and requires very a small step to achieve enough accuracy.

3.5.2 Runge-Kutta methods

Runge-Kutta is one of the most used integration methods. This method includes intermediate steps based on the slope at the midpoint of each interval, and then uses the values of both t and y at the midpoint to make the real step across the interval. Runge-Kutta of k-order is defined as follows:

$$y_{n+1} = y_n + h \sum_{i=1}^{s} b_i k_i, \tag{3.5.2}$$

where

$$k_i = f(t_n + c_i h, y_n + h(\sum_{j=1}^{i-1} a_{ij} k_j)), \tag{3.5.3}$$

$$a_{ij}(for 1 \leq j < i \leq s),\ b_i(for i = 1, .., s)\ and\ c_i(for i = 2, .., s)$$

and

$$\sum_{j=1}^{i-1} a_{ij} = c_i.$$

The higher accuracy of this method allows to use higher values of time steps, which is useful for adjustments in time scale between living and model neurons (see 4). In this thesis, the simulations have been carried out using 6(5) Runge-Kutta (Hull et al., 1972), including the integration of the models in hybrid circuits, which require real-time performance for the interaction with living cells.

Chapter 4

Hybrid Circuits

In this chapter, we introduce the advantages of hybrid circuits implemented through dynamic-clamp techniques and present their advantages. We highlight their potential to study the origin and role of robust sequential activations. Dynamic-clamp techniques allow to interact with the living system using realistic closed-loop stimulations by implementing synapses between living neurons or *in vivo* synaptic inputs among others. In particular, these techniques allow to connect a living neuron with a model neuron or with a whole model circuit, building up a *hybrid circuit*. Finally, in this chapter, we discuss the technical requirements necessary to construct hybrid circuits.

4.1 Introduction

Interacting with neural networks beyond the conventional voltage- or current-clamp techniques by using *dynamic clamp* goes back almost three decades ago; see for a review (Chamorro et al., 2012). Dynamic-clamp techniques allow to alter the conductance of a neuron by injecting a controlled current taking into account its own membrane potential (Robinson and Kawai, 1993a; Sharp et al., 1993a,b; Cymbalyuk et al., 2002; Nowotny et al., 2003; Prinz et al., 2004a; Hooper et al., 2015; Sakurai and Katz, 2017). Dynamic-clamp techniques can be used to simulate voltage dependent and independent conductances, synapses between neurons, *in vivo* synaptic inputs and *hybrid circuits*. Hybrid circuits are networks built by connecting computer modeled neurons and synapses to living cells. The advantage of hybrid circuits is that they combine the best features of computer modeling and experimental electrophysiology to build highly realistic input or closed-loop interactions. For instance, the rich dynamics of living systems and the variability of the rhythm can be incorporated in a hybrid system built up with neuron models. In the same way, experimental studies can benefit from computational tools to explore intrinsic and connection parameters, and stimulation dynamics that would not be possible with traditional electrophysiology.

4.2 Dynamic-clamp and close-loop interactions

Typically, experiments in electrophysiology employ a constant/ramp or periodic stimulation and classical techniques such as voltage, patch or current clamp to interact with a

living neuron or circuit. These traditional experimental protocols are types of open-loop interactions, in which stimuli are predetermined beforehand and are independent of the system activity, see ***Figure 4.1*** panel A. However, there are mechanisms of neural information processing which cannot be fully addressed by means of these protocols.

Alternatively, complex stimulation protocols in which inputs depend on the ongoing activity of the neuron can be designed. This type of stimulation protocols is also known as closed-loop interactions (***Figure 4.1*** panel B). With this type of stimulation, it is possible to reveal history-dependent neural dynamics and provide insight into the origin of neural circuits properties. Closed-loop interactions have been generalized into a wide variety of activity dependent stimulations such as closed-loop drug-microinjection, closed-loop video-event driven stimulation, closed-loop mechanical stimulation, see (Chamorro et al., 2012), among others.

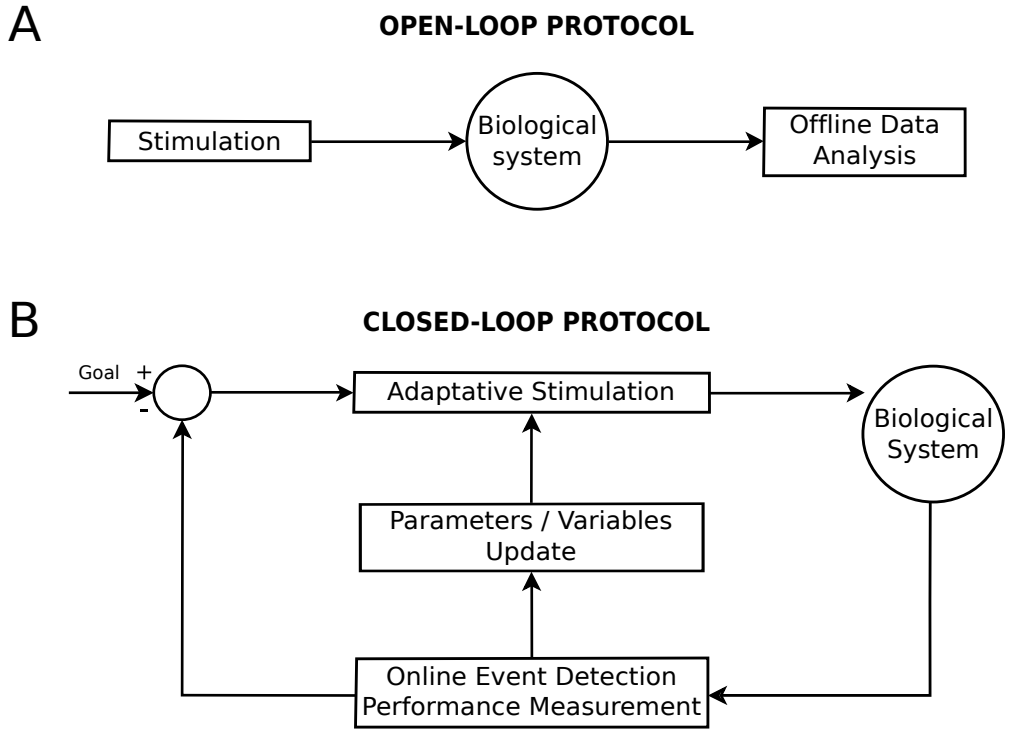

Figure 4.1: Schematic representation of open-loop and general closed-loop protocols of stimulation in neuroscience research. Panel A: In an open-loop protocol, the stimulus is designed and predetermined before any interaction takes place. The data recording during the experiment is typically analyzed offline. Panel B: in a closed-loop protocol, the stimulus is applied to achieve a certain goal, thus a performance measure is used to determine whether the system has reached the desired goal or not. In a general closed-loop implementation, the biological system is measured and events are detected online. Then, the parameters and variables are updated according to the performance and the stimulus is delivered to the system. Once the stimulus is applied, the biological system is measured again, as the interaction cycle continues.

The dynamic clamp technique allows to implement close-loop stimulations using the neuron membrane potential. Any time- or voltage- dependent conductance that can be described mathematically and therefore simulated in a computer can be used to interact with a neuron using dynamic clamp (Robinson and Kawai, 1993a; Sharp et al., 1993a,b; Prinz et al., 2004a). The resulting current injected to the neuron is calculated using the difference between the measured membrane potential and the reversal potential for a particular conductance, which is multiplied by the value of the computed conductance. For instance, this

method can be used to study the effects of leakage conductances on neuronal dynamics (Cymbalyuk et al., 2002; Prinz et al., 2004a), see ***Figure 4.2*** panel A. In general, it can be used to explore the impact of different intrinsic membrane conductances on neuronal activity. Dynamic clamp can also be used to create artificial synaptic currents between living neurons (see ***Figure 4.2*** panel B). In this case, the neuron on which the dynamical clamp is being implemented acts as the postsynaptic element, and another neuron acts as the presynaptic element (Nowotny et al., 2003; Hooper et al., 2015; Sakurai and Katz, 2017). Similarly, bidirectional connectivity such as a mutual chemical inhibition or a bidirectional electrical synapse can be implemented by recording the voltage of each cell and delivering the corresponding modeled current on each of them. Living neurons can also interact with neuron models or whole computational circuits implementing artificial synaptic currents, see ***Figure 4.2*** panel C. In this thesis, we have denominated these systems as *hybrid circuits*. Finally, another application of the dynamic clamp protocol is simulating realistic synaptic inputs in *in vivo* conditions, such as in slice preparations. In these circumstances, dynamic clamp allows to simulate a similar environment to which neurons normally operate.

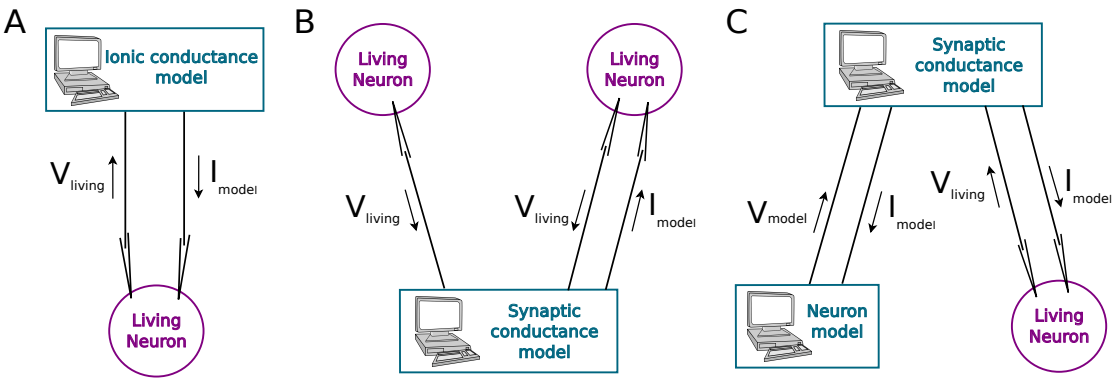

Figure 4.2: Schematic representation of different applications of the dynamic-clamp technique. Dynamic-clamp interactions allow to implement closed-loop interactions depending on the activity of the neuron. First, voltage is measured (event detection) and a current is delivered into the cell (stimulation) as a function of this voltage as calculated by a synaptic or membrane conductance model. This closed-loop cycle is continuously repeated to model the effect of the ionic or synaptic conductance. Panel A: scheme of the implementation of dynamic-clamp to create an ionic conductance model. Panel B: scheme of the implementation of dynamic-clamp to create artificial synaptic currents between living neurons. Panel C: scheme of the application of the dynamic-clamp technique to connect a living neuron with a model neuron, i.e., a *Hybrid Circuit*.

4.3 Hybrid circuits

Hybrid circuits are networks built up by connecting model neurons to living cells by means of computed synapses e.g. see (Yarom, 1991; Szucs et al., 2000; Pinto et al., 2000; Varona et al., 2001a; LeMasson et al., 2002; Nowotny et al., 2003; Oprisan et al., 2004; Arsiero et al., 2007; Grashow et al., 2010; Brochini et al., 2011; Wang et al., 2012; Thounaojam et al., 2014; Hooper et al., 2015; Norman et al., 2016; Broccard et al., 2017). Hybrid circuits allow us to manipulate parameters or features we wish to study with the same degree of precision and freedom that we have in a model, while maintaining their interaction with real neurons and neural circuits dynamics. Thus, hybrid circuits allow to combine the best features of computer modeling and experimental electrophysiology. Hybrid circuits make use of dynamic clamp protocols to implement the current to be injected in the neuron using its instantaneous membrane potential (Robinson and Kawai, 1993b; Sharp et al., 1993b; Prinz

et al., 2004a; Destexhe and Bal, 2009; Nowotny and Varona, 2012), see ***Figure 4.2*** panel C. Any neuron and/or synapse model that can be computed in real-time can be used to build the hybrid circuit. In this thesis, in particular in part IV, we have employed hybrid circuits to study sequential activations of the pyloric rhythm. For these experiments, the LP neuron was chosen to build the hybrid circuit since it does not have electrical connections to any other cell in the circuit and participate directly in the sequence (LP-PY-PD) of the triphasic rhythm (see section 2.5.2). ***Figure 4.3*** shows a scheme of the hybrid circuit built up with the pyloric circuit discussed in this work.

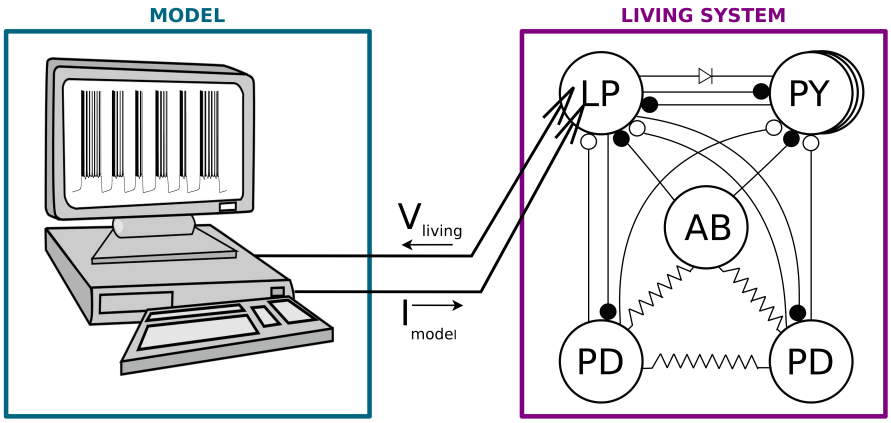

Figure 4.3: Scheme of the hybrid circuit established with the pyloric CPG. Hybrid circuits are networks built up by connecting model neurons to living cells by means of computed synapses. We have used hybrid circuits to study sequential activations of the pyloric rhythm. LP neuron was chosen to build the hybrid circuit. The neuron and synapse models described in chapter 3 are convenient candidates to implement hybrid circuits.

4.4 Real-time and automatic calibration algorithms

In spite of the large applicability of hybrid circuits, their use is usually limited by the difficulty in their implementation. Hybrid circuit construction often requires specific hardware and real-time software to implement accurately the stimulation cycles while recording intracellular activity (Christini et al., 1999; Pinto et al., 2001; Muñiz et al., 2005; Arsiero et al., 2007; Muñiz et al., 2009; Kemenes et al., 2011; Nowotny and Varona, 2012; Linaro et al., 2015; Patel et al., 2017). To achieve an accurate dynamic-clamp performance, an uninterrupted rapid sampling of the membrane potential and a fast computation of the current that has to be injected back into the neuron is required. Thus, frequently real-time software technology is required to manage the type of interactions needed in hybrid circuit experiments (Amaducci et al., 2019).

An additional problem in the construction of hybrid circuits is related to the handling of time and amplitude scale differences between living and model neurons and synapses. The amplitude and time scale adjustments also have to be addressed specifically for each preparation. Furthermore, experimentalists frequently have to deal with voltage drifts and the natural evolution of the membrane potential and changes in the electrode resistance during minutes or hours of experiments. This task is time-consuming and often a major drawback when building a hybrid circuit. There are algorithms that facilitate the building of hybrid circuits for different neuron and synapse models (Amaducci et al., 2019; Reyes-Sanchez et al., 2018). These algorithms calibrate and adapt automatically the time and

amplitude of voltage and current scales, which facilitates the construction of closed-loop interactions with living neurons in real-time.

Part II

Results: Robust dynamical invariants in sequential neural activity

Chapter 5

Characterization of variability of spiking-bursting activity in CPGs

While there is a vast list of efforts that address the generation and function of brain rhythms, the dynamical origin of the balance between robustness and flexibility in building sequential activations, which underlie many of such rhythms, has not been investigated in detail. A first step towards finding the dynamical principles that shape neuronal sequences is analyzing both regular and irregular rhythms instead of exclusively steady states as typically done in previous works. In particular, in this chapter we study and characterize regular and irregular pyloric CPG rhythms. Irregular regimes were obtained by two means: intrinsic irregularity in control experiments and irregularity induced by ethanol. Ethanol was very effective in revealing the rich sequential dynamics of the circuit and it did not disrupt the LP-PY-PD sequence (Elices et al., 2019).

5.1 Introduction

Typically, experimental and computational works on CPGs study their output rhythm only in a steady state with regular spiking-bursting activity, discarding irregular activity as well as transient changes. However, there are several experimental and modeling studies that have quantified the regularity of CPG rhythmic activity, particularly in the pyloric circuit of the stomatogastric ganglion of crustacean. Most studies have dealt with rhythm variability across preparations, e.g. see (Hooper, 1997a; Bucher et al., 2005; Rabbah and Nadim, 2005; Soofi et al., 2014). It is known that part of the variability observed in a preparation of the pyloric CPG is due to the interaction with the slower dynamics of the gastric CPG, which is bidirectionally connected to the pyloric network, e.g. see (Selverston and Moulins, 1987; Clemens et al., 1998; Bartos et al., 1999; Thuma and Hooper, 2003). Other works have addressed the role of specific connections, particularly inhibitory feedback to stabilize the overall CPG rhythm (Nadim et al., 2011; Hooper et al., 2015). Nevertheless, there have been few attempts to characterize transient dynamics and the ongoing balance between robustness and flexibility in preparations without external stimulation through long intracellular recordings.

Since, external and intrinsic inputs continuously arrive to the circuit inducing variability in the rhythm, the analysis of irregular regimes can unveil important properties of the balance between robustness and flexibility in building sequential activations and rhythm

coordination. Thus, to expose this process we have studied irregular rhythms in the pyloric CPG, i.e., activity that presented high variability in period, phase between neurons, or burst duration in the same experiment. In particular, we used two sources of rhythm irregularity: intrinsic variability in the preparation, and irregularity induced by ethanol. We have also studied the variability in the rhythm when the connectivity of the circuit is altered by removing the fast connections with Picrotoxine. Our departing hypothesis is that the analysis of non-periodic regimes together with the knowledge regarding the asymmetry in the connectivity can unveil properties of the underlying robust dynamics controlling rhythm coordination, which remain unnoticed in regular rhythm regimes.

5.2 Methods

5.2.1 Electrophysiology

Adult male and female shore crabs (*Carcinus maenas*) were purchased locally and maintained in a tank with 13-15 ºC artificial seawater. Crabs were anesthetized by ice for 15 min before the dissection. The procedures followed the European Commission and Universidad Autónoma de Madrid animal treatment guidelines. The stomatogastric nervous system was dissected following standard procedures and pinned in a Sylgard-coated dish containing *Carcinus maenas* saline (in mM: 433 $NaCl$, 12 KCl, 12 $CaCl_2 \cdot 2H_2O$, 20 $MgCl_2 \cdot 6H_2O$, 10 $HEPES$, adjusted to pH 7.60 with 4 M $NaOH$). After desheathing the STG, neurons were identified by their membrane potential waveforms and the spikes times in the corresponding motor nerves. Membrane potential from neurons was recorded using 3 M KCl filled microelectrodes (50 $M\Omega$) and a DC amplifier (ELC-03M, NPI Electronic, Hauptstrasse, Tamm, Germany). Extracellular recordings were made using stainless steel electrodes in Vaseline wells on the motor nerve and amplified with an AC amplifier neuroprobe (model 1700, A-M Systems, Bellevue, WA, USA).

5.2.2 Data extraction

Data were acquired at 10 KHz using an A/D board (PCI-MIO-16E-4, National Instruments). Spike timings were obtained from intracellular recordings using Dataview (https://www.st-andrews.ac.uk/~wjh/dataview/), first applying a FIR filter and then a threshold-crossing criterion to detect the beginning of each spike. Since we used a high threshold and worked with intervals, calculated by subtracting consecutive time references, the error introduced by using the beginning of the spike is mostly canceled out. In each recording, the distribution of the spikes was used to select the time windows that defined the intra and inter burst intervals, and particularly the first and last spike of each burst (see Matlab scripts in appendix C). The accuracy of the scripts was carefully verified for each experiment. Preparations were exposed to concentrations of (170 mM) Ethanol (Panreac), added directly to the bath. Glutamatergic synaptic inputs were blocked using 10^{-7} M picrotoxin (PTX; Sigma-Aldrich). Only preparations that completed all categories of treatment were included for this analysis.

Time references and interval measures

To analyze and quantify regular and irregular recordings, we considered several interval measures based on precise time references at the beginning and at the end of the bursts (see ***Figure 5.3*** middle panel): PD and LP burst duration $BD_{PD,LP}$: intervals from the first spike to the last spike of PD and LP neuron, respectively; $LPPD\ delay$: interval from the last LP spike to the first PD spike; $LPPD\ interval$: interval defined from the LP first spike to the PD first spike; $PDLP\ delay$: interval from the last PD spike to the first LP spike in the following burst; $PDLP\ interval$: interval from the first PD spike to the first LP spike in the following burst; $Period$: interval from first LP spike to the next first spike in the following LP burst. We quantified these measures in long intracellular recordings (15 min on average). There were some extreme cases in irregular rhythms induced by ethanol where time references were not well defined and the corresponding activity had to be removed from the statistics shown below. The number of bursts that had to be dismissed in these experiments ranged from 1 to 17% and 0 to 27% of the total number of bursts of LP and PD neurons, respectively, in the recordings.

The coefficient of variation defined as $C_v = \sigma/\mu \cdot 100\,(\%)$, depicted in the boxplots for the results shown in this chapter, was calculated as an average of the C_{v_i} of each experiment in an ensemble N specified in each plot.

$$C_v = \langle C_{v_i} \rangle = \langle \frac{\sigma_i}{\mu_i} \rangle \cdot 100,\ \ for\ i \in \{1, 2, ..., N\} \tag{5.2.1}$$

The significance level α used for the null hypothesis significance test for correlations of data was adjusted according to the Bonferroni correction, which modifies the desired overall alpha level α_0 compensating for the number of hypotheses to be tested m as the following:

$$\alpha = \frac{\alpha_0}{m} \tag{5.2.2}$$

In this case, the number of hypotheses is the correlations between different combinations of the defined time intervals ($m = 12$). Thus, setting $\alpha_0 = 0.01$, the final significance level applied was $\alpha = 8 \cdot 10^{-4}$.

A t-test was also performed to test the significance of the correlation coefficients among experiments for each hypothesis m.

Standardized cycle intervals z in ***Figure 6.8*** were calculated as follows:

$$z_j = \frac{x_j - \mu}{\sigma}, for\ each\ j\ cycle, \tag{5.2.3}$$

where x is the interval value.

5.3 Results

Irregular activity can be seen in cases of intrinsic variability in the pyloric CPG preparation, which may be a result of the external neural modulation, slightly damaged neurons

or severed modulator nerves, etc. Panel A in ***Figure 5.1*** shows an example of extracellular (LVn) and intracellular recordings from PD and LP neurons in a stomatogastric ganglion with intrinsic variability. There are clear differences from the regular activity recordings shown in ***Figure 2.8***: hyperpolarizations of both neurons are irregular and, while PD bursts remain more constant, LP presents longer plateaus and higher variability in burst duration. Irregularity can also be induced chemically, e.g. evoked by application of ethanol (***Figure 5.1***, panel B) which is known to affect neural dynamics (see an example on rhythmic motor patterns in Maze et al. (2006)). Pyloric rhythm under ethanol is characterized by a remarkably flexible and long PD burst duration and, variability in hyperpolarization in both neurons. At the same time, LP burst duration presents much less variability as compared to the PD neuron. Despite the large irregularity induced by ethanol, the sequence LP-PY-PD in the rhythm is still preserved. After washing or ethanol evaporation, regular activity is recovered.

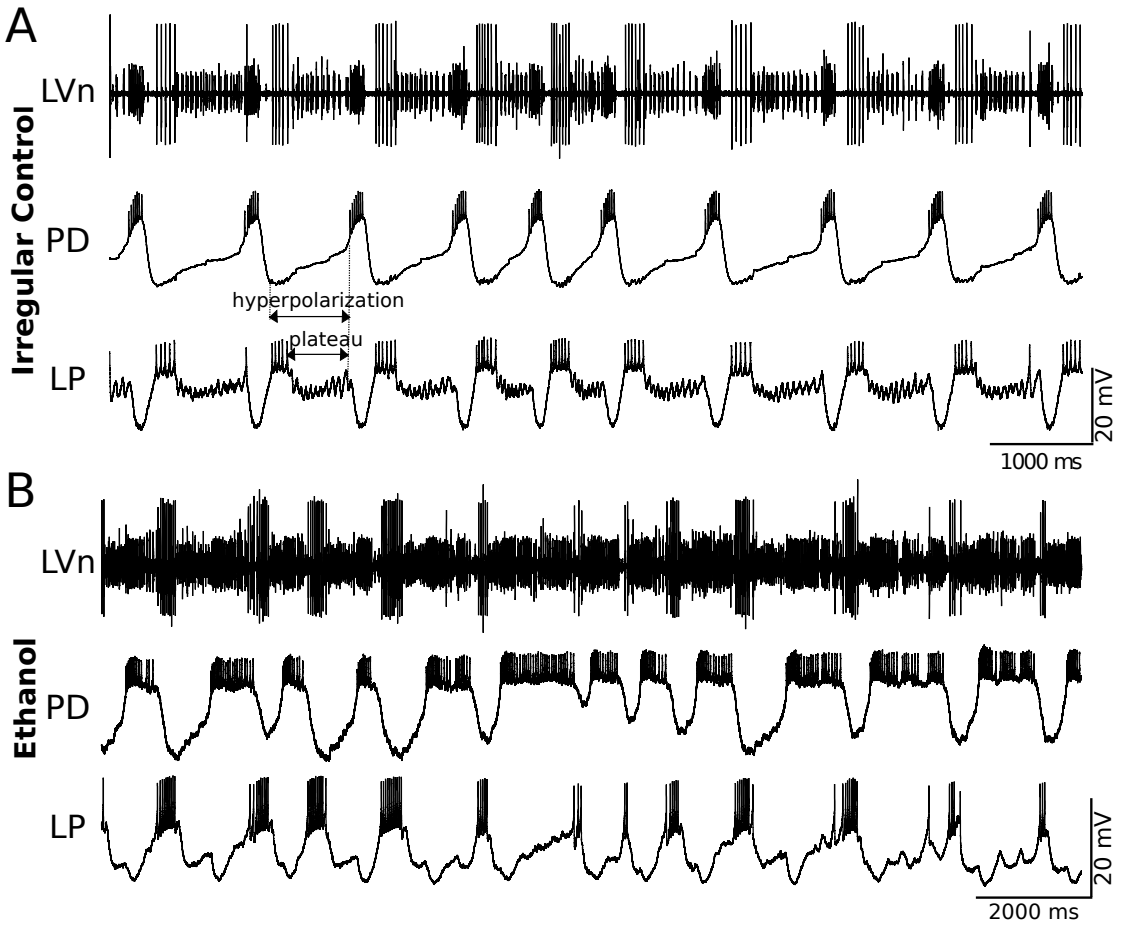

Figure 5.1: Examples of irregular sequential activity produced by the pyloric CPG. The traces correspond to simultaneous extracellular recordings of the LVn nerve (upper trace) and intracellular recordings of PD and LP neurons in the intact CPG. Panel A: Example of transient irregular spiking-bursting activity in control conditions. Note the irregular hyperpolarizations and variability in LP plateaus as compared to the regular trace shown in regular control conditions. Panel B: Example of irregular spiking-bursting activity with addition of ethanol (170 mM). Note that PD neuron presents flexible and long burst durations while LP neuron has more restricted burst durations. In all cases, the sequence of neuron activations LP-PY-PD is preserved, in spite of the intrinsic or induced irregularity.

The analysis of variability of CPG rhythms in all conditions was assessed by defining specific intervals with precise time references using the first and last spike of bursts from intracellular recordings. We chose seven intervals (defined in ***Figure 5.2***): $Period$, $LPPD\ delay$

(corresponding to PY neuron activity), $LPPD\ interval$, PD burst duration BD_{PD}, LP burst duration BD_{LP}, $PDLP\ delay$ and $PDLP\ interval$, and studied variability in long recordings using their coefficient of variation ($C_v = \sigma/\mu \cdot 100(\%)$).

Note that some of these intervals are different from those used in other pyloric CPG studies that consider as time reference the beginning of the PD burst. In most studies, the PD neuron burst beginning is used as the time reference for cycle period and delays of the other so-called follower neurons Hooper (1997a, 1998); Bucher et al. (2005). A considerable variability across individual preparations was previously observed in phase-frequency relationships when the pacemaker group is used as the time reference Bucher et al. (2005); Rabbah and Nadim (2005). Since PD neurons have strong inertia from electrical coupling among all cells in the pacemaker group, the selected time reference frame is more suitable to address the balance between flexibility and robustness, see also Hooper (1997b).

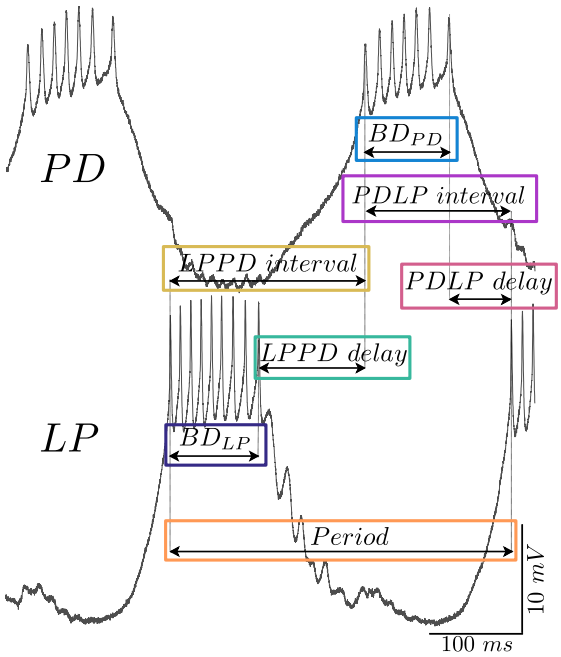

Figure 5.2: Scheme of the definition of the measured time intervals considered in this study to characterize the CPG cycle-by-cycle rhythm. BD_{PD} and BD_{LP}: burst duration defined as the time interval from the first spike to the last spike of PD and LP neurons, respectively; $LPPD\ delay$: interval defined from the LP last spike to the PD first spike; $LPPD\ interval$: interval defined from the LP first spike to the PD first spike; $PDLP\ delay$: interval defined from the PD last spike to the next first LP of the following burst; $PDLP\ interval$: interval defined from the PD first spike to the next first LP of the following burst; $Period$: interval from the LP first spike to the next LP first spike in the following burst.

Figure 5.3 compares the average of the coefficient of variation of the considered intervals, described in the central panel, for preparations with departing regular (left panel) and irregular (right panel) activity in control conditions and under ethanol by means of boxplots. Boxes in darker color correspond to control conditions. In regular control preparations, the values of the C_v of the six intervals went from 4% to 15%, the highest corresponding to $PDLP\ delay$ and BD_{LP}. One can observe that in control conditions variability was small but still left room for flexibility. In the case of intrinsic irregular activity, variability increased in all intervals except for BD_{PD}. Under the influence of ethanol (lighter hue boxes), both regular and irregular preparations increased the variability in all intervals. In particular, BD_{PD} ($88\% - 130\%$), $LPPD\ delay$ ($80\% - 79\%$) and $PDLP\ interval$ ($67\% - 84\%$) presented a larger variability while BD_{LP} was lower ($40\% - 36\%$). Note that $BD_{LP,PD}$ and $LPPD\ delay$

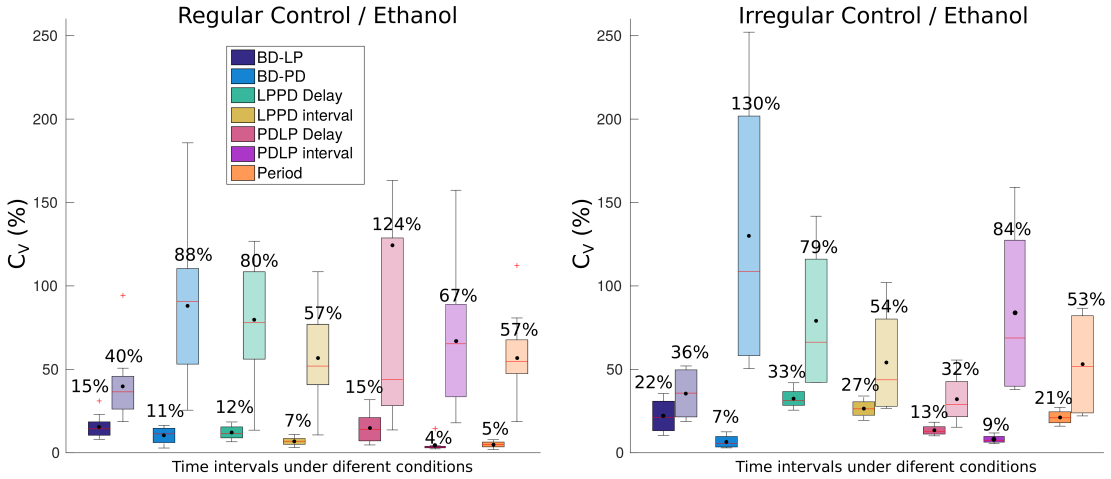

Figure 5.3: Definition and variability analysis of temporal intervals considered in this study to characterize the CPG cycle-by-cycle rhythm. Left and right panels: Boxplots of the coefficient of variation for the six measures in control conditions (darker color) and under the influence of ethanol (lighter hue boxes). Mean values (black dots) are displayed on top of each box. Left panel: Quantification of the variability in long recordings for preparations that were regular in control conditions (N=12). The coefficients of variation are small ($4-15\%$) in control conditions. Under the influence of ethanol, in lighter colored boxes, there is a large increase in variability for BD_{PD} (88%), $LPPD\ delay$ (80%) and $PDLP\ delay$ (124%) while BD_{LP} is more restricted in variability (40%). Right panel: Intrinsically irregular preparations (N=4). One can observe an increase in variability of $LPPD\ delay$ and $LPPD\ interval$ due to the irregular hyperpolarization intervals in control conditions (see ***Figure 5.1***). After applying ethanol, there is even larger variability in BD_{PD} (130%), $PDLP\ interval$ ($67\%-84\%$) and $LPPD\ delay$ (79%) while BD_{LP} variability remains more restricted (36%).

together with $PDLP\ delay$ build the triphasic rhythm. The interquartile range of the boxes indicates the variability among preparations and, in the case of ethanol, it highlights the differences of its effect on the rhythm. Overall, the system showed a wide range of variability specific to the distinct intervals that shape the rhythm with large variability in some, such as BD_{PD}, and smaller variability in others (e.g., BD_{LP}). ***Table 5.1*** shows values of the individual coefficient of variation CV(%) of the considered intervals for 9 representative experiments in control and ethanol conditions.

Table 5.1: Values of the coefficient of variation CV(%) of the considered intervals for 9 representative experiments in control and ethanol conditions (same preparations as in ***Figure 6.3*** and ***Figure 6.4***). Other experiments show similar results.

Control CV(%)	$Exp1$	$Exp2$	$Exp3$	$Exp4$	$Exp5$	$Exp6$	$Exp7$	$Exp8$	$Exp9$	$< Exp >$
BD_{LP}	22	35	10	26	16	23	15	11	14	19
BD_{PD}	3	13	4	3	7	9	6	15	16	8
$LPPD\ delay$	12	31	26	42	31	15	9	16	17	22
$LPPD\ inter.$	8	26	19	34	27	10	7	4	9	16
$PDLP\ delay$	5	12	13	10	18	11	5	21	18	13
$PDLP\ inter.$	3	8	7	5	12	4	3	4	4	5
$Period$	5	20	16	27	22	7	5	3	7	12

Ethanol CV(%)	$Exp1$	$Exp2$	$Exp3$	$Exp4$	$Exp5$	$Exp6$	$Exp7$	$Exp8$	$Exp9$	$< Exp >$
BD_{LP}	36	24	19	47	52	94	37	44	23	42
BD_{PD}	29	66	50	152	252	99	82	45	26	89
$LPPD\ delay$	127	42	42	142	90	110	100	121	38	90
$LPPD\ inter.$	108	29	27	102	58	76	81	78	26	65
$PDLP\ delay$	26	30	56	28	15	163	30	49	89	54
$PDLP\ inter.$	18	42	38	96	160	53	64	32	21	58
$Period$	81	26	22	78	87	52	61	54	21	53

To characterize further the variability of the sequence intervals we have studied their duration distribution. ***Figure 5.4*** and ***Figure 5.5*** show histograms of the interval durations of a representative example in control and ethanol conditions, respectively. In control conditions, the duration of the intervals ranged from 30-500 ms. Note that BD_{PD} histogram is bimodal since the number of spikes in the burst was oscillating, which also affects to $PDLP\ delay$. Under the influence of ethanol, the duration of the intervals ranged from 50-1200 ms. Note the change in the scale of the duration for the different intervals, especially in case of BD_{PD}, which reached almost 1000 ms. This particular histogram presents a long-tailed shape, which means that large durations are not the most frequent. However, it is important to observe that the peak of the histogram corresponds to 200 ms which is twice the value of the control experiment.

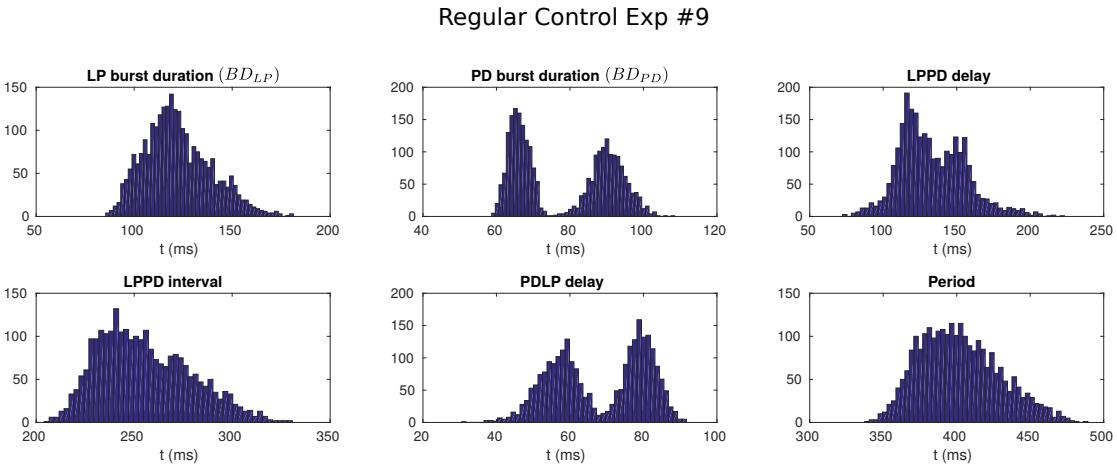

Figure 5.4: Histograms of the interval duration distributions of a representative example in control conditions (Experiment 9 in ***Table 5.1***). In particular, this example was classified in the group of regular control preparations in ***Figure 5.3***. Note that all intervals present relatively low variability. BD_{PD} histogram is bimodal due to an oscillation in the number of spikes in the burst, which also affects to $PDLP\ delay$.

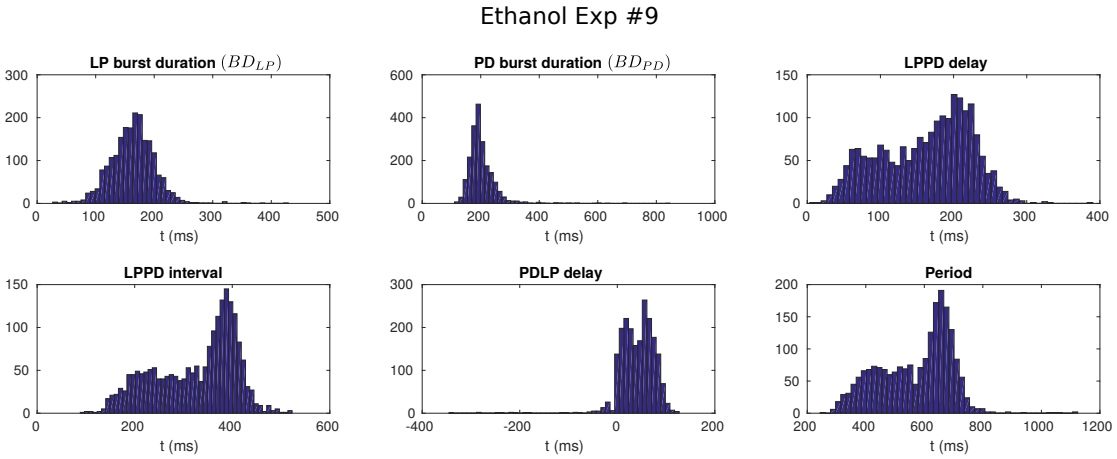

Figure 5.5: Histograms of the interval duration distributions of a representative example in ethanol conditions (Experiment 9 in ***Table 5.1*** and the same preparation as in ***Figure 5.4***). Note the change in the scale of the duration for the different intervals, especially in the case of BD_{PD}, which reaches almost 1000 ms. Negative values in $PDLP\ delay$ correspond to cycles in which the end of the PD burst partially overlaps the beginning of the LP burst.

One notable property of the pyloric CPG network is its asymmetric inhibitory connectivity. This connectivity could play a key role in explaining the compensation process that creates the rhythm. Thus, we studied variability after applying picrotoxin (PTX) $5 \cdot 10^{-7}\ M$, a glutamatergic synapse blocker, which blocked the fast inhibitory synapses (see left panel in ***Figure 5.6***). Right panel shows an example of PD and LP activity after applying PTX. One can observe the irregular shape of the LP bursting activity, allowed by the low PTX concentration, the absence of LP IPSPs in the PD trace and the removal of the LP plateau. A comparison of the coefficient of variation in three conditions, control, PTX and PTX+EtOH, is shown in ***Figure 5.7***. In control conditions, the variability was small for all measures $(5\% - 15\%)$. After applying PTX there was a slight increase in C_v for all measures except for $LPPD\ delay$ that reached 163%. Adding ethanol increased the variability even further $(43\% - 201\%)$ with

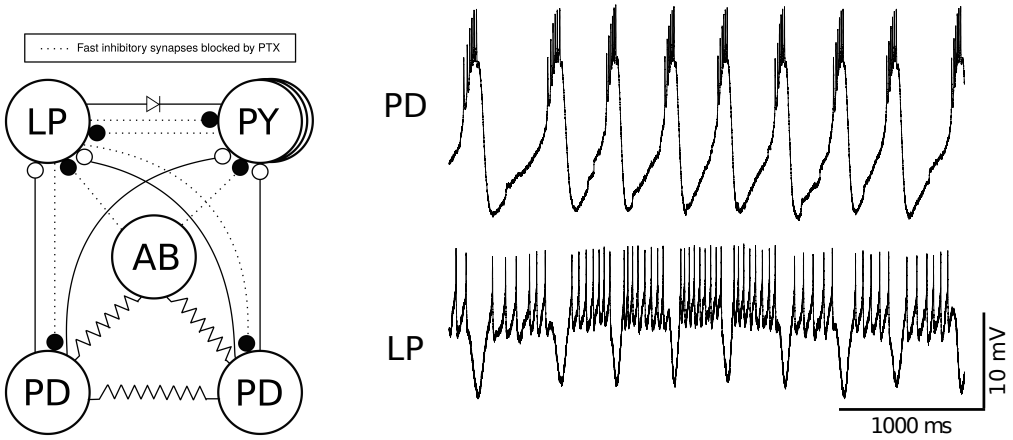

Figure 5.6: Results of blocking fast inhibitory synapses with *PTX*. Left panel: Scheme of the connectivity of the pyloric CPG after applying picrotoxin (PTX) $5 \cdot 10^{-7}$ M. Dotted lines correspond to blocked fast inhibitory synapses. Right panel: Example of the spiking-bursting activity of the circuit after applying PTX. The traces correspond to simultaneous intracellular recordings of PD (upper trace) and LP (lower trace) neurons. Note that the characteristic IPSPs typically seen in the PD neuron trace are no longer present.

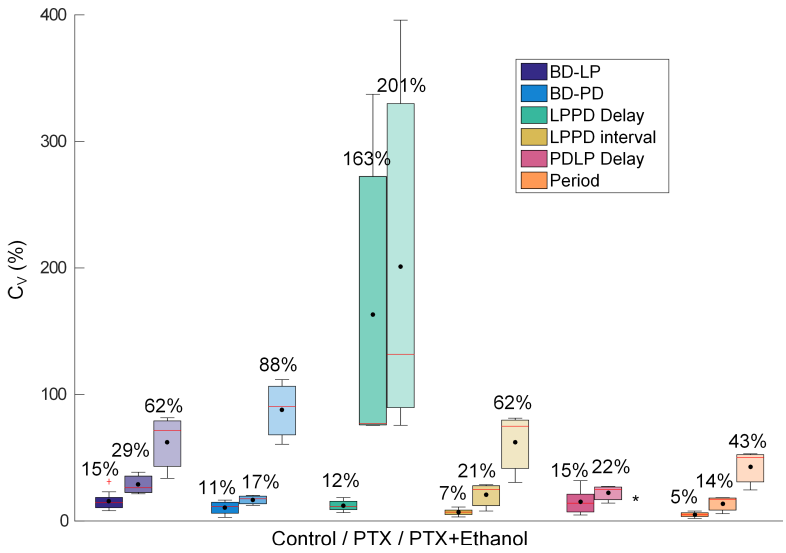

Figure 5.7: Coefficient of variation (C_v) for the seven measures in three conditions: control, first column for each measure (darkest color); after applying PTX $5 \cdot 10^{-7}$ M (N=3), middle column; after adding ethanol to the PTX dilution (N=3), third column (lightest hue boxes). The highest variability in control conditions corresponds to BD_{LP} and $PDLP\ delay$ (15%), while after applying PTX the highest C_v corresponds to $LPPD\ delay$ with 163%, which is almost 14 times higher than in control. Variability in the other 5 measures also increases with PTX although more slightly. Adding ethanol to the PTX solution increases variability even further $(43\% - 201\%)$.

values similar to those obtained in experiments after applying ethanol alone (c.f. ***Figure 5.3***) except for BD_{LP} and $LPPD\ delay$, which showed larger variability after removing the connections from the PYs and AB with PTX.

5.4 Discussion

Most experimental and computational studies on CPGs focus their analysis on regular regimes, frequently discarding non-regular transient activity Selverston et al. (2000); Soofi et al. (2014). However, the analysis of irregular CPG rhythms, rich in transient dynamics and not only in steady state activity, can unveil important properties of the robust neuron and network dynamics underlying sequence programming and coordination. Irregular rhythms were obtained in this study by two means: intrinsic irregularity, and biophysical disruption with ethanol. Moderate ethanol application did not disrupt the anti-phase relationship between LP and PD neurons, thus the robustness of the sequence was kept, but evoked variable burst duration and hyperpolarization intervals. The effect of ethanol was reversible and in most cases, the neurons returned to their original rhythm after ethanol was washed out or evaporated.

As opposed to traditional regular activity recordings, irregular rhythms caused by intrinsic factors in the preparation presented high variability in hyperpolarization intervals and waveforms in both LP and PD neurons. LP presented larger plateaus and higher variability in burst duration while PD activity remained less variable. Irregularity induced by ethanol, however, presented remarkably flexible and long PD burst duration, while LP burst duration was more restricted. Ethanol also induced variability in the hyperpolarization intervals in both neurons. Despite the variability displayed in all intervals, both in control conditions and ethanol, as shown by the analyses of the coefficients of variation (***Figure 5.3*** and ***Table 5.1***) and the histograms (***Figure 5.4*** and ***Figure 5.5***), the sequence LP-PY-PD in the rhythm is preserved. For further analysis, PTX was used along with ethanol to study how removing fast synapses in the circuit affected variability.

Chapter 6

Dynamical invariants

In chapter 5, we studied and characterized regular and irregular sequential rhythms of the pyloric CPG. In particular, we analyzed the intervals involved in the CPG rhythm with intrinsic irregularity and irregularity induced by ethanol. Ethanol resulted very effective in evoking highly irregular rhythms but it did not disrupt the LP-PY-PD sequence. In this chapter, we study the dynamical principles shaping the CPG rhythm that could underlay the optimal functioning of the motor system. Here, we present a cycle-by-cycle analysis that unveils dynamical invariants in the sequential activations that build the CPG rhythm in long intrinsic regular or irregular rhythm recordings and also in recordings under the effect of ethanol, which allowed to demonstrate the adjustments between key intervals that build the sequence. PTX was used along with ethanol to study the effect of removing fast synapses in the circuit (see ***Figure 5.6***) on the invariants. We observed that the specific asymmetric connectivity of the pyloric network plays a key role in shaping the invariants. The analysis shows that there are dynamical principles that conform a set of rules to shape the time intervals that build the sequence in each cycle in regular and irregular rhythms.

6.1 Introduction

Several studies have suggested the maintenance of CPG phase-frequency relationship when altering the rhythm speed by applying different stimulation protocols in the pyloric pacemaker neurons (AB-PDs), e.g. see (Hooper, 1997a,b; Weaver and Hooper, 2003a; Hooper et al., 2009) or by temperature changes (Soofi et al., 2014). Phase maintenance is typically addressed by quantifying average delays and periods and comparing across preparations, in most cases discarding irregular activity transients (Hooper, 1997a,b; Soofi et al., 2014). However, considerable variability across individual preparations has been observed in phase-frequency relationships when the pacemaker group is used as the time reference (Bucher et al., 2005; Rabbah and Nadim, 2005). In most studies, the PD neuron burst beginning is used as the time reference for cycle period and delays of the other so-called follower neurons (Hooper, 1997a, 1998; Bucher et al., 2005). Since connectivity is asymmetric and non-open (Huerta et al., 2001) and neurons are heterogeneous, using an adequate time reference frame in the analysis of neuronal sequential activations with asymmetric connectivity can be crucial to understand the dynamical principles that shape neuronal sequences.

In spite of the large variability seen in the experiments, in this chapter we report two

robust *dynamical invariants* in the form of linear correlations between pivotal time intervals that build the sequence. These invariants were strongly preserved under different conditions and were found using a time reference frame that took into account the asymmetric topology of the system. Because our previous characterization of the rhythms shows that the intervals that build the sequence display distinct variability, it is not trivial that any of them is correlated with the period. We characterized these invariants and related them to the underlying balance of influences between the rich intrinsic dynamics of neurons and the asymmetric connectivity of the circuit. We hypothesize that dynamical invariants participate in the instantaneous coordination of the different muscles innervated by the CPG neurons, and therefore can be linked to the efficient cycle-by-cycle performance of motor activity of the system in different circumstances.

Considering regular bursting activity and a dynamic-clamp protocol that altered a CPG synapse, previous work reported a dynamical invariant in which the ratio between the resulting change in average burst duration and the change in average phase lag between PD and LP neurons was tightly preserved in all preparations (Reyes et al., 2008). Here we follow this terminology, but we refer to robustly preserved instantaneous interval relationships within the variability of a preparation, as opposed to cross-preparation averaged phase maintenance. We believe this term reflects better the transient information exchange in the circuit.

The novelty of our approach resides in the analysis of long recordings in which the variability of the activity is kept intact, i.e., we did not extract steady state regimes with nearly periodic activity from the recordings and/or average intervals among preparations as in previous studies. Rather, we address the changes in a cycle-by-cycle ongoing CPG rhythm and argue that all neurons participate in the production and tuning of the system, so that each contributes to the instantaneous negotiation of the resultant pattern. We characterized cycle-by-cycle variability in long intrinsic regular or irregular rhythm recordings and also in recordings under the effect of ethanol to search for intervals that sustained a robust relationship with the period and, thus, defined a dynamical invariant (Elices et al., 2019). Information regarding variability cannot be ignored when characterizing the instantaneous generation and coordination of neural sequences. This information is lost under traditional average analyses (Hooper, 1997a,b; Soofi et al., 2014).

In this chapter, we show that the flexibility from rich intrinsic neuron dynamics is actively bounded by the connectivity in a cycle-by-cycle negotiation that produces coordinated sequential activity, even during transients. Here, we report the transient adaptation of the sequence timings in which the linear relationship with the period is kept at all costs.

6.2 Results

6.2.1 Sequences in control and under ethanol conditions

In order to identify factors shaping the CPG transient rhythm negotiation, i.e., the process of balancing flexibility and robustness of timings and sequence, we analyzed the cycle-by-cycle intervals defined in section 5.3 in regular and irregular rhythms. The underlying question is whether there is any property or temporal relationship in the ongoing rhythm, in addition to the sequence of neuron activations, which is preserved under different conditions (regular rhythms, intrinsic irregularity or ethanol), i.e., a *dynamical invariant*.

Departing from well-defined time references at the burst beginning and end in the LP and PD neurons, we analyzed $Period$, $LPPD\ delay$, $LPPD\ interval$, $PDLP\ delay$, $PDLP\ interval$ and burst durations $BD_{PD,LP}$ (see ***Figure 5.2***), and searched for preserved correlations between pairs of intervals, even when the rhythm was very irregular. We performed this analysis cycle-by-cycle in long continuous intracellular recordings in both control and experiments under ethanol. The results of these analyses are summarized in ***Table 6.1*** and ***Table 6.2***. It is important to note that most relationships between intervals were not preserved, such as $BD_{PD,LP}$ and $PDLP\ delay$ as a function of the $Period$, BD_{LP} or $LPPD\ interval$ as a function of BD_{PD} or $BD_{PD,LP}$ as a function of the $LPPD\ delay$ (see ***Table 6.1*** and ***Table 6.2*** columns 1-9).

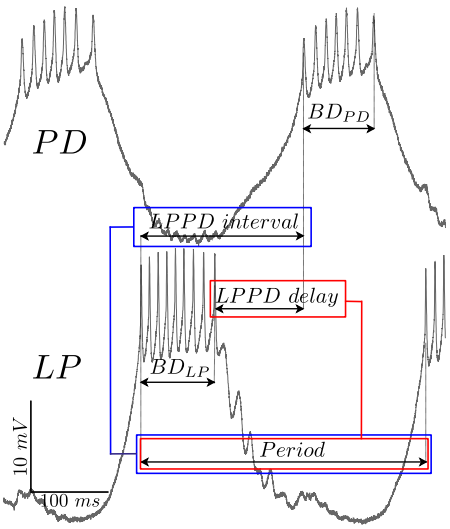

Figure 6.1: Intervals that build dynamical invariants.

However, we found two relationships that presented strong linear correlations in both control and under ethanol conditions: the measured $LPPD\ delay$ and $Period$, and $LPPD\ interval$ and $Period$ (see ***Figure 6.1***, ***Figure 6.2***, ***Table 6.1*** and ***Table 6.2***). $PDLP\ interval$ presented correlation with the $Period$, however it was weaker and not consistent among preparations. Additionally, under ethanol conditions, a couple of experiments also showed correlation between PD burst duration and $Period$ (see ***Table 6.2***) but it was not consistent through the rest of the experiments, as it was with both invariants. In these cases, the higher correlation with the $Period$ can be explained in terms of the very long PD bursts duration. What is unique in the intervals participating in the invariants is that the correlation exists for any interval duration category and is present in every preparation, thus we defined them as dynamical invariants. These dynamical invariants consistently remained tightly preserved with the slope of the linear regression close to one for different preparations and under different conditions.

Approximate phase maintenance observed in previous studies was revealed by averaging intervals across preparations (see Introduction). Following the same procedure by calculating interval averages for each preparation, correlation is found between all intervals and the averaged period and even among them in control and in most cases in ethanol conditions (see ***Table 6.1*** and ***Table 6.2*** last column). In our cycle-by-cycle analysis, strong correlation is only found between $LPPD\ interval[Period]$ and $LPPD\ delay[Period]$.

Table 6.1: Values of the Pearson correlation coefficient ρ obtained for the different combinations of instantaneous intervals considered in this study for 9 representative experiments in control conditions (same preparations as in ***Table 6.2***, ***Figure 6.3*** and ***Figure 6.4***). Other experiments show similar results. Regression analysis indicated that both $LPPD\ interval$ and $delay$ (framed in the table) have a strong correlation with $Period$ consistently in all the experiments. $PDLP\ interval$ present correlation with $Period$ but is not consistent among preparations, and other measured variables are not correlated. A t-test for significance of the correlation coefficients (N=16) is also included in the table. Last column represents the Pearson correlation coefficient among interval averages calculated for the 16 preparations. * Slope significantly different from 0 ($p < 8 \cdot 10^{-4}$).

Control	ρ_{Exp1}	ρ_{Exp2}	ρ_{Exp3}	ρ_{Exp4}	ρ_{Exp5}	ρ_{Exp6}	ρ_{Exp7}	ρ_{Exp8}	ρ_{Exp9}	t-test	$\rho_{<Exp>}$
$LPPD\ inter.[Period]$	0.976*	0.997*	0.997*	0.999*	0.997*	0.970*	0.981*	0.952*	0.988*	1	1.000*
$LPPD\ delay[Period]$	0.876*	0.939*	0.991*	0.988*	0.992*	0.715*	0.854*	0.392*	0.750*	1	0.999*
$BD_{PD}[Period]$	0.376*	0.587*	0.341*	0.029	-0.132	0.185*	0.108*	0.442*	0.202*	0	0.931*
$BD_{LP}[Period]$	-0.170*	0.352*	0.070	0.055	0.512*	0.352*	0.147*	0.135*	0.374*	0	0.924*
$BD_{PD}[BD_{LP}]$	-0.160*	0.293*	-0.090	0.279*	0.201	0.028	0.105	0.098*	0.153*	0	0.876*
$BD_{PD}[LPPD\ inter.]$	0.342*	0.562*	0.314*	0.016	-0.154	0.147*	0.067	0.366*	0.172*	0	0.930*
$BD_{PD}[LPPD\ delay]$	0.354*	0.496*	0.326*	-0.024	-0.185	0.129*	0.012	0.107*	0.065	0	0.927*
$BD_{LP}[LPPD\ delay]$	-0.592*	0.018	-0.039	-0.092	0.424*	-0.366*	-0.357*	-0.844*	-0.315*	0	0.905*
$PDLP\ delay[Period]$	0.509*	0.355*	0.769*	0.173*	-0.417*	0.161*	0.315*	-0.110*	0.098*	0	0.929*
$PDLP\ delay[BD_{LP}]$	-0.105*	0.072*	-0.084	-0.006	-0.254	-0.185*	-0.030	-0.131*	-0.130*	0	0.764*
$PDLP\ inter.[Period]$	0.632*	0.771*	0.787*	0.172*	-0.426*	0.375*	0.511*	0.809*	0.722*	1	0.977*
$PDLP\ inter.[BD_{LP}]$	-0.163*	0.304*	-0.100*	0.068	-0.194	-0.203*	0.071	-0.043	0.064	0	0.843*

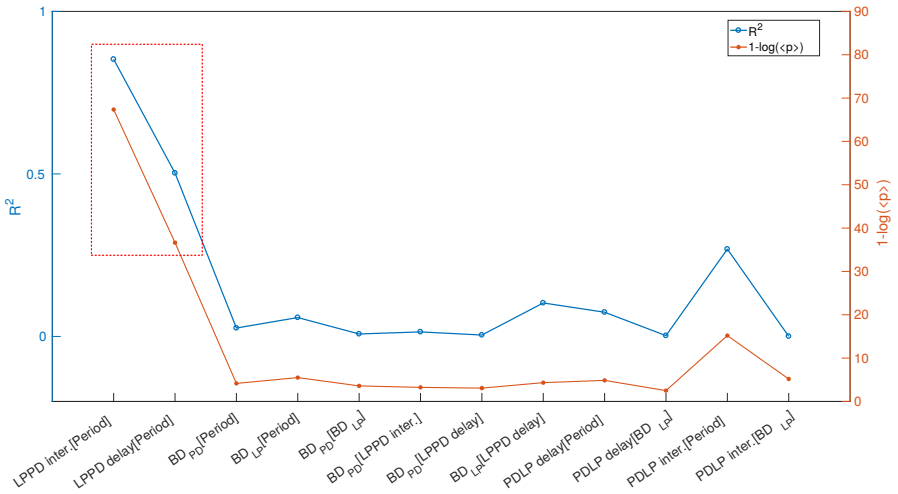

Figure 6.2: Comparison of the mean correlation R^2 and P-values for the 12 combinations of time intervals shown in ***Table 6.1*** (N=16). Note the larger values of R^2 in $LPPD\ inter.[Period]$ and $LPPD\ delay[Period]$ indicating a strong correlation. Other interval combinations yield much lower correlations as quantified by the R^2 values.

Figure 6.3 depicts these two preserved relationships for 9 representative experiments in control conditions with their corresponding linear regression. The analysis includes both regular and intrinsically irregular rhythms (indicated with †). The linear regression shows that the ratio between the change from one cycle to the next in $LPPD\ interval, delay$ and the change in $Period$ is constant. The strong linear correlations indicated the presence of these invariants despite the rhythm variability ($R^2 > 0.9$ for $LPPD\ interval[Period]$). We also included the special case of Exp. 8 in ***Figure 6.3*** with $R^2_{LPPD\ delay[Period]} = 0.154$. This low coefficient of correlation can be attributed to the very small variability in control conditions resulting from a remarkably fast and highly regular rhythm in this experiment, which hides the invariant relationship.

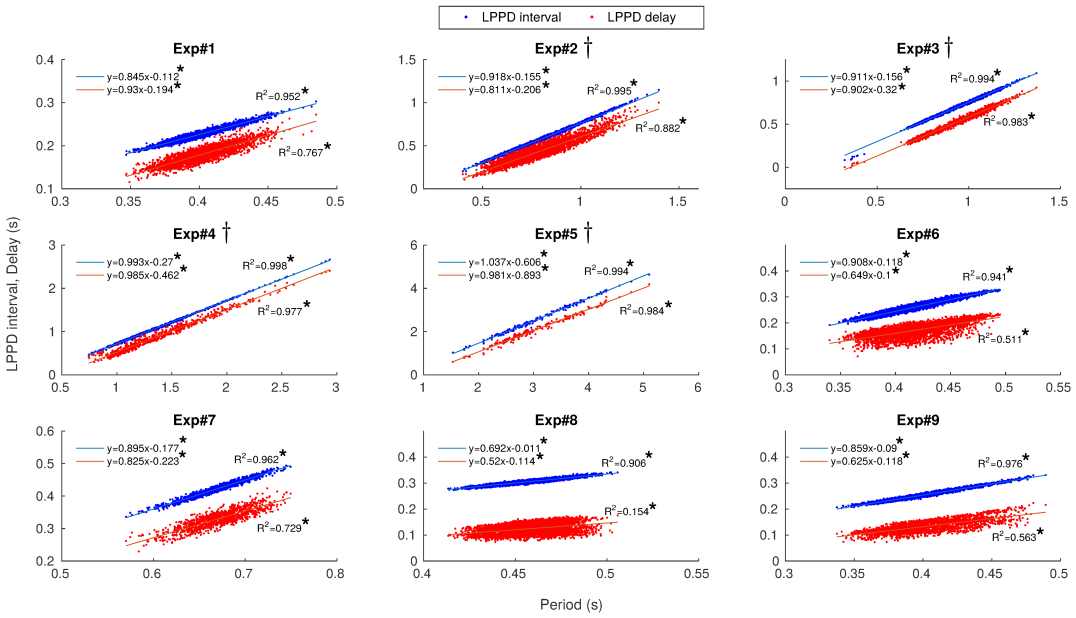

Figure 6.3: Presence of the two dynamical invariants in *control conditions* in 9 representative preparations. The correlation between $LPPD\ interval$ and $Period$ is shown in blue while the correlation between $LPPD\ delay$ and $Period$ is shown in red. Each point corresponds to one pyloric cycle of continuous recordings. Linear regressions are depicted for each experiment. Regression analysis showed that both $LPPD\ interval$ and $LPPD\ delay$ values increased with the $Period$. The linear dependence is indicated by R^2 values displayed for each experiment in the corresponding panel. † Intrinsically irregular preparations. * Slope significantly different from 0 ($p < 8 \cdot 10^{-4}$).

Figure 6.4 depicts these relationships for the same preparations illustrated in ***Figure 6.3*** under the influence of ethanol applied after control. Even in this condition, in which the variability of the measured intervals was very large, the invariants were still present. Note that now Exp. 8 yields $R^2 > 0.9$ for both invariants. Under the influence of ethanol, the CPG rhythm can display very long bursts (lasting in some cases over 6 seconds). During some sections of the recordings in ethanol conditions, bursts in the sequence were lost. These sections that did not contain the required time references were removed from the statistics as illustrated in ***Figure B.1***. ***Table B.1*** shows the percentage of dismissed burst, which never exceeded 26% of the whole recording. The presence of the invariant in ethanol suggests that variability in $BD_{PD,LP}$ and variability in $LPPD\ delay$ compensate each other cycle-by-cycle to sustain the invariants in the rhythm.

Table 6.2: Values of the Pearson correlation coefficient ρ obtained for the different combinations of instantaneous intervals considered in this study for 9 representative experiments in ethanol conditions (same preparations as in ***Table 6.1***, ***Figure 6.3*** and ***Figure 6.4***). Other experiments show similar results. Regression analysis indicated that both $LPPD\ interval$ and $delay$ (framed in the table) have a strong correlation with $Period$ consistently in all the experiments. $PDLP\ interval$ present correlation with $Period$ but is not consistent among preparations, and other measured variables are not correlated. A t-test for significance of the correlation coefficients (N=16) is also included in the table. Last column represents the Pearson correlation coefficient among interval averages calculated for the 16 preparations. * Slope significantly different from 0 ($p < 8 \cdot 10^{-4}$).

Ethanol	ρ_{Exp1}	ρ_{Exp2}	ρ_{Exp3}	ρ_{Exp4}	ρ_{Exp5}	ρ_{Exp6}	ρ_{Exp7}	ρ_{Exp8}	ρ_{Exp9}	t-test	$\rho_{<Exp>}$
$LPPD\ inter.[Period]$	0.998*	0.676*	0.773*	0.866*	0.774*	0.894*	0.923*	0.979*	0.950*	1	0.918*
$LPPD\ delay[Period]$	0.997*	0.630*	0.743*	0.851*	0.756*	0.821*	0.910*	0.957*	0.913*	1	0.890*
$BD_{PD}[Period]$	0.395*	0.707*	0.591*	0.643*	0.934*	0.366*	0.564*	0.120*	0.531*	1	0.728
$BD_{LP}[Period]$	0.011	0.445*	0.386*	0.411*	0.155	0.376*	0.341*	0.505*	0.621*	1	0.548
$BD_{PD}[BD_{LP}]$	0.03	0.028	-0.039	0.151*	0.034	0.105*	0.232*	-0.091*	0.169*	0	0.335
$BD_{PD}[LPPD\ inter.]$	0.352*	-0.011	-0.020	0.178*	0.497*	0.130*	0.204*	-0.031	0.330*	0	0.417
$BD_{PD}[LPPD\ delay]$	0.350*	-0.027	-0.009	0.165*	0.510*	0.089*	0.186*	-0.009	0.346*	0	0.380
$BD_{LP}[LPPD\ delay]$	-0.036	0.341*	0.241*	0.294*	-0.040	0.010	0.184*	0.322*	0.391*	0	0.385
$PDLP\ delay[Period]$	-0.053	0.318*	0.088*	-0.002	-0.037	0.131*	0.347*	0.711*	0.427*	0	0.601
$PDLP\ delay[BD_{LP}]$	-0.062	0.134*	0.055	0.057	0.229*	-0.222*	0.442*	0.306*	0.162*	0	0.112
$PDLP\ inter.[Period]$	0.349*	0.785*	0.647*	0.644*	0.936*	0.591*	0.592*	0.629*	0.857*	1	0.824*
$PDLP\ inter.[BD_{LP}]$	-0.007	0.063	-0.024	0.157*	0.042	-0.105*	0.276*	0.173*	0.292*	0	0.330

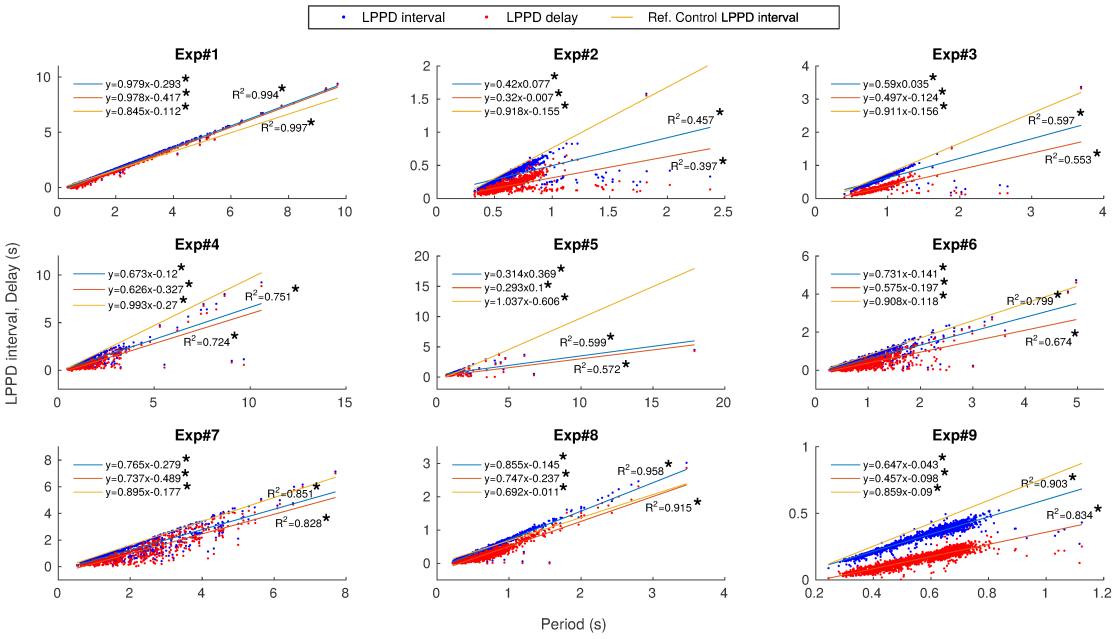

Figure 6.4: Presence of the two dynamical invariants under the influence of *ethanol* for the corresponding 9 preparations displayed in ***Figure 6.3***. The correlation between the measured $LPPD\ interval$ and $Period$ is shown in blue while the correlation between $LPPD\ delay$ and $Period$ is shown in red. Each point corresponds to one pyloric cycle. Linear regressions are depicted for each experiment. Regression analysis showed that both $LPPD\ interval$ and $LPPD\ delay$ values increased with the $Period$. The linear dependence is indicated by R^2 values displayed for each experiment in the corresponding panel. Line in orange corresponds to the linear regression between $LPPD\ interval$ and $Period$ in control conditions shown in ***Figure 6.3*** and is provided to facilitate the comparison. * Slope significantly different from 0 ($p < 8 \cdot 10^{-4}$).

6.2.2 Sequences under PTX

Asymmetric connectivity could play a key role in explaining the compensation process that creates the invariants, so that, if key synapses are removed, invariants should change or even disappear. ***Figure 6.5*** compares the invariant correlations after applying PTX in 9 preparations. One can observe that the dynamical invariant $LPPD\ delay[Period]$ was not preserved in the absence of fast synapses with slopes tending to 0 in all experiments, as opposed to the dynamical invariant $LPPD\ interval[Period]$ that maintains a tendency similar to the corresponding control. ***Table 6.3*** also shows the correlation coefficients between the rest of the combinations of intervals after applying PTX for the same 9 experiments. Under these conditions, most relationships between intervals were not preserved except for the invariant $LPPD\ interval[Period]$. $PDLP\ interval$ presented correlation with the $Period$, however it was weaker and less consistent among preparations. Three of these experiments ($Exp\#10$, $Exp\#11$ and $Exp\#12$) were also subjected to ethanol and ***Figure 6.6*** shows the correlations of these experiments under three conditions: control, PTX, and PTX and ethanol. A possible explanation for the preservation of the $LPPD_{interval}[Period]$ invariant is the LP burst duration variability, which manages to compensate PD variability, even under the effect of ethanol.

Table 6.3: Values of the Pearson correlation coefficient ρ obtained for the different combinations of instantaneous intervals considered in this study for 9 representative experiments after applying PTX $5 \cdot 10^{-7}\ M$ (same preparations as in ***Figure 6.5***). Other experiments show similar results. A t-test for significance of the correlation coefficients is also included in the last column of the table. * Slope significantly different from 0 ($p < 8 \cdot 10^{-4}$).

PTX	ρ_{Exp10}	ρ_{Exp11}	ρ_{Exp12}	ρ_{Exp13}	ρ_{Exp14}	ρ_{Exp15}	ρ_{Exp16}	ρ_{Exp17}	ρ_{Exp18}	t-test
$LPPD\ inter.[Period]$	0.968*	0.953*	0.936*	0.878*	0.940*	0.483*	0.899*	0.938*	0.939*	1
$LPPD\ delay[Period]$	-0.192*	0.018	0.431*	0.036	0.750*	-0.053	0.097*	-0.092	0.195*	0
$BD_{PD}[Period]$	0.002	0.178*	0.258*	0.196*	0.698*	0.534*	0.453*	0.117	0.437*	0
$BD_{LP}[Period]$	0.585*	0.920*	0.631*	0.464*	0.310*	0.397*	0.671*	0.808*	0.480*	1
$BD_{PD}[BD_{LP}]$	0.035	0.106*	0.154*	0.078	0.261*	0.266*	0.265*	0.110	0.196*	1
$BD_{PD}[LPPD\ inter.]$	-0.037	0.064	0.190*	0.184*	0.629*	0.292*	0.353*	0.035	0.442*	0
$BD_{PD}[LPPD\ delay]$	-0.065	-0.168*	0.057	0.030	0.463*	-0.075*	0.035	-0.149	0.126*	0
$BD_{LP}[LPPD\ delay]$	-0.901*	-0.241*	-0.345*	-0.827*	-0.311*	-0.656*	-0.581*	-0.590*	-0.734*	1
$PDLP\ delay[Period]$	0.286*	0.319*	-0.006	0.572*	0.895*	0.303*	0.813*	-0.202*	0.519*	0
$PDLP\ delay[BD_{LP}]$	-0.028	0.046	-0.186*	0.118*	0.144*	-0.503*	0.444*	-0.309*	0.119*	0
$PDLP\ inter.[Period]$	-0.974*	-0.562*	-0.568*	-0.941*	-0.713*	-0.686*	-0.875*	-0.719*	-0.861*	1
$PDLP\ inter.[BD_{LP}]$	0.435*	0.620*	0.419*	0.241*	-0.108*	0.716*	0.156*	0.705*	0.305*	0

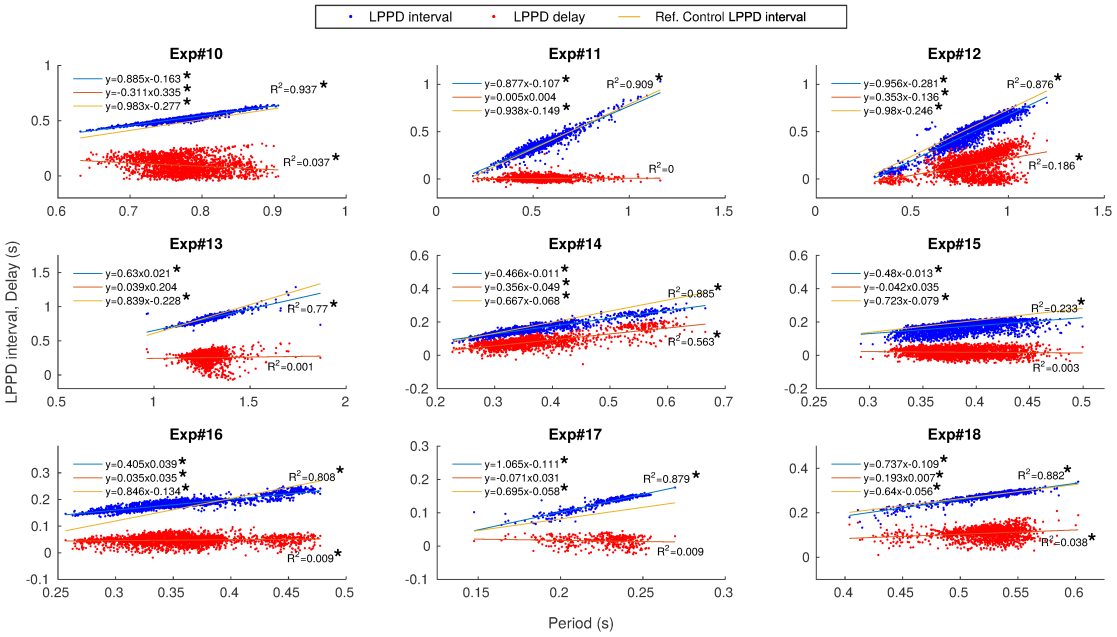

Figure 6.5: Comparison of the two dynamical invariants after applying PTX $5 \cdot 10^{-7}$ M in 9 preparations. The correlation between the measured $LPPD\ interval$ and $Period$ is shown in blue while the correlation between $LPPD\ delay$ and $Period$ is shown in red. Each point corresponds to one pyloric cycle. Linear regression is depicted for each experiment. Regression analysis showed that only the $LPPD\ interval$ increased with the $Period$. The linear dependence is indicated by R^2 values displayed for each experiment in the corresponding panel. * Slope significantly different from 0 ($p < 8 \cdot 10^{-4}$). Line in orange corresponds to the linear regression between the measured $LPPD\ interval$ and $Period$ in control conditions.

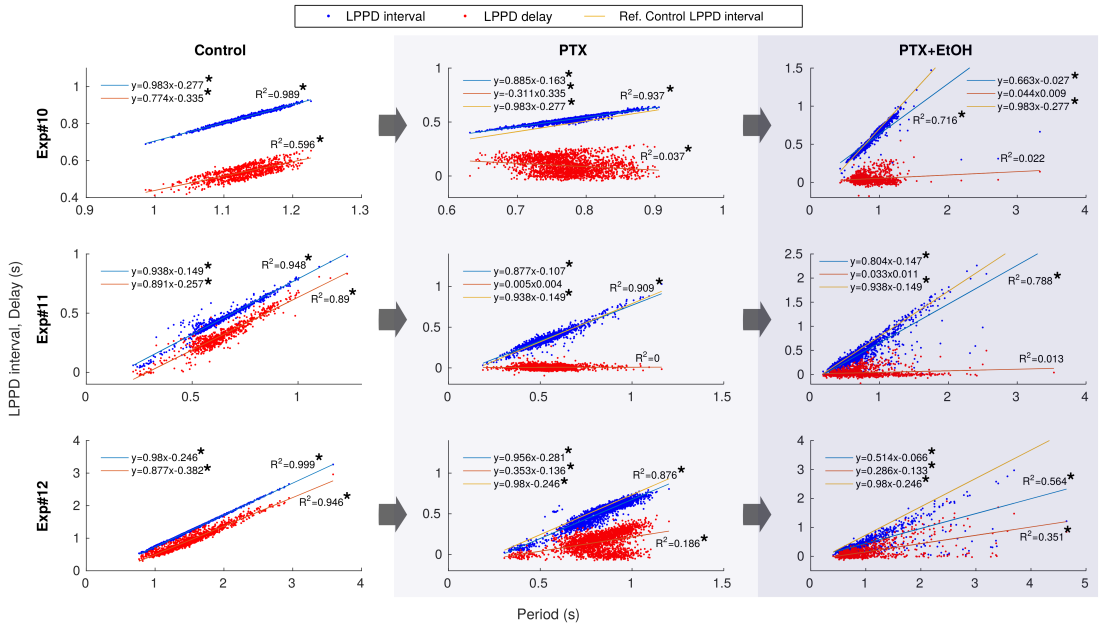

Figure 6.6: Comparison of the two dynamical invariants in three conditions: *control*, *PTX* and *PTX + Ethanol* in three different preparations ($Exp\#10$, $Exp\#11$ and $Exp\#12$ in ***Figure 6.5***). The correlation between the measured $LPPD\ interval$ and $Period$ is shown in blue while the correlation between the $LPPD\ delay$ and $Period$ is shown in red. Each point corresponds to one pyloric cycle. Regression analysis showed that only the $LPPD\ interval$ increased with the $Period$. The linear dependence is indicated by R^2 values displayed for each experiment in the corresponding panel. * Slope significantly different from 0 ($p < 8 \cdot 10^{-4}$). Line in orange corresponds to the linear regression between the measured $LPPD\ interval$ and $Period$ in the control conditions shown in the first column.

6.2.3 Cycle-by-cycle analysis

A major contribution of our work is the demonstration of cycle-by-cycle adjustments that give rise to the invariants, which can be indirectly be seen in ***Figure 6.3***, ***Figure 6.4***, ***Figure 6.5*** and ***Figure 6.6***. Even though in these figures each point corresponds to one pyloric cycle, the temporal relationship between points is lost in this type of representation. The cycle-by-cycle adaptation of the intervals that build the sequence of the CPG rhythm can also be visually noticed in a video of the ongoing rhythm (Elices et al., 2019). ***Figure 6.7*** illustrates the representation of the time series in the video with the instantaneous intervals highlighted in color and the corresponding representation of the points in the linear correlation analysis.

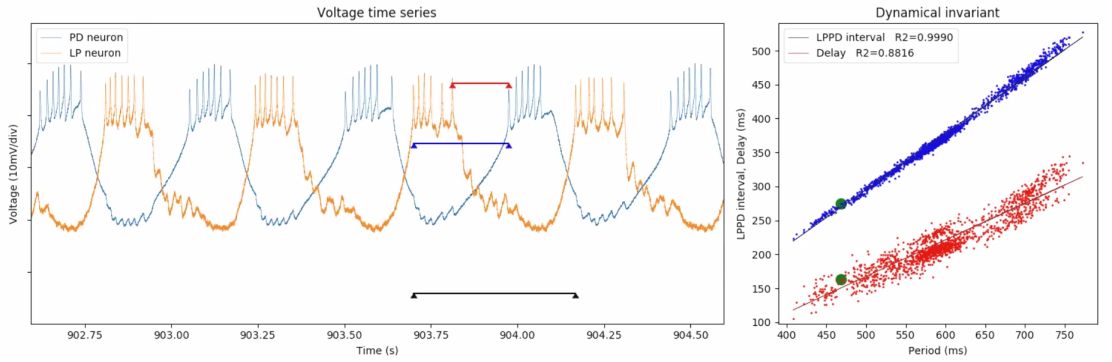

Figure 6.7: Capture of the video of the evolution of the time intervals giving rise to dynamical invariants. Left panel depicts LP and PD voltage time series showing the instantaneous $LPPD\ interval$ (blue), $LPPD\ delay$ (red) and $Period$ (black) in an illustrative experiment. Right panel shows the evolution of the dynamical invariants in time along the regression lines. See video at https://www.biorxiv.org/content/10.1101/379909v1.supplementary-material (Elices et al., 2019).

To better illustrate the instantaneous compensations of the different intervals in each cycle we highlight two representative examples of transient changes in an intrinsically irregular preparation and under the influence of ethanol, shown in ***Figure 6.8***. Panel A in ***Figure 6.8*** shows the evolution of each interval $Period$, BD_{LP}, BD_{PD}, $LPPD\ delay$, $LPPD\ interval$, $PDLP\ delay$ and $PDLP\ interval$ for each cycle period (Exp #9 in ***Figure 6.3***). One can observe that $LPPD\ delay$ and $LPPD\ interval$ closely follow the $Period$ despite its variability. Note that the variability in BD_{LP} , BD_{PD} and $PDLP\ delay$ is much lower and unrelated to the $Period$. Panel B depicts all the intervals standardized so that their variability is presented in the same range. In this representation, the intervals that give rise to the invariants evolve on top of each other (see inset). However, the evolution of the intervals BD_{LP}, BD_{PD} and $PDLP\ delay$ intertwines each other approximately compensating their variability among them. Panels C and D show analogous cycle-by-cycle representations to A and B respectively for an illustrative experiment under the influence of ethanol (Exp #6 in ***Figure 6.4***). Note that when there is a really long PD burst, $PDLP\ delay$ interval can be negative if there is a certain overlap of the PD and LP burst. In addition, it is likely for BD_{PD} to be proportional to the corresponding long period in these cycles (see ***Figure 5.1***). The intervals participating in the dynamical invariants, on the other hand, are correlated to the period for any interval duration category in each cycle and it is consistent in every experiment. Despite the induced large variability, $LPPD\ delay$ and $LPPD\ interval$ closely follow the $Period$.

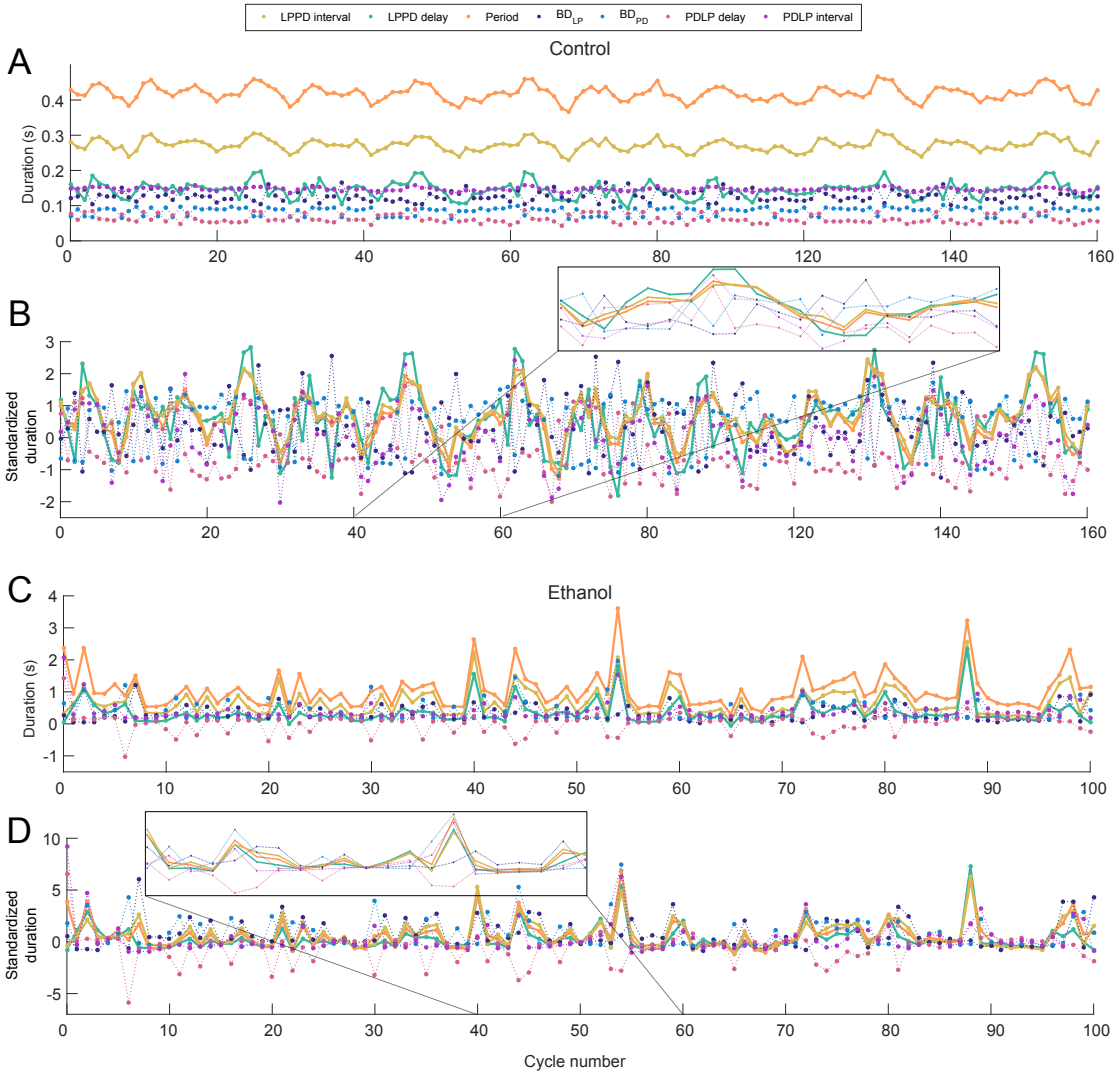

Figure 6.8: Cycle-by-cycle transient changes in the studied intervals. Panel A, intervals $Period$, BD_{LP}, BD_{PD}, $LPPD\ delay$, $LPPD\ interval$ and $PDLP\ delay$ for each cycle. Note that despite the variability in the $Period$, $LPPD\ delay$ and $LPPD\ interval$ closely follow it. Panel B shows the intervals as in Panel A, but with standardized duration. In this representation, the variability of all intervals is in the same range. Note that the standardized $LPPD\ delay$, $LPPD\ interval$ and $Period$, which give rise to the invariants, evolve on top of each other while the evolution of the others intertwines. Analogous representations of the cycle-by-cycle transient changes under the influence of ethanol are shown in Panels C and D. $LPPD\ delay$ and $LPPD\ interval$ closely track $Period$ despite the induced variability. Both insets show a blow up to highlight the common evolution of the three intervals involved in the invariants (solid lines).

6.3 Discussion

Using an adequate time reference frame and experimental conditions to expose transient dynamics, our characterization of cycle-by-cycle variability in CPG circuits has revealed the presence of dynamical invariants in neural sequences. Cycle-by-cycle analysis allowed to center the study of dynamical invariants in transient regimes, without losing the temporal relationship between pivotal time intervals building the sequence. Results show that

$LPPD\ delay$ and $LPPD\ interval$ closely follow the changes in $Period$ despite the variability underlying both dynamical invariants. These invariants were present not only in regular control conditions but also in intrinsic irregular conditions and when high irregularity was induced by ethanol. In control conditions, the presence of both invariants was a very robust result, since they were found in all experiments performed (n=42). One plausible explanation for the invariants is that the intervals, BD_{LP}, BD_{PD} and $PDLP\ delay$ approximately compensate their variability in each pyloric cycle. The invariant $LPPD\ interval[Period]$ is more precise than $LPPD\ delay[Period]$, this is probably because $LPPD\ interval$ contains the added variability of both BD_{LP} and $LPPD\ delay$. It is important to note that other explored relationships among CPG activity intervals did not lead to strong correlations in the form of invariants. This might imply that they are not as relevant for the rhythm negotiation and, thus, have unrelated variability to fulfill another role. Since in our experiments we only used intracellular recordings of LP and PD neurons, we cannot discard the presence of additional preserved relationships among other neurons. Extracellular recordings did not provide additional information due to the difficulty in isolating individual units with accuracy.

It is important to emphasize, that in this work we considered different time intervals from the commonly analyzed latency onset and offset, which are defined using the PD neuron first spike (Hooper, 1997a,b; Bucher et al., 2005; Soofi et al., 2014). When connectivity is asymmetric, the selection of the time references to define the intervals is crucial for exposing potential dynamical invariants. LP neuron receives fewer connections than other neurons in the pyloric circuit. Therefore, it has more flexibility to adapt and coordinate its activity with the rest of the circuit elements in a cycle-by-cycle basis, making this neuron a better candidate as a time reference, see also (Hooper, 1997b). In addition, note that the two invariants observed during cycle-by-cycle transients are different from the approximate phase maintenance reported in previous works that used cross-preparations analysis, steady activity recordings, and other time references (Hooper, 1997a,b; Bucher et al., 2005; Soofi et al., 2014). Approximate phase maintenance, obtained by averaging phase and periods in different preparations or in the same preparation under different treatments (Hooper, 1997a,b; Weaver and Hooper, 2003a; Hooper et al., 2009; Tang et al., 2010; Bucher et al., 2005; Soofi et al., 2014), might reflect some aspects of the unveiled invariants, but not their presence in cycle-by-cycle analysis, in particular during transients. In our analysis, averaging intervals within preparations (see last column in ***Table 6.1***) always provided linear relationships between all intervals and the period across experiments due to all sources of interval variability canceling each other. However, only the intervals participating in the invariants are strongly correlated to the period in a cycle-by-cycle analysis in long recordings. This means that the variability of these two intervals in each cycle is restricted by a linear relation and thus results in a rule for the coordination of the sequence.

For further analysis, PTX was used along with ethanol to study how removing fast synapses in the circuit affected the invariants and tilted the interacting forces of the network that negotiate timings within a robust sequence. We observed that the specific asymmetric connectivity of the pyloric network plays a key role in shaping the invariants. After removing glutamatergic synaptic inputs by applying PTX, the correlation $LPPD\ delay[Period]$ was completely gone while $LPPD\ interval[Period]$ was still maintained. Preservation of this last invariant is probably due to the LP burst duration variability, which manages to compensate the PD variability, even under the effect of ethanol.

The experimental results from the analysis of irregular CPG rhythms presented in this work illustrate that rich dynamics of neurons and connections in the pyloric circuit contribute to regulate flexibility and coordination to readily negotiate their specific timing within the sequential activity. The CPG tends to preserve cycle-by-cycle temporal relationships between neurons even under extreme conditions which points out to circuit's highly

effective negotiating properties and the dynamical arrangement of the motor rhythm to balance robustness and flexibility. CPGs could use the reported invariants and other preserved relationships to program their function under distinct circumstances, which may underlie their remarkable context-specific autonomous adaptability and functional efficiency.

Part III

Results: Role of asymmetric connectivity in shaping robust sequential activity in a conductance model

Chapter 7

Closed-loop control of a minimal central pattern generator network

In the previous chapter, we showed that the pyloric rhythm presents a strong robustness of transient dynamics in keeping not only the activation sequences but also specific cycle-by-cycle temporal relationships in the form of linear correlations between pivotal time intervals, which we named dynamical invariants. We also observed that the specific asymmetric connectivity of the pyloric network plays a key role in shaping the invariants.

In order to study the mechanisms that give rise to the dynamical invariants, here we assess the role of connectivity to generate regular and irregular activity in a CPG model based on a minimal network architecture, i.e., a half-center oscillator. We adaptively modified synaptic maximum conductances using a closed-loop algorithm to expose and map regular and irregular activity regimes.

7.1 Introduction

As we have shown in the previous chapter, central pattern generators are neural circuits that produce robust sequences from flexible constituent time intervals to control muscle function. These circuits have what is called a non-open topology, i.e., all neurons in the CPG receive input from other neurons in the circuit (Huerta et al., 2001; Stiesberg et al., 2007). The building block of these rhythm generator networks is typically based on reciprocal inhibition between pairs of neurons, which underlies many properties of the network-driven spiking-bursting activity and of the phase relationships among neurons in these circuits (Selverston, 2010; Sakurai et al., 2014).

Experimental observations in crustacean CPG neurons show that the oscillatory behavior of these cells within the CPG network is more regular than the behavior observed in isolated cells (Abarbanel et al., 1996; Elson et al., 1999; Varona et al., 2001a). In fact, nonlinear analyses of membrane potential time series have shown the chaotic nature of the isolated neurons (Abarbanel et al., 1996). Chaotic behavior is easily regularized through the cooperative activity of the neurons in the CPG, which typically produces a periodic rhythm to control motor movements (Elson et al., 1999; Selverston et al., 2000; Varona et al., 2001b). Rich intrinsic dynamics allow CPG neurons to rapidly negotiate network rhythms as a function of external input through reciprocal interactions. In intact preparations, the observed

CPG network rhythm is usually very regular and robust as shown in ***Figure 2.8***. Network modifications or the action of specific substances such as ethanol can lead to irregular spiking-bursting activity (see ***Figure 5.1***).

In this chapter, we show that a simple closed-loop protocol can be used to study and map the conditions under which the connectivity of two reciprocally inhibitory chaotic neurons, that implement a well-characterized conductance based model, display regular rhythm regimes, see (Elices and Varona, 2015). In particular, the protocol explores the maximum conductance of the inhibitory synapse to one of the neurons in this minimal CPG circuit. We also discuss how the circuit can also be regularized by external inhibitory stimulation.

7.2 Methods

7.2.1 Neuron model

In this study, we used the Komendantov-Kononenko model explained in section 3.2.1. This conductance-based model has been extensively used to reproduce the spiking-bursting activity of different neuron types (e.g. see (Komarov et al., 2008; Latorre et al., 2013b)). The parameters used in this study were set for the chaotic bursting regime (see ***Table A.1*** in the Appendix A.1). ***Figure 7.1*** shows the typical irregular spiking-bursting activity that the model displays in this regime.

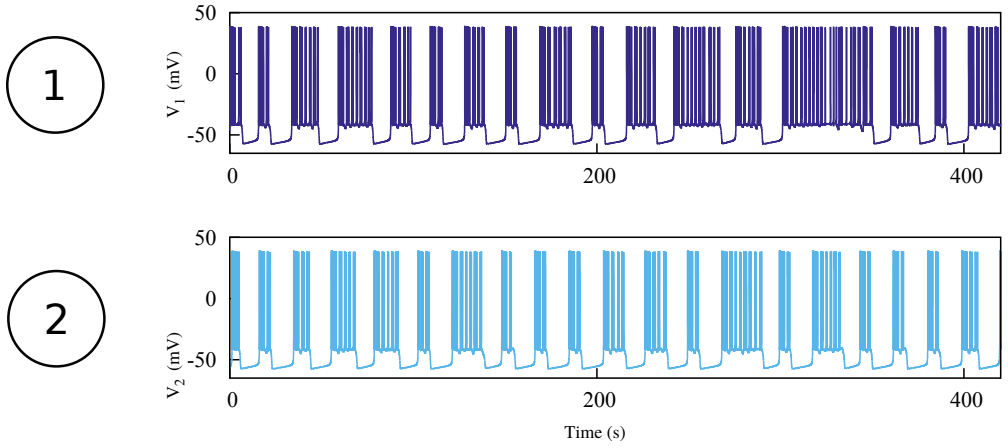

Figure 7.1: Chaotic bursting activity of two single Komendantov-Kononenko model neurons. Initial conditions: $V_1^0 = -47.0, V_2^0 = -58.0$, model parameters are the same as in (Komendantov and Kononenko, 1996) for the chaotic regime.

7.2.2 Minimal CPG network

The system considered consists of a minimal network built up with two Komendantov-Kononenko neurons connected with a bidirectional fast chemical inhibitory synapse, a characteristic half-center oscillator (left panel in ***Figure 7.2***). These chemical synaptic currents were modeled with a fast graded chemical synapse (see section 3.3.2)

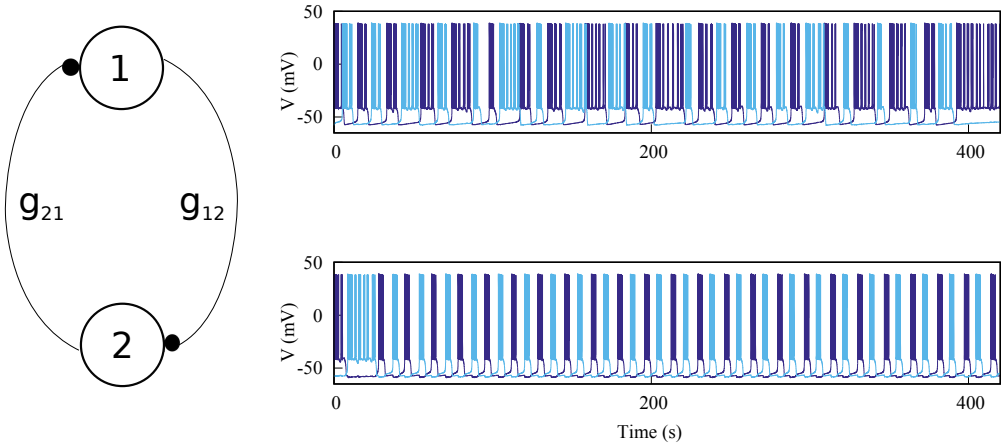

Figure 7.2: Minimal network built up connecting two neurons with two chemical inhibitory synapses. The activity can be irregular or regular depending on the maximal conductances of the synapses. Parameters: Top panel g_{21}=0.005 μS, g_{12}=0.044 μS; Bottom panel g_{21}=0.022 μS, g_{12}=0.024 μS, P_1^f=16.3628 s, RD_1^f=0.3763 %, P_2^f=16.3668 s, RD_2^f=0.1720 %, ϕ_{12}=7.9010 s, ϕ_{21}= 8.4650 s.

The values of the synapse parameters used in our simulations are shown in ***Table 7.1***.

E_{syn}	V_{fast}	s_{fast}
-65.0	44.7	0.31

Table 7.1: Parameters for the fast inhibitory chemical synapse model used in this study.

The network generates alternating bursting activity between both neurons due to the mutual inhibition. Depending on the maximal conductance values used for the inhibitory synapses, the activity can be regular or irregular, see ***Figure 7.2***. The departing point in all simulations discussed in this chapter was the alternating irregular spiking bursting activity of this minimal circuit (top panel in ***Figure 7.2***).

7.2.3 Closed-loop protocol to explore activity regularization

In this study, we used a simple closed-loop algorithm to control the dynamics of the network and achieve a specific goal: a regular alternating bursting activity in the minimal CPG circuit, see (Elices and Varona, 2015). This aim required choosing a performance measure in order to monitor the activity of the system. This measure, which we have called *Regularization Degree* (RD), is the standard deviation of the burst period recorded in the last five bursts at a given time. Thus, it was considered that the system reached the closed-loop goal if the regularization degree was below a certain value ($RD < 0.95$ in the simulations discussed below, as this value provides a reasonable regular spiking-bursting activity comparable to our experimental CPG rhythm recordings).

In the proposed closed-loop, we modified online one of the synaptic conductances, g_{21}, in an activity-dependent manner (see ***Figure 7.3***). The protocol was implemented by changing the value of g_{21} based on the regularity of recent burst periods, as follows: Every time a new burst *n* is generated in neuron 1, its period P_1^n is compared to the average of

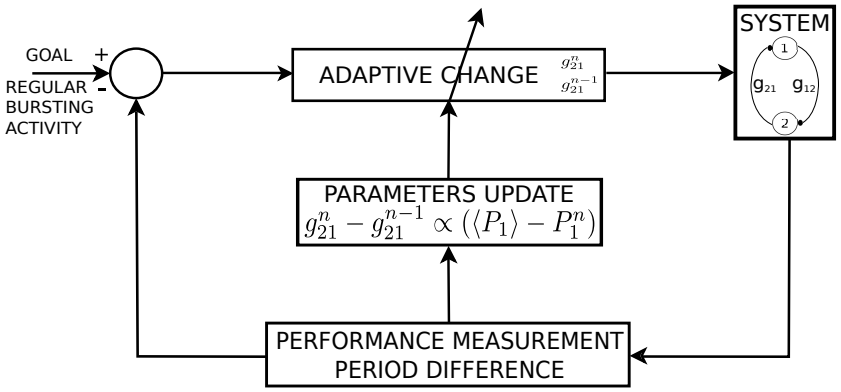

Figure 7.3: Schematic representation of the proposed closed-loop algorithm. To achieve a certain goal, regular alternating bursting activity in the circuit, a performance measure is used to determine whether the system has reached the desired goal or not. In the algorithm proposed in this research, the performance measure is given by the difference between the period of the last burst P_1^n and the average of the last five bursts $\langle P_1 \rangle$. Then, the parameters of the system are updated according to this measure and a new value is set by changing the conductance g_{21} as it is described in section 7.2.3.

the last five bursts' periods $\langle P_1 \rangle$. Then,

- If $P_1^n \in \left[\langle P_1 \rangle - P_w, \langle P_1 \rangle + P_w\right]$, the conductance g_{21} remains unchanged.
- If $P_1^n < (\langle P_1 \rangle - P_w) \rightarrow g_{21}^n = g_{21}^{n-1} = \alpha \cdot \left(\langle P_1 \rangle - P_1^n\right)$,
- If $P_1^n > (\langle P_1 \rangle + P_w) \rightarrow g_{21}^n = g_{21}^{n-1} = \alpha \cdot \left(P_1^n - \langle P_1 \rangle\right)$,

where P_w and α are parameters to set the allowed deviation from the period average and the rate of conductance change, respectively. Note that new conductance values depend on the recent past history of the bursting activity. In the simulations described in the next section, we used the following values: $P_w = 0.5\ s$ and $\alpha = 0.001$. The chosen values and the monitoring of the last five bursts provided a good balance between a reasonable online measurement of the regularity and a fast convergence to the closed-loop goal.

7.3 Results

The closed-loop protocol described above was used to regularize the spiking-busting activity of the circuit while sustaining the alternating rhythm of the two neurons. The departing point was the alternating irregular activity shown in the top panel of ***Figure 7.2***. The algorithm updated the value of one of the synaptic conductances, g_{21}, according to the difference between the current period, P_1^n, and the average of the periods of the last five bursts, $\langle P_1 \rangle$, as summarized in ***Figure 7.3***.

Figure 7.4 illustrates an example of the evolution of the circuit activity under the closed-loop protocol. The initial value of the synaptic conductance that changed during the protocol was g_{21}^0=0.04 μS, and it evolved to g_{21}^f=0.0291 μS at the end of the protocol. The other conductance remained fixed g_{12}=0.024 μS. One can observe that the system needed little time to reach a regular alternating bursting activity. In this example, the final bursting

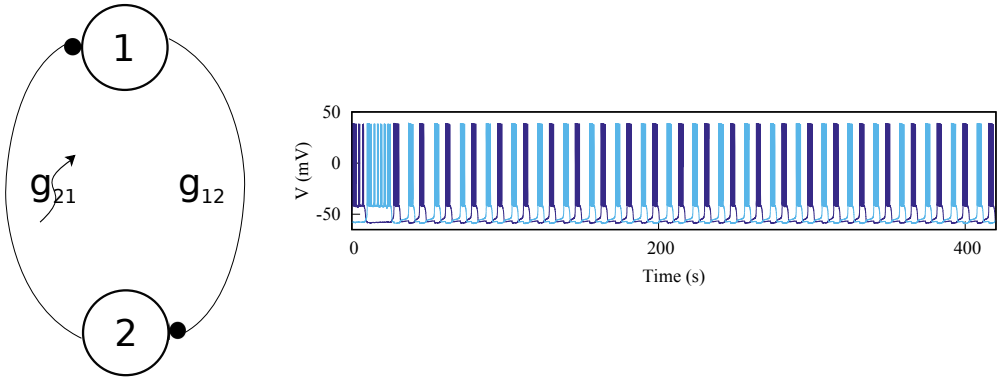

Figure 7.4: Activity of the system using the proposed closed-loop algorithm that changes the g_{21} conductance to regularize the spiking-bursting activity of the circuit. The protocol tries to find a suitable value of a single synaptic conductance, which drives the system into a regular bursting activity. Parameters: g_{21}^{0}=0.04→ g_{21}^{f}=0.0291 μS, g_{12}=0.024 μS, P_1^f=16.4842 s, RD_1^f=0.3655 %, P_2^f=16.4778 s, RD_2^f=0.3187 %, ϕ_{12}=8.9550 s, ϕ_{21}=7.5228 s.

periods were very similar for both neurons (P_1^f=16.4842 s, P_2^f=16.4778 s), and their regularization degree was well below 0.95% (RD_1^f=0.3655 %, RD_2^f=0.3187 %). Moreover, in this particular case, the alternating bursting activity was nearly symmetric since the interburst intervals between both neurons were similar (ϕ_{12}=8.9550 s, ϕ_{21}=7.5228 s).

$g_{21}^{0} \rightarrow g_{21}^{f}$ (μS)	g_{12} μS)	P_1^f (s)	RD_1^f (%)	P_2^f (s)	RD_2^f (%)	ϕ_{12} (s)	ϕ_{21} (s)
0.0130 → 0.0138	0.0160	16.1862	0.3124	16.1884	0.5200	7.7746	8.4138
0.0200 → 0.0116	0.0160	16.1752	0.1720	16.1814	0.2577	7.5416	8.6398
0.0250 → 0.0213	0.0160	16.3034	0.1855	16.3026	0.1625	8.8358	7.4668
0.0280 → 0.0183	0.0160	16.2372	0.2638	16.2436	0.2871	8.4540	7.7896
0.0450 → 0.0110	0.0160	16.1638	0.7111	16.1856	0.2939	7.5154	8.6702
0.0180 → 0.0158	0.0240	16.3716	0.6151	16.3824	0.6946	7.1950	9.1874
0.0230 → 0.0261	0.0240	16.4110	0.5967	16.4128	0.5600	8.5232	7.8896
0.0250 → 0.0206	0.0240	16.3522	0.1939	16.3658	0.6735	7.7476	8.6182
0.0280 → 0.0201	0.0240	16.3526	0.5535	16.3672	0.2135	7.6936	8.6736
0.0300 → 0.0213	0.0240	16.3630	0.3162	16.3600	0.4817	7.7874	8.5726
0.0330 → 0.0348	0.0240	16.6464	0.8114	16.6434	0.3666	9.5626	7.0808
0.0350 → 0.0224	0.0240	16.3592	0.6145	16.3686	0.6530	8.0204	8.3482
0.0400 → 0.0291	0.0240	16.4842	0.3655	16.4778	0.3187	8.9550	7.5228
0.0280 → 0.0298	0.0350	16.6174	0.4224	16.6218	0.2926	7.5674	9.0544
0.0350 → 0.0304	0.0350	16.6162	0.4445	16.6204	0.3007	7.6110	9.0094
0.0380 → 0.0395	0.0350	16.7380	0.5404	16.7344	0.3611	9.1442	7.5902
0.0400 → 0.0312	0.0350	16.6044	0.6406	16.6170	0.1673	7.7810	8.8360
0.0430 → 0.0399	0.0350	16.7496	0.3720	16.7408	0.5269	9.1724	7.5684
0.0450 → 0.0347	0.0350	16.6124	0.4317	16.6320	0.3347	8.3612	8.2708
0.0380 → 0.0373	0.0440	16.8644	0.2154	16.8654	0.3007	7.3504	9.5150
0.0400 → 0.0364	0.0440	16.8656	0.3720	16.8684	0.4079	7.3122	9.5562
0.0430 → 0.0409	0.0440	16.8138	0.6306	16.8226	0.6248	7.9142	8.9084
0.0450 → 0.0401	0.0440	16.8264	0.2871	16.8328	0.5671	7.7454	9.0874
0.0480 → 0.0449	0.0440	16.8536	0.6119	16.8374	0.6086	8.5202	8.3172
0.0500 → 0.0438	0.0440	16.8218	0.3655	16.8356	0.4587	8.5102	8.3254
0.0550 → 0.0548	0.0440	17.1988	0.5455	17.1968	0.5154	10.1168	7.0800

Table 7.2: Representative results of the regularization of the spiking-bursting activity using the closed-loop protocol described in section 7.2.3.

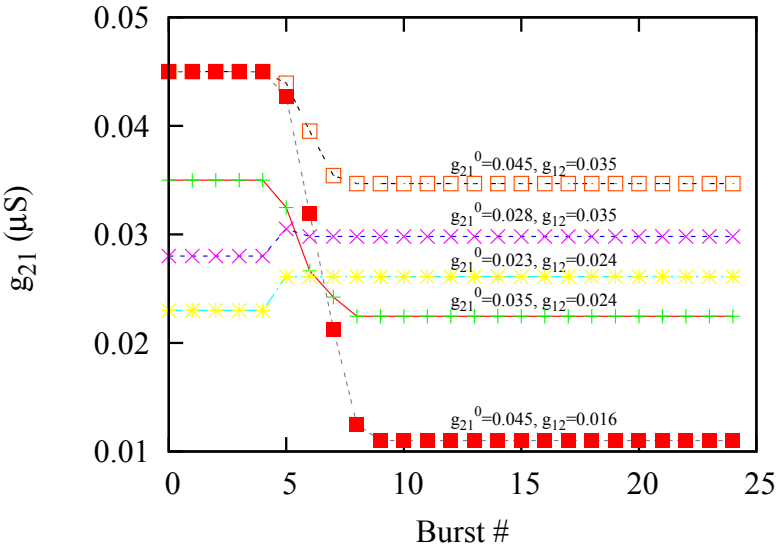

Figure 7.5: Examples of evolution of the conductance g_{21} during the simulations with the closed-loop protocol. The figure shows the different conductance values after each burst. One can observe that g_{21} reached the final value that led to the regularization goal after very few bursts.

Table 7.2 summarizes the analysis of representative results of applying the closed-loop protocol to circuits with different values of g_{21}^0 and g_{12}. The table displays the final value of the conductance g_{21}^f, as well as the neurons' corresponding final periods $P_{1(2)}^f$, regularization degrees $RD_{1(2)}^f$ and time intervals between neurons $\phi_{12(21)}$. For all these examples, the circuit displayed regular alternating bursting activity after the closed-loop g_{21} adaptation (since $RD < 0.95\%$) although with different interburst interval relationships, as reflected by the values of ϕ_{12} and ϕ_{21} between consecutive bursts.

Figure 7.5 shows several examples, taken from ***Table 7.2***, of the g_{21} conductance value update evolution that led to the regularization goal under the closed-loop protocol. One can observe that after very few bursts the conductance reached the final value g_{21}^f and remained unchanged until the simulation finished. This final value can be higher or lower than the departing conductance value g_{21}^0, and the number of bursts needed to reach it usually varied from 1 to 5.

Not all departing values of the conductance led to regularization under this protocol. Left panel in ***Figure 7.6*** depicts a map of g_{12} and g_{21}^0 conductance values that led to a regular spiking-bursting activity. One can see that there is a certain symmetry in these values, so that they are within a range around the fixed value of g_{12}. If the departing value of the conductance g_{21}^0 did not belong to this range, the algorithm was not able to find a g_{21}^f value that led to regular activity. Right panel in this figure shows the final values of the conductance g_{21}^f that achieved the regularization goal. Note that these final conductance values also tended to remain close to the fixed g_{12} values. Changing the parameters used in the closed-loop algorithm, e.g., choosing another rate for the conductance change α (including making it an adaptive parameter) and/or the allowed deviation from the period average, P_w, may allow us to find other goal-compatible values of the g_{21} conductance.

Another way to regularize the spiking-bursting activity of the network is by means of external stimulation. This is a common regularization protocol in experimental research and it is typically implemented using periodic current injection, e.g. see (Elson et al., 1999;

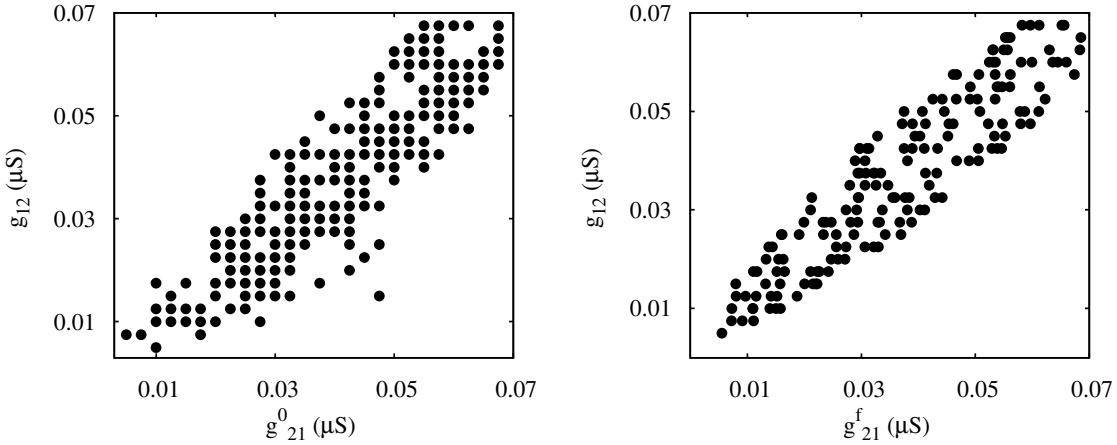

Figure 7.6: Maps of departing and final conductances using closed-loop protocol. Left panel: Map of departing conductances values g_{12} and g_{21}^0 that led to regularization of the spiking-bursting activity where the incremental step for g_{12} and g_{21}^0 was 0.0025 μS. Black circles represent values that led to regular activity ($RD < 0.95\%$). Right panel: map displaying the final conductance values g_{21}^f that resulted in a regular CPG rhythm.

Szücs et al., 2001; Denker et al., 2005). Here we have considered several scenarios with a negative pulse stimulation on one or on the two neurons of the circuit. For our analysis, we distinguished between stimulation that takes into account the current state of the system and stimulation that is delivered in an open-loop independently of the current state of the neurons.

Top panel in ***Figure 7.7*** shows the activity observed when only one neuron was stimulated using a periodic current injection of small amplitude (0.02 nA, 5 s long square pulses) delivered without any information regarding the current state of the system. The regularization measures in this example yielded RD_1^f=198.2582 %, RD_2^f=316.0967 % and thus the regularity goal was not achieved. To regularize the activity under this protocol by delivering periodic square pulses to only one neuron, the current injection amplitude had to be very large (2.1 nA) and, as a consequence, the neuron dynamics displayed non-physiological membrane potential waveforms that drove the neuron dynamics to low hyperpolarized voltage values every time the stimulus was applied (see bottom panel in ***Figure 7.7***). Under the same scenario, we considered the case in which we provided a minimal information about the current activity to deliver the stimulation (e.g., the current injection starts at the beginning of the neuron's first burst), the results obtained were very similar; the amplitude of the current that we have to inject to achieve regularity was very large.

On the other hand, we stimulated both neurons at the same time with synchronous square periodic current injections of small amplitude (0.02 nA), without taking into a count any information regarding the state of the system (***Figure 7.8***). The resulting activity was regular $RD < 0.95\%$ (RD_1^f=0.4578 %, RD_2^f=0.3929 %) and nearly symmetric: ϕ_{12}=10.5360 s, ϕ_{21}=9.4630 s. Therefore, the coordination between the neurons induced by the synchronous current injection (a common transient hyperpolarization reset) was enough to regularize the activity. After introducing a fixed delay (5.0 s) between both stimulation signals, as it is illustrated in ***Figure 7.9***, one can observe that the minimal amplitude of the signal needed to regularize the activity (0.042 nA) was higher than when simultaneous stimuli were used, still without driving the voltage to non-physiological membrane voltage waveforms. Note also the expected larger asymmetry in the interburst intervals resulting from the stimulation delay (ϕ_{12}=14.7910 s, ϕ_{21}=5.2150 s). Finally, we considered an

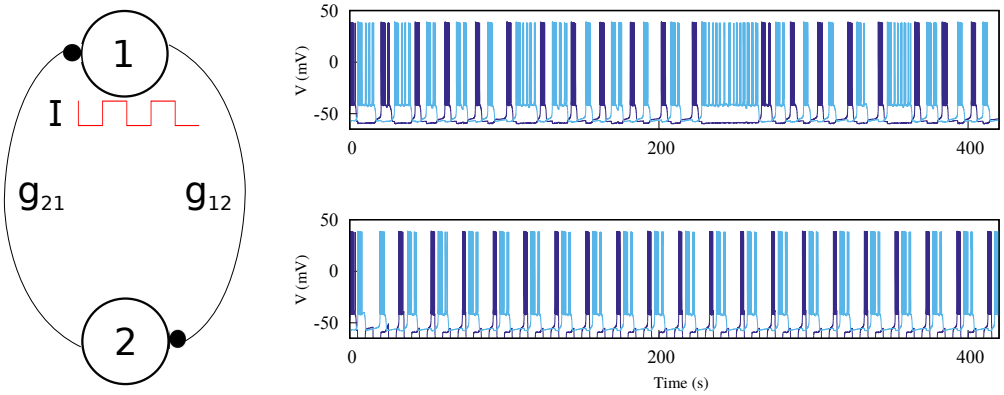

Figure 7.7: Activity of the system stimulating one of the neurons using a periodic square current pulse delivered independently of the state of the system. Time series show that this method required large amplitude pulses that induced non-physiological membrane potential waveforms to achieve the regularization goal. Parameters: Top panel: g_{21}=0.07 μS, g_{12}=0.025 μS; Signal: amplitude=0.02 nA, duration= 5.0 s, RD_1^f=198.2582 %, RD_2^f=316.0967 % ; Bottom panel: g_{21}=0.07 μS, g_{12}=0.025 μS; Signal: amplitude=2.1 nA, duration= 5.0 s, P_1^f=20.0016 s, RD_1^f=0.1356 %, P_2^f=20.0026 s, RD_2^f=0.0800 %, ϕ_{12}=15.6260 s, ϕ_{21}=4.3760 s.

activity-dependent stimulation to both neurons, so that stimulation signals to each of the cells started at the beginning of their corresponding first bursts (see ***Figure 7.10***). One can observe that the activity was regular (RD_1^f=0.4409 %, RD_2^f=0.2530 %) and nearly symmetric (ϕ_{12}=10.6040 s, ϕ_{21}=9.3960 s). It is important to note, that the amplitude of the signals needed to regularize the alternating rhythm (0.021 nA) was lower than in the previous case, where we introduced a delay between the signals without taking into account the current state of the system.

7.4 Discussion

Closed-loop techniques in basic and applied neuroscience research contribute to reveal neural dynamics and provide new control possibilities of healthy and pathological states by activity-dependent stimulation cycles. These techniques are successfully applied at different description levels of the nervous system, from single neurons in *in vitro* preparations all the way up to human rehabilitation protocols and brain computer interfaces (Destexhe and Bal, 2009; Rolston et al., 2010; Chamorro et al., 2012; Amini and Hosseini-Golgoo, 2012; Schiff, 2012; Sulzer et al., 2013; van Boxtel and Gruzelier, 2014). Theoretical studies can also use these types of protocols to explore and map the model parameter space, search for specific relevant dynamics, and assess robustness and comparison with experimental results.

The motor function of CPG circuits is related to the production of robust yet flexible rhythms, in most cases in the form of regular spiking-bursting activity in each of their member neurons. This is also the function that is given to CPG-based bio-inspired circuits in robotic applications (Ijspeert, 2008; Herrero-Carrón et al., 2011). CPGs show a remarkable ability to adapt to different situations, e.g. behavioral contexts, by changing the speed and/or phase relationships while keeping the regularity of the activity produced. On the other hand, some CPG neurons have shown chaotic activity when isolated, which contributes to their flexibility to negotiate rhythms within the circuit (Elson et al., 1999; Varona

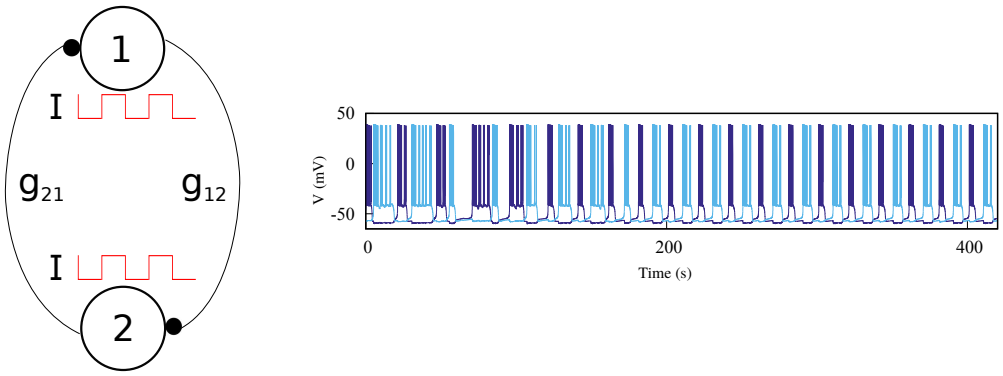

Figure 7.8: Activity of the system stimulating simultaneously both neurons with synchronous square periodic signals delivered independently of the state of the system. The results show that when both neurons were stimulated with the same timing, regular activity was easily achieved. Parameters: g_{21}=0.07 μS, g_{12}=0.025 μS; Signal: amplitude=0.02 nA, duration= 5.0 s, P_1^f=20.0012 s, RD_1^f=0.4578 %, P_2^f=19.9984 s, RD_2^f=0.3929 %, ϕ_{12}=10.5360 s, ϕ_{21}=9.4630 s.

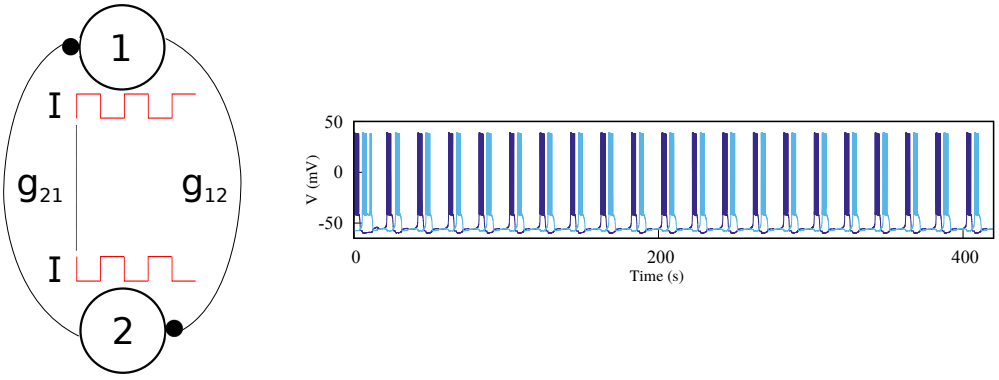

Figure 7.9: Activity of the system stimulating both neurons using square periodic signals with a fixed delay (5.0 s) between the stimuli delivered to each of the neurons. The final activity of the system was regular, with asymmetric intervals between both neurons. The minimum amplitude of the stimuli that was needed for regularization was higher in this case than when using simultaneous stimuli (cf. ***Figure 7.8***). Parameters: g_{21}=0.07 μS, g_{12}=0.025 μS; Signal: amplitude=0.042 nA, duration= 5.0 s, delay=5.0 s, P_1^f=20.0022 s, RD_1^f=0.3250 %, P_2^f=20.0014 s, RD_2^f=0.3450 %, ϕ_{12}=14.7910 s, ϕ_{21}=5.2150 s.

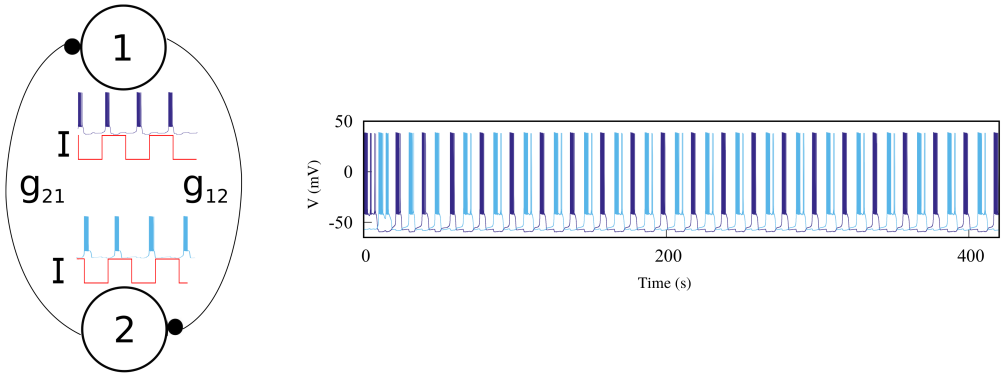

Figure 7.10: Activity of the system stimulating both neurons using a square periodic signal that begins when the first burst of the neuron starts. The results illustrate that taking into account minimal information about the current activity to deliver the stimulation, regular activity was more easily achieved. The amplitude needed for regularization was lower than when a stimulus with a fixed delay between signals was used, without any information about the current state of the system. Parameters: g_{21}=0.07 μS, g_{12}=0.025 μS; Signal: amplitude=0.021 nA, duration= 5.0 s, P_1^f=20.0036 s, RD_1^f=0.4409 %, P_2^f=20.003 s, RD_2^f=0.2530 %, ϕ_{12}=10.6040 s, ϕ_{21}=9.3960 s.

et al., 2001a). A minimal circuit with reciprocal inhibition, typically a half-centered oscillator, is under the core of this ability.

The dynamical mechanisms that lead to regularized activity of spiking-bursting neurons have been widely addressed in several experimental studies (Elson et al., 1998, 1999; Varona et al., 2001a; Szücs et al., 2009; Hooper et al., 2015) and theoretical work with a wide variety of models ranging from conductance-based models to map models, e.g. see (Rabinovich et al., 1997; Varona et al., 2001b; Cazelles et al., 2001; Rulkov, 2001; Duarte et al., 2009; Used et al., 2012; Doloc-Mihu and Calabrese, 2014; Rabinovich et al., 1999). Although some studies have included the role of sensory feedback (Simoni and DeWeerth, 2007) in a half-center oscillator, the closed-loop control of the irregular activity in this minimal CPG circuit is largely understudied. In this chapter, we have explored a simple closed-loop protocol to regularize the activity of a minimal CPG circuit by changing one of its inhibitory conductances, see also (Elices and Varona, 2015). Our results showed that the protocol was effective in this task. In our study, we adaptively modified one of the synaptic maximum conductances. The control of both conductances simultaneously could be addressed by considering a protocol that did not drive them into diverging directions in relation to the closed-loop goal. External stimulation was not very effective in regularizing activity if only one neuron was stimulated with moderate current pulses that kept the membrane potential in a physiological regime as shown in the discussed examples. On the other hand, asynchronous external stimulation to the two neurons was more effective when taking into account the state of the circuit. The study described above serves as a basis to propose new closed-loop experiments to further explain the remarkable capacity of CPG neurons to produce robust yet flexible rhythms. Once we have characterized the regularization of chaotic dynamics in a half-center oscillator with fast synapses, in the next chapter we extend the analysis to more asymmetric configurations.

Chapter 8

Asymmetry Factors Shaping Regular and Irregular Bursting Rhythms in Central Pattern Generators

In this chapter, we continue our study in the mechanisms of generation of regular and irregular activity from the perspective of the asymmetry observed in the connectivity of most CPG circuits. In particular, we use a half-center oscillator model with different degrees of complexity to perform a parametric search of regular regimes and assess the role of asymmetry in strength and temporal scale to generate these rhythms.

8.1 Introduction

As we have previously highlighted, many CPGs are built with a non-open network architecture, i.e., a connection topology in which every neuron receives at least one synapse from another member of the CPG (Huerta et al., 2001). The building block in this type of connection architecture is often an oscillator circuit of reciprocally inhibitory neurons (Miller and Selverston, 1982; Sakurai et al., 2014; Selverston, 2010). Therefore, minimal circuits such as half-center oscillators involving mutually inhibitory neurons are convenient networks to address CPG function. In particular, the concept of a half-center oscillator has been extensively used to study CPG rhythm generation, both in experimental, e.g. see (Miller and Selverston, 1982; Sharp et al., 1996; Yakovenko et al., 2005; Brookings et al., 2012; Sakurai et al., 2014), and theoretical works, e.g. (Nadim et al., 1995; Cymbalyuk et al., 2002; Bem and Rinzel, 2004; Wojcik et al., 2014; Reyes et al., 2015; Doloc-Mihu and Calabrese, 2016). Most of these studies focus on the analysis of alternating regular rhythms, and only a few works address the presence of irregular spiking-bursting activity in mutually inhibitory neurons, e.g. (Varona et al., 2001a; Doloc-Mihu and Calabrese, 2011; Elices and Varona, 2015, 2017; Nagornov et al., 2016).

Using conductance-based models and realistic connection topologies inspired by the crustacean pyloric CPG, in this chapter we address the study of asymmetry connectivity factors shaping CPG spiking-bursting rhythms. In particular, we show the existence of asymmetric maximal synaptic conductances and time constants that shape regularized and robust alternating spiking-bursting activity in half-center oscillator circuits, and we assess their role in the rhythm configuration. We also discuss the modulation of the regularity by

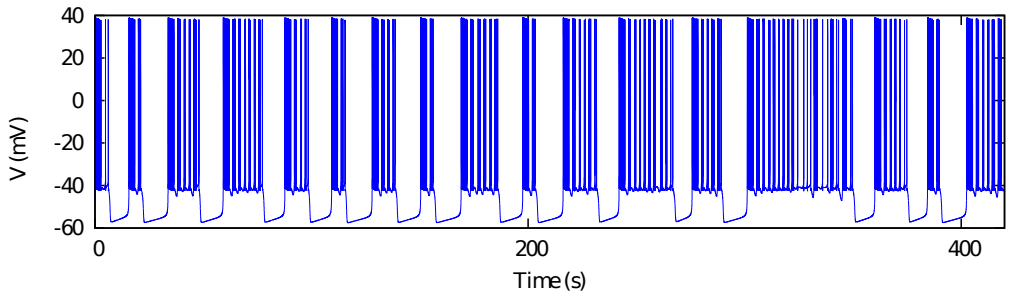

Figure 8.1: Chaotic bursting activity of a single Komendantov-Kononenko model neuron. See model parameter in ***Table A.1***, see also (Komendantov and Kononenko, 1996). $V_0 = -47.0$

additional gap-junction connections to the half-center oscillator. Finally, we show how a closed-loop protocol can adapt online the synaptic time constants based on the regularity of the burst periods. We argue that this closed-loop interaction is an effective methodology in characterizing the coordination properties that arise from both the connection topology and the individual dynamics of the spiking-bursting neurons in these circuits when there is no time to explore the whole parameter space, as in experimental approaches.

8.2 Methods

8.2.1 Neuron model

For our analysis, we used the conductance based Komendantov-Kononenko model, explained in section 3.2.1. The parameters used in our simulations were set for the chaotic bursting regime (see ***Table A.1*** in A.1). ***Figure 8.1*** illustrates the irregular bursting activity of the model in this regime, which resembles the observed behavior in isolated CPG neurons (Abarbanel et al., 1996; Elson et al., 1998).

8.2.2 Network topologies

Synaptic asymmetries in both strength and duration are known to be present in the mutual inhibition between CPG neurons (Marder and Eisen, 1984). For our study on the asymmetry factors shaping regular and irregular bursting rhythms, we used three different topologies of mutually inhibitory neurons that we describe below, see also (Elices and Varona, 2017).

Mutually inhibitory oscillator circuit with symmetric synaptic temporal dynamics

Following the logic of the previous chapter for comparison purposes, we first considered a half-center oscillator topology, i.e., a minimal network built up with two model neurons connected with mutually inhibitory chemical synapses that have symmetric temporal characteristics but considering the possibility of different maximal conductances in each synapse (see left panel in ***Figure 8.2***A). The associated synaptic currents were modeled with

a fast graded synapse, a common type of chemical synapse in many CPGs 3.3.2. The values of the synapse parameters used in our simulations are $E_{syn} = -65mV$, $V^f = -49mV$, $s^f = 0.31mV^{-1}$. The mutually inhibitory connections in the circuit lead the neurons to a rhythm negotiation in the form of alternating bursting activity. The activity produced by the circuit can be regular or irregular depending on the value of the maximal conductances of the synapses as it can be observed in the right panels of ***Figure 8.2***A. In this analysis we have considered that the activity is regular if the coefficient of variation of the period C_v during five consecutive bursts is less than 5% ($C_v < 5\%$).

Mutually inhibitory oscillator circuit with asymmetric synaptic temporal dynamics

As we have seen before, temporal asymmetry is present between the LP and the PD neurons in the crustacean pyloric CPG (Marder and Eisen, 1984). For further characterization of the role of asymmetry shaping CPG spiking-bursting rhythms, one of the *fast* graded inhibitory synapses in the previous circuit was replaced by a *slow* graded inhibitory synapse (see right panel in ***Figure 8.2***B). The slow synaptic current model used was 3.3.3. k_1 and k_s were used as additional control parameters to introduce asymmetry in the temporal evolution of the synaptic currents. Examples of regular and irregular alternating bursting activity generated by this type of circuit are shown in the left panels of ***Figure 8.2***B.

Topology with gap-junction induced asymmetry

In addition to the asymmetric inhibitory connectivity in the network, we considered a third circuit in which neuron two of the previous circuit were replaced by two electrically coupled cells, as it is illustrated in the left panel of ***Figure 8.2***C. Gap-junctions add additional inertia to the neurons connected by this type of synapse, which tend to synchronize (Elson et al., 1999; Varona et al., 2001a). This topology with electrical coupling is also present in several CPGs and in particular in the crustacean stomatogastric ganglion (Selverston and Moulins, 1987). The equation used to model the gap junction is indicated in 3.3.1. The value for the gap-junction conductance used was $g^{gj}_{prepost} = 0.0045mS$. Note that this third topology involves two slow inhibitory graded synapses to neuron 1 (see ***Figure 8.2***C), and one fast graded inhibitory synapse to each of the electrically coupled cells (neurons 2 and 3). Again, the values of the maximal synaptic conductances determine the regular or irregular rhythm in the circuit (see right panels in ***Figure 8.2***C).

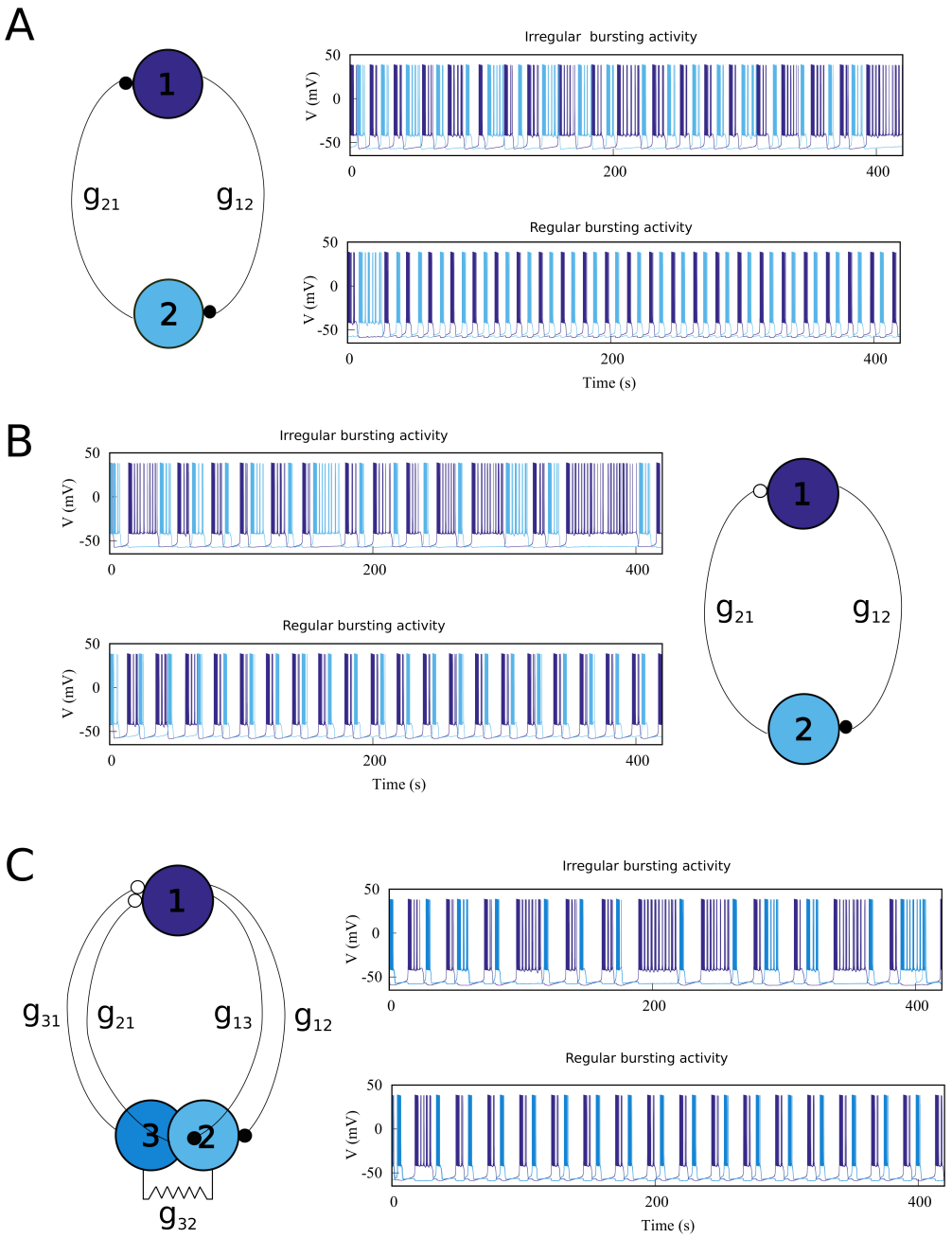

Figure 8.2: The three different topologies of mutually inhibitory spiking-bursting neural circuits considered in this study. The activity can be irregular or regular depending on the maximal conductances of the synapses and the rest of parameters that control the asymmetry level in each circuit. Panel A: mutually inhibitory oscillator circuit with temporal symmetric synapses. Black filled circles represent fast graded chemical synapses, see (***Equation 3.3.2***). Parameters: Top panel g_{21}=0.005 μS, g_{12}=0.044 μS (irregular rhythm); Bottom panel g_{21}=0.022 μS, g_{12}=0.024 μS (regular rhythm). Panel B: Mutually inhibitory oscillator circuit with temporal asymmetric synapses. The empty circle represents a slow chemical synapse, see (***Equation 3.3.3***, ***Equation 3.3.4***). Parameters: k_1 =0.6 ms^{-1}, k_2= 0.27 ms^{-1}, Top panel g_{21}=0.0155 μS, g_{12}=0.0255 μS; Bottom panel g_{21}=0.0235 μS, g_{12}=0.0055 μS. Panel C: Asymmetric topology with gap-junctions modeled with (***Equation 3.3.1***). Parameters: k_1 =0.6 ms^{-1}, k_2= 0.27 ms^{-1}, Top panel $g_{21,31}$=0.05 μS, $g_{12,13}$=0.03 μS; Bottom panel $g_{21,31}$=0.035 μS, $g_{12,13}$=0.055 μS.

8.3 Results

8.3.1 Regularized activity in mutually inhibitory oscillator circuits

As a departing point, we have considered a half-center oscillator topology with symmetric fast temporal dynamics in the synapse model (see left panel in ***Figure 8.2***A). This temporal symmetric circuit generates regular and irregular alternating bursting activity depending on the values of synaptic maximal conductances. Simulations were run to explore the synaptic maximal conductances that resulted in regular or irregular activity according to the criterion of having the coefficient of variation C_v of this activity below a 5% threshold. ***Figure 8.3*** illustrates the map of conductances g_{12} and g_{21} that led to regularized rhythms (black dots) consisting of alternating bursting between the two neurons. White spaces represent regions where irregular spiking-bursting activity was found. One can observe that this map is nearly symmetric, i.e., regions that led to regularized spiking-bursting rhythms correspond to values of maximal conductances g_{12} and g_{21} that do not differ much beyond $0.02\mu S$. Thus, for temporal symmetric fast inhibitory synapses, regularization occurs for closely symmetric maximal conductance values.

The right panel in ***Figure 8.2*** shows two examples of regular and irregular alternating bursting activity for representative values of g_{12} and g_{21} conductances. Note the symmetric interburst interval relationships of the regular spiking bursting rhythm, which corresponds to the nearly symmetric values of the maximal conductances.

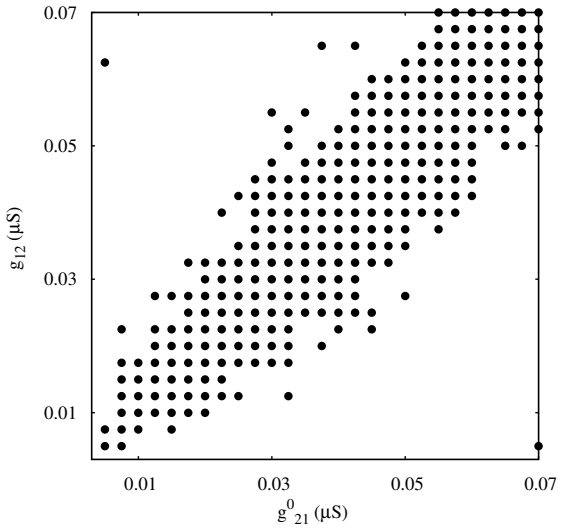

Figure 8.3: Map of conductances g_{12} and g_{21} that led to regularization of the spiking-bursting activity for the connection topology with fast symmetric temporal dynamics. The incremental step for both g_{12} and g_{21} was 0.0025 μS. Black circles represent values that led to regular activity ($C_v < 5\%$). The symmetric distribution of the circles in the map reflects the balanced temporal dynamics of the fast synapses, which in general allows only moderate differences in the maximal conductances to achieve regularity. A similar map was shown in ***Figure 7.6*** that was generated using different sets of parameters, see methods in sections 8.2.2 and 7.2.2.

8.3.2 Regularized activity in mutually inhibitory oscillator circuits with temporal asymmetry

Here we focus on the analysis of a mutually inhibitory circuit with temporal synaptic asymmetry. In this case, we considered mutual inhibition with a slow synapse in one direction and a fast synapse in the other (see left panel in ***Figure 8.2***B). This asymmetry is present in half-center oscillators that built up central pattern generators (Marder and Eisen, 1984). ***Figure 8.4*** represents the map of conductances g_{12} and g_{21} that led to regularized rhythms consisting of alternating spiking-bursting activity between the two neurons. It is important to emphasize that in this case asymmetry in the maximal conductances coexists with the temporal asymmetry of the slow and fast synapses in the circuit. Note the reduced size and the sparser distribution of maximal conductances that led to regularized spiking-bursting rhythms, which was caused by the synaptic imbalance introduced by the temporal asymmetry. ***Figure 8.2***B illustrates two examples of regular and irregular spiking-bursting activity, respectively, for representative values of g_{12} and g_{21} conductances. One can see the asymmetric interburst intervals of the regular rhythm as compared to the one depicted in ***Figure 8.2***A.

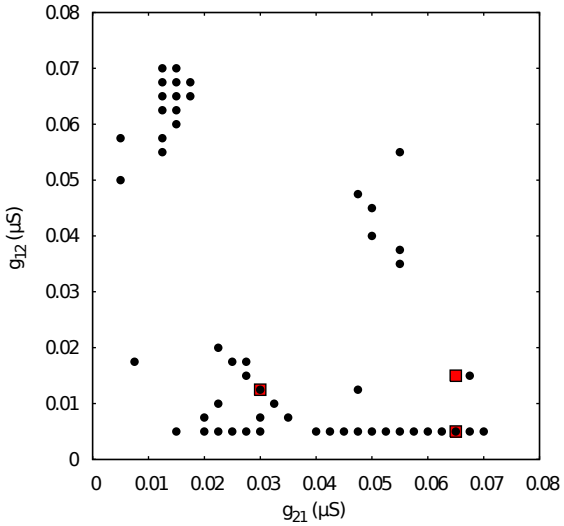

Figure 8.4: Map of conductances g_{12} and g_{21} of the temporal asymmetric mutually inhibitory circuit that led to regularization of the spiking-bursting activity. The incremental step for both g_{12} and g_{21} was 0.0025 μS. Black circles represent values that led to regular activity ($C_v < 5\%$). The map shows a reduced number of configurations of parameters that led to regular activity as a consequence of the temporal asymmetry in the connection between the neurons. Parameters: k_1 =0.6 ms^{-1}, k_2= 0.27 ms^{-1}. Red squares correspond to specific values of g_{12} and g_{21} that were used for an analysis of k_1 vs k_2 maps.

Next, we chose representative values of the maximal conductances in the temporal asymmetric circuit (indicated by red squares in ***Figure 8.4***) and using the same methodology, we explored the parameter space of the time constants k_1 and k_2, which control the temporal aspects of the slow synapse. ***Figure 8.5*** shows this analysis for fixed g_{21}=0.03μS and g_{12}=0.0125 μS, corresponding to a regularized activity regime in ***Figure 8.4***. Note the presence of k_2 bands where regularity occurred for large regions of k_1 values for this particular selection of maximal conductances. The size of these bands, and thus the size of the regions with regular activity, depend on the values of the maximal conductances of the mutually inhibitory circuit.

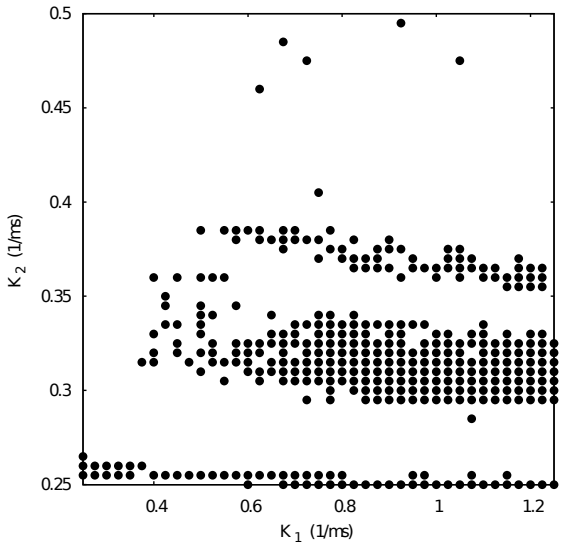

Figure 8.5: Map of slow synaptic time constants k_1 and k_2 of the temporal asymmetric mutually inhibitory oscillator circuit that led to regularization of the spiking-bursting activity. Parameters: g_{21}=0.03 μS, g_{12}=0.0125 μS (see red squares in ***Figure 8.4***). The incremental step for k_1 and k_2 was 0.025 ms^{-1} and 0.005 ms^{-1}, respectively. Black circles represent values that led to regular activity ($C_v < 5\%$).

Figure 8.6 shows the k_1 vs k_2 map for fixed g_{21}=0.065μS and g_{12}=0.005 μS. Note that such conductance values also correspond to regular spiking-bursting activity in the map depicted in ***Figure 8.4***. In spite of the large maximal conductance difference, the resulting combination of conductance and temporal asymmetries in the mutual inhibition led to a broad region of regular spiking-bursting activity. Irregular regimes are mostly in the region defined by $k_2 < 0.3$

We selected from ***Figure 8.4*** a set of maximal conductances that correspond to irregular spiking-bursting activity (e.g. g_{21}=0.065μS and g_{12}=0.015 μS) and varied k_1 vs k_2 to produce the map with reduced regularity bands shown in ***Figure 8.7***. Nevertheless, one can observe that the temporal asymmetry can compensate the conductance unbalance to achieve regular regimes.

8.3.3 Regularized activity in mutually inhibitory oscillator circuits with gap-junction induced asymmetry

Finally, in addition to the asymmetric connectivity in the network, we have considered another source of asymmetry common in many CPG's (Selverston and Moulins, 1987) by replacing one of the neurons in the former circuit with two electrically coupled cells (see left panel in ***Figure 8.2***C). The gap-junction synchronizes the activity of neurons 2 and 3. It is important to note that in this configuration there are two slow and two fast inhibitory graded synapses. Note also the interburst interval asymmetry of the regular regimes in this configuration. To analyze the contribution of this topological asymmetry to the generation of regular and irregular rhythms, we have fixed the synaptic time constants to k_1=0.6 ms^{-1}, k_2=0.27 ms^{-1} and the gap-junction conductance $g^{gj}_{23,32}$=0.0045 μS.

Figure 8.8 shows the map of conductances g_{12} and g_{21} that led to regularized alternat-

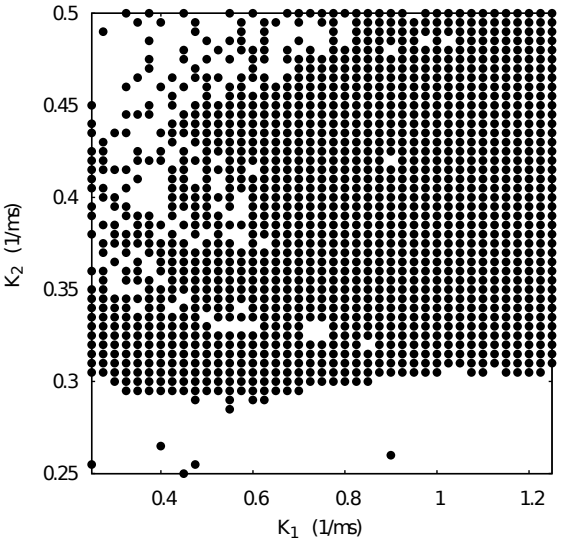

Figure 8.6: Map of slow synaptic time constants k_1 and k_2 of the temporal asymmetric mutually inhibitory oscillator circuit that led to regularization of the spiking-bursting activity. Parameters: g_{21}=0.065 μS, g_{12}=0.005 μS (see red squares in ***Figure 8.4***). The incremental step for k_1 and k_2 was 0.025 ms^{-1} and 0.005 ms^{-1} respectively. Black circles represent values that led to regular activity ($C_v < 5\%$).

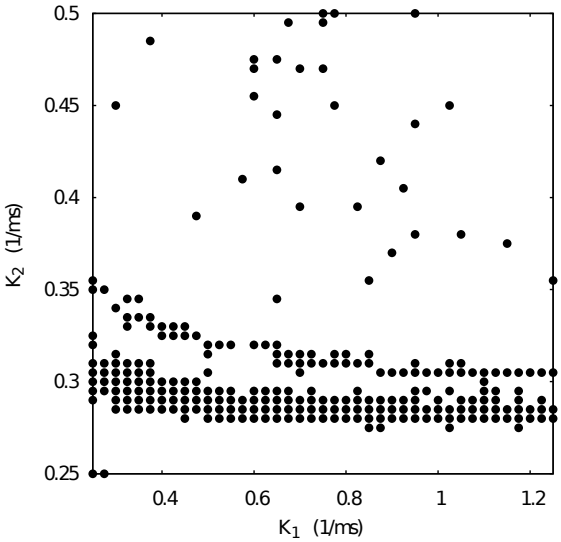

Figure 8.7: Map of slow synaptic time constants k_1 and k_2 of the temporal asymmetric mutually inhibitory oscillator circuit that led to regularization of the spiking-bursting activity. Parameters: g_{21}=0.065 μS, g_{12}=0.015 μS (see red squares in ***Figure 8.4***). The incremental step for k_1 and k_2 is 0.025 ms^{-1} and 0.005 ms^{-1} respectively. Black circles represent values that lead to regular activity ($C_v < 5\%$).

ing bursting activity in this configuration. One can observe that the regularity regions were larger than in the corresponding case for the circuit with only temporal synaptic asymmetry (cf. ***Figure 8.4***). This result hints that the gap-junction connectivity, with its associated dynamical inertia, could contribute to enlarge the regions of regular spiking-bursting activity in living half-center oscillators.

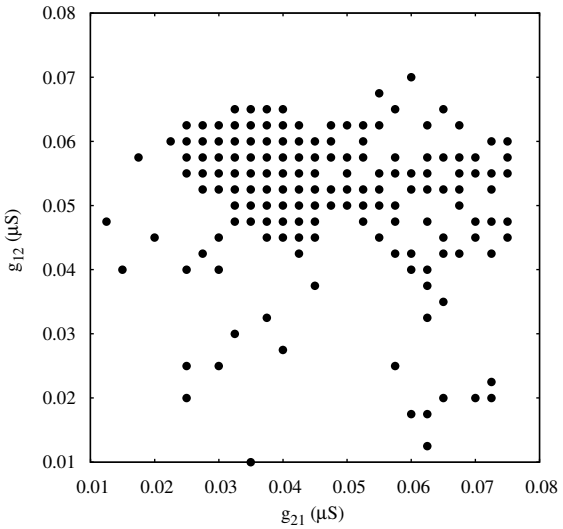

Figure 8.8: Map of conductances g_{12} and g_{21} of the circuits with gap-junction induced asymmetry that led to regularization of the spiking-bursting activity where the incremental step for both g_{12} and g_{21} is 0.0025 μS. Black circles represent values that lead to regular activity ($C_v < 5\%$). Parameters: k_1=0.6 ms^{-1}, k_2=0.27 ms^{-1}, $g^{gj}_{23,32}$=0.0045 μS.

8.3.4 Closed-loop exploration for regular bursting rhythms

In the previous sections, we have presented a modeling study in minimal mutually inhibitory circuits of the asymmetry factors that contribute to shape regular and irregular spiking-bursting rhythms. The hypotheses drawn in these sections can be tested experimentally. Dynamic clamp can be used to modify maximal conductances and synaptic temporal characteristics by building hybrid circuits composed of living neurons and artificial synapses 4. As the time to perform such experiments is restricted and the number of configurations that can be tested is typically small, a close-loop exploration method can be used (Reyes-Sanchez et al., 2018). The closed-loop algorithm can control the dynamics by changing a set of parameters of the network to achieve a specific goal (e.g. the regularization of the bursting activity). These sets of parameters are updated in every iteration according to a designed rule (which should be simple due to time restrictions) until the goal is achieved.

Following the same logic as in chapter 7, we have validated the method in the context of the half-center oscillator model with temporal asymmetric synapses and g_{21}=0.065 μS, g_{12}=0.005 μS. In this case, the closed-loop algorithm updated the value of the synaptic time constants $k_{1,2}$, according to the difference between the current period P_1 and the average of the periods of the last five bursts $\langle P_1 \rangle$, trying to find a suitable new set of values that led to regular activity $C_v < 5\%$, which was the goal of this closed-loop exploration. The departing points were different sets of configurations of the synaptic time constants k^0_1 and k^0_2 that drove the system into alternating irregular spiking-bursting activity. Every time a new burst *n* was generated in neuron 1, the algorithm checked if the coefficient of variation of the period calculated for the last 5 bursts C_v was below the established regularity threshold 5%. Then, the values of the synaptic time constants were updated as follows:

$$k^n_{1,2} = k^{n-1}_{1,2} - \alpha \cdot \left(\langle P_1 \rangle - P^n_1 \right),$$

where α was the rate for the synaptic time constant change, $\langle P_1 \rangle$ was the average period of neuron 1 calculated with the last five bursts and P_1^n was the current period. In this study we set $\alpha = 0.01$. This value and the monitoring of the last five bursts provided a good balance between a reasonable online measurement of the regularity and a fast convergence to the closed-loop goal.

Figure 8.9 shows the evolution of three sets of departing time constants k_1^0 and k_2^0 during the closed-loop protocol displayed over a map of slow synaptic time constants that led to regularized rhythms (gray circles), see ***Figure 8.6***. In these three examples, the departing values are located in empty regions in the maps ($C_v > 5\%$) and at the end of the protocol, the new set of values k_1^f and k_2^f are located within the gray circles area ($C_v < 5\%$). Noting the color code, one can observe that the changes in $k_{1,2}^n$ became quite large during the first few interactions since this change is proportional to the difference between the period at that cycle and the average of the periods of the last five bursts. The protocol was able to find the regular spiking-bursting regimes in only a few iterations. The departing irregularity and the achieved regularized activity of the circuit after the closed-loop protocol are shown in ***Figure 8.10***.

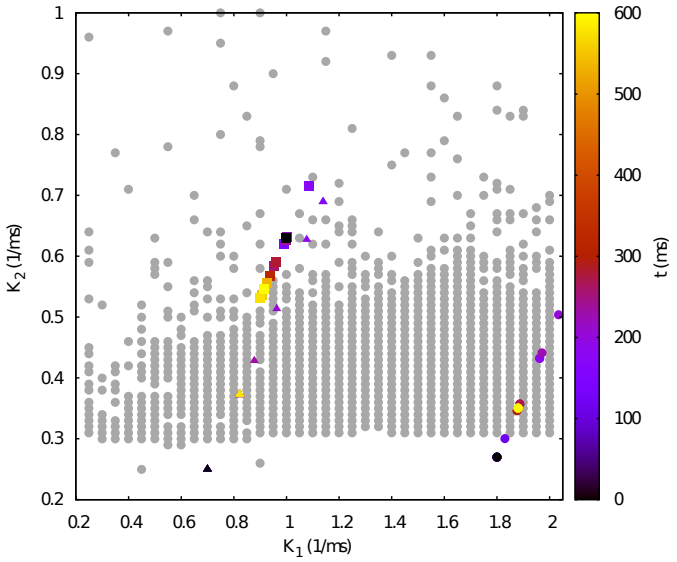

Figure 8.9: Evolution of the synaptic time constants k_1 and k_2 of the low synapse in a half-center oscillator during closed-loop exploration for regular bursting rhythms. The figure shows the evolution of the values of k_1 and k_2 in time (color bar in s) for three different departing values (coded in black): squares points, k_1^0=1.00 ms^{-1}, k_2^0=0.63 ms^{-1}; triangle points, k_1^0=0.70 ms^{-1}, k_2^0=0.25 ms^{-1}; circle points, k_1^0=1.80 ms^{-1}, k_2^0=0.27 ms^{-1}. Final values after the closed-loop exploration (coded in yellow): squares points, k_1^f=0.92 ms^{-1}, k_2^f=0.55 ms^{-1}; triangle points, k_1^f=0.82 ms^{-1}, k_2^f=0.37 ms^{-1}; circle points, k_1^f=1.89 ms^{-1}, k_2^f=0.35 ms^{-1}. Gray circles in the background represent the map of slow synaptic time constants k_1 and k_2 that led to regularization of the spiking-bursting activity, using the same parameter configuration as in ***Figure 8.6***. The incremental step for k_1 and k_2 was 0.05 ms^{-1} and 0.01 ms^{-1} respectively. The protocol searched for a suitable value of both synaptic time constants which drove the system into a regular bursting activity, $C_v < 5\%$ (gray circle points). Parameters: g_{21}=0.065 μS, g_{12}=0.005 μS.

This closed-loop protocol allows different configurations and optimizations. The experimenter can choose to modify time constants k_1 and k_2 simultaneously or one at a time, for example only k_2 to unveil the regularity bands shown in ***Figure 8.5*** and ***Figure 8.7***. The protocol can also include a nonlinear dependence on the difference between the current and the averaged bursting period, as well as other search methods (e.g. gradient descent,

stochastic search) and alternative performance measurements to evaluate online the regularization goal.

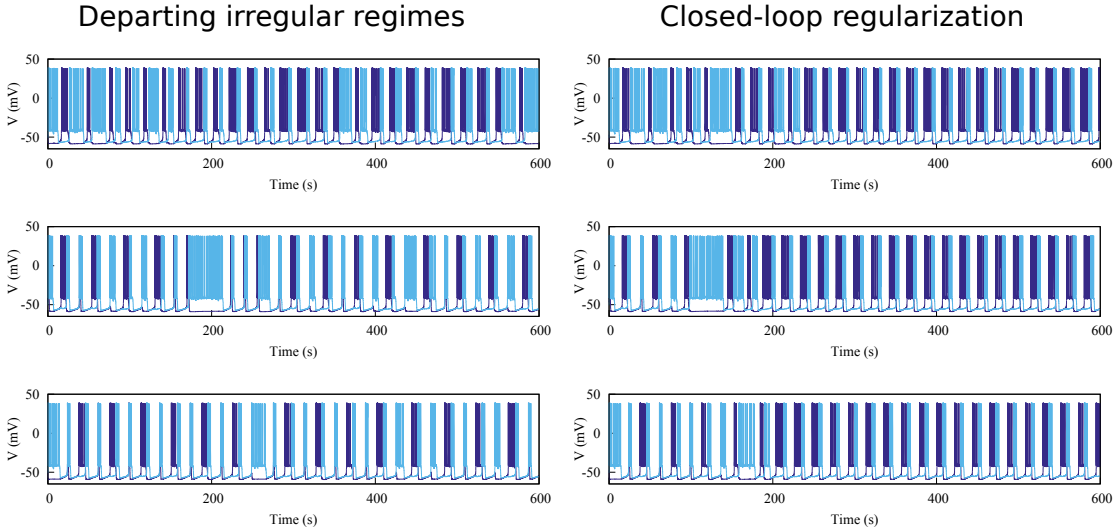

Figure 8.10: Departing irregular regimes and closed-loop exploration for regular activity for the three cases discussed in ***Figure 8.9*** in a circuit with synaptic temporal asymmetry. Left panels show the departing irregular activity for the following slow synaptic time constants: k_1^0=1.00 ms^{-1}, k_2^0=0.63 ms^{-1}, k_1^0=0.70 ms^{-1}, k_2^0=0.25 ms^{-1} and k_1^0=1.80 ms^{-1}, k_2^0=0.27 ms^{-1}. Right panels show the regularization obtained through the closed-loop (cf. evolution of time constants in ***Figure 8.9***). Note that the protocol was able to find the regular regimes in a very short time. Maximal conductance parameters: g_{21}=0.065 μS, g_{12}=0.005 μS.

8.4 Discussion

Using realistic conductance-based models of half-center oscillator based CPG circuits, in this chapter we have addressed the study of synaptic asymmetry to shape robust alternating spiking-bursting rhythms. In particular, we focused on the analysis of the asymmetry of synaptic maximal conductances and time constants in the reciprocal inhibition of half-center oscillators. We have mapped the regimes of regular and irregular coordinated rhythms as a function of these parameters. We have shown that asymmetry both in the maximal conductances and in the temporal dynamics of mutually inhibitory neurons, including modulation by gap-junction connectivity, can synergistically contribute to shape large regions of regular spiking-bursting regimes in central pattern generator circuits. Regular rhythms resulting from realistic asymmetric synaptic configurations display specific interburst interval relationships that reflect the balance among the distinct sources of asymmetry.

Irregularity regimes are typically disregarded both in experimental and theoretical CPG research. One reason for this is that regular rhythms, as recorded in experimental setups, are more easily associated with observable rhythmic CPG motor functions. Several theoretical studies have shown that regular regimes could be more efficient for specific motor tasks (Huerta et al., 2000, 2001; Stiesberg et al., 2007). However, coordinated irregularity is also present in living CPGs under normal and pathological circumstances and might mediate key aspects of the rhythm negotiation in these circuits. Recent brute force approaches

to map the parameter space in half-center oscillator models inspired by the leech heartbeat CPG have also pointed out the presence of irregular regimes (Doloc-Mihu and Calabrese, 2011, 2016). In this chapter, we have shown that the asymmetric synaptic parameter space for the existence of regular and irregular coordinated rhythms in a conductance-based half-center oscillator is large. Previous modeling efforts that did not explore synaptic asymmetry hinted that intrinsic neuron irregularity easily disappeared under mutual inhibition in CPG half-center oscillator circuits, e.g. see (Varona et al., 2001a,b). Here we have seen how half-center oscillations can be modulated and coordinated by asymmetrical factors in the mutual inhibition of its constituent neurons, (Elices and Varona, 2017). The study of irregular regimes in the case of realistic asymmetric synapses can shed further light to understand the balance between robustness and flexibility in central pattern generator circuits.

There are known asymmetries in the connectivity of CPG half-center oscillators. However, their role in shaping the circuit rhythm has not been explored in detail. In this chapter, we have shown that a closed-loop protocol adapting online the synaptic parameters under a regularization goal can be an effective methodology to map and characterize the coordination properties that arise from both the connection topology, including their asymmetry, and the individual neuronal dynamics in these circuits. We believe that customized versions of this protocol can be used in experimental setups, where there is no time to explore the whole parameter space, to address the hypotheses drawn by the discussed model.

Chapter 9

Role of asymmetry connectivity in shaping robust sequences activity in a conductance model

In this chapter, we relate the work presented in chapter 6 with the two previous chapters by considering a simplified model of the pyloric CPG. Since the analyses of the experiments indicate that the asymmetric connection may be, at least partially, involved in producing the dynamical invariants observed experimentally, here we study how the triphasic rhythm is generated by means of the connectivity and address the study of the presence of the dynamical invariants in CPG models.

9.1 Introduction

Previous studies in the pyloric CPG have reported approximate phase maintenance for motor function (Grillner and Kashin, 1976; Dicaprio et al., 1997; Fischer et al., 2001). In particular, modeling works have tried to explain phase maintenance in terms of short-term depression or the interaction between synaptic depression and the kinetics of different currents by inducing fixed frequency variations (Greenberg and Manor, 2005; Hooper et al., 2009). Model databases, which are known to have regions of irregular bursting activity, are only used in the regular regimes to address this phase maintenance (Soofi et al., 2012). There is a vast variety of models of the pyloric CPG, each one with specific realistic aspects and simplifications. However, to our knowledge, none of them can replicate the intrinsic variability observed in the autonomous rhythm as quantified experimentally *in vitro* (Elices et al., 2019) or *in vivo* (Rezer and Moulins, 1983; Clemens et al., 1998; Soofi et al., 2014).

In chapter 6 we studied both regular and irregular pyloric CPG rhythms and unveiled two robust dynamical invariants in the form of linear relationships between pivotal time intervals that build the sequence. We also observed that the specific asymmetric connectivity of the pyloric network plays a key role in shaping the invariants. Moreover, our model study in last chapter showed that asymmetry both in the maximal conductances and in the temporal dynamics of mutually inhibitory neurons can synergistically contribute to shape wide regimes of regular spiking-bursting activity in central pattern generators.

Departing from our model work in the previous chapter, here we have considered a

Table 9.1: Values for the fixed maximal conductances (units in μS) and time constants (units in ms^{-1}) used in the Hodgkin-Huxley description for the modeling study reported in this paper.

g_{PD_1PY}	g_{PD_2PY}	g_{LPPY}	g_{PYLP}	$g_{PD_1PD_2}$	$K1_{PD_{1,2}LP}$	$K2_{PD_{1,2}LP}$	$K1_{PD_{1,2}PY}$	$K2_{PD_{1,2}PY}$
0.005	0.0057	0.006	0.00611	0.004	0.6	0.4	0.6	0.27

simplified model of the pyloric CPG to study the influence of the asymmetry in time scale and strength of the connections in producing the triphasic sequence (LP-PY-PD) and the presence or absence of the invariants in the CPG rhythm.

9.2 Methods

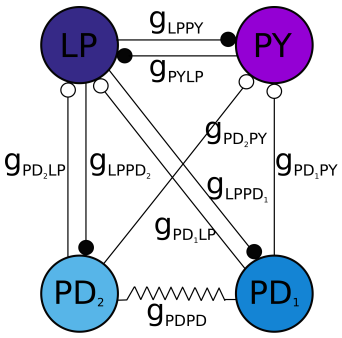

Figure 9.1: Schematic circuit of the model. Black and white circles represents fast and slow chemical synapses respectively.

The neuron model used in this study is again the Hodgkin–Huxley type model proposed by Komendantov and Kononenko; see section 3.2.1. The parameters used in this study are the same as those specified in the appendix of (Komendantov and Kononenko, 1996) for the chaotic bursting regime to introduce intrinsic variability within the rhythm. Graded chemical slow and fast synapses were implemented as described in section 3.3, see also (Latorre et al., 2006; Elices and Varona, 2015, 2017). Values for the maximal conductances and time constants of the synapses used in all simulations are shown in ***Table 9.1***. All the equations of our models were numerically solved with a 5(6) Runge-Kutta variable step method and implemented in Julia.

The model was built up with four neurons whose schematic circuit is depicted in ***Figure 9.1***. In this model circuit, the neuron that represents LP is connected to two electrically coupled PD neurons. Note that the connectivity between the LP and the PD neurons preserves also the asymmetry observed experimentally, with slow and fast graded chemical synapses as discussed in the previous chapter. In addition, the LP is connected to a PY neuron with asymmetric fast graded chemical synapses. The electrically coupled PD neurons were connected to the single LP neuron and PY neuron with slow chemical synapses. Therefore, the circuit represents the kernel of the living pyloric system that gives rise to a *triphasic rhythm* (LP-PY-PD sequence), see 2.5.2.

9.3 Results

The analyses of the experimental data discussed in chapter 6 indicate that the asymmetric connection may be involved, at least partially, in producing the invariant. To address this question, we have considered the simplified model of the CPG describe above to study how the time scale and strength of the connections underlie the triphasic rhythms (LP-PY-PD sequence) and if the dynamical invariants can be reproduced in this model circuit.

Four different rhythms were produced by adjusting the value of the maximal con-

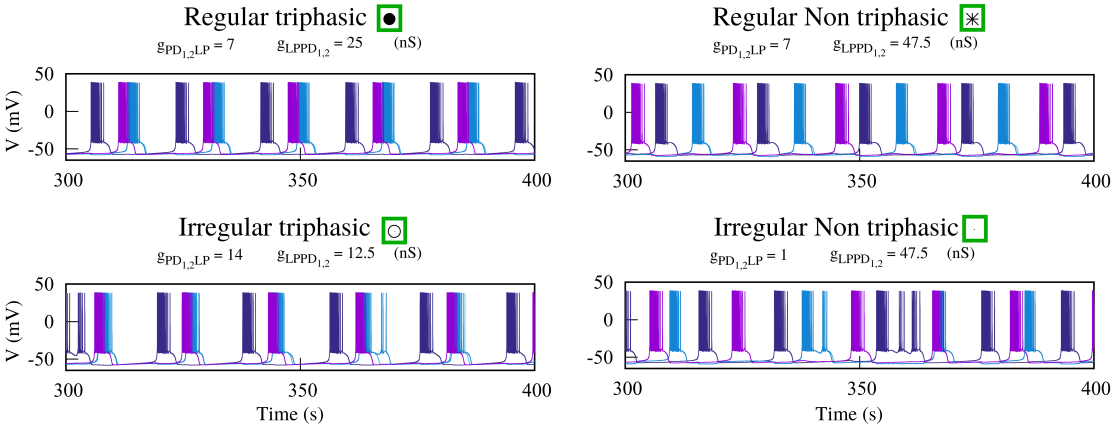

Figure 9.2: Examples of activity of the circuit in four different regimes based on the values of maximal conductances used. Left upper panel: regular triphasic (LP-PYs-PDs order) spiking-bursting activity ($g_{PD_{1,2}LP} = 7\ nS$, $g_{LPPD_{1,2}} = 25\ nS$); Left bottom panel: irregular triphasic spiking-bursting activity ($g_{PD_{1,2}LP} = 14\ nS$ $g_{LPPD_{1,2}} = 12.5\ nS$); Right upper panel: regular non-triphasic spiking-bursting activity ($g_{PD_{1,2}LP} = 7\ nS$ $g_{LPPD_{1,2}} = 47.5\ nS$); Right bottom panel: irregular non-triphasic spiking-bursting activity ($g_{PD_{1,2}LP} = 1\ nS$ $g_{LPPD_{1,2}} = 47.5\ nS$).

ductances: regular (defined as $C_v < 5\%$); irregular triphasic (LP-PY-PD sequence) spiking-bursting activity (in ***Figure 9.2***), which can be related to the activity produced by a CPG in control conditions and under ethanol, respectively; and regular and irregular non-triphasic spiking-bursting rhythms (defined as generating sequences different than the LP-PY-PD activation order). The values of the maximal conductance, $g_{PD_{1,2}LP}$ $g_{LPPD_{1,2}}$ that led to these different types of behavior are represented in maps in ***Figure 9.3***.

The map on the left panel corresponds to the realistic version of the circuit shown in panel A with fast and slow synapses. The majority of the explored pairs of maximal conductances corresponded to regular and irregular triphasic rhythms, which are represented by colored filled and empty circles, respectively. The map on the right corresponds to a symmetric version of the circuit in which the slow synapses were replaced by fast synapses. In this case, the number of combinations of maximal conductances that produced both regular and irregular triphasic activity was significantly lower. It can be observed that both asymmetric maximal conductances and inhibitory synaptic time scales contributed to the shaping of wide regimes of regular and irregular triphasic spiking-bursting activity. In both figures, the color palette represents the Pearson correlation coefficient ρ between $Period$ and the $LPPD\ interval$ in the model for pairs presenting triphasic rhythm. Most of the explored pairs of maximal conductances had low correlation coefficients and therefore the dynamical invariant $LPPD\ interval[Period]$ was not present for the explored configurations. When the $Period$ is represented against $LPPD\ interval$ (analogously as in ***Figure 6.3***), for pairs of conductances with high values of ρ, the cycle-by-cycle points values are clustered in groups without a clear linear tendency. Further analysis of these configurations of maximal conductances revealed low excess kurtosis, which confirmed their data distribution was heterogeneous, and therefore a linear regression is not a good fit (circles in black). Thus, we can conclude that the invariant $LPPD\ interval[Period]$ was not present in the wide variety of explored configurations of the model. Analysis for $LPPD\ delay[Period]$ yields the same conclusions (not shown).

To characterize the variability of the regular and irregular triphasic rhythms generated by the circuit (see ***Figure 9.1***) we have studied the duration distribution of the sequence intervals. ***Figure 9.4*** and ***Figure 9.5*** show histograms of the interval durations of a repre-

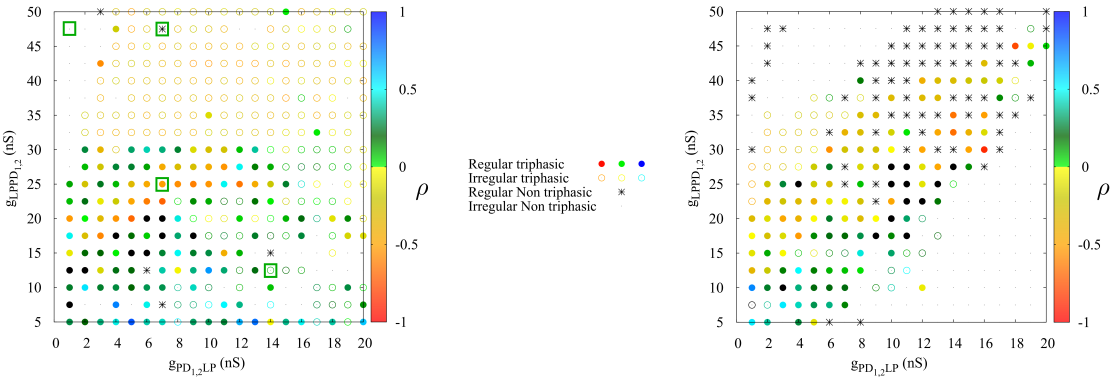

Figure 9.3: Maps of the maximal conductances that lead to the different types of rhythms. Left panel corresponds to the more realistic circuit with fast and slow synapses. Both asymmetric maximal conductances and inhibitory synaptic time scales contribute to the shaping of wide regimes of regular and irregular triphasic spiking-bursting activity. Right panel corresponds to a symmetric version of the circuit using only fast synapses. Regular and irregular triphasic activity is more restricted in this case. Color palette in both figures represents the Pearson correlation coefficient ρ between $Period$ and the $LPPD\ interval$ in the model. Most of the values are close to zero. Further analysis of the higher values reveals a low excess kurtosis ($EK < -1.0$), which means their data distribution is heterogeneous, thus the linear regression does not correctly represent the relationship (circles in black).

sentative example in regular and irregular triphasic regimes, respectively. This analysis is analogous to the one performed in chapter 5. The coefficients of variation of the intervals for different configurations of maximal conductances in both triphasic regimes are shown in ***Table 9.2***. One can observe that despite the high variability present in several time intervals of irregular regime configurations, in particular in BD_{LP}, the distributions of the interval durations obtained in the model are very different from the distributions obtained in the living system. In the model, certain intervals BD_{LP}, $LPPD\ interval$ and $Period$ presented cluster distributions characterized by "forbidden" interval durations that produce more discrete histograms. This is absent in the analyses of the experimental data recordings, which always produced continuous histograms (c.f. ***Figure 5.4*** and ***Figure 5.5***).

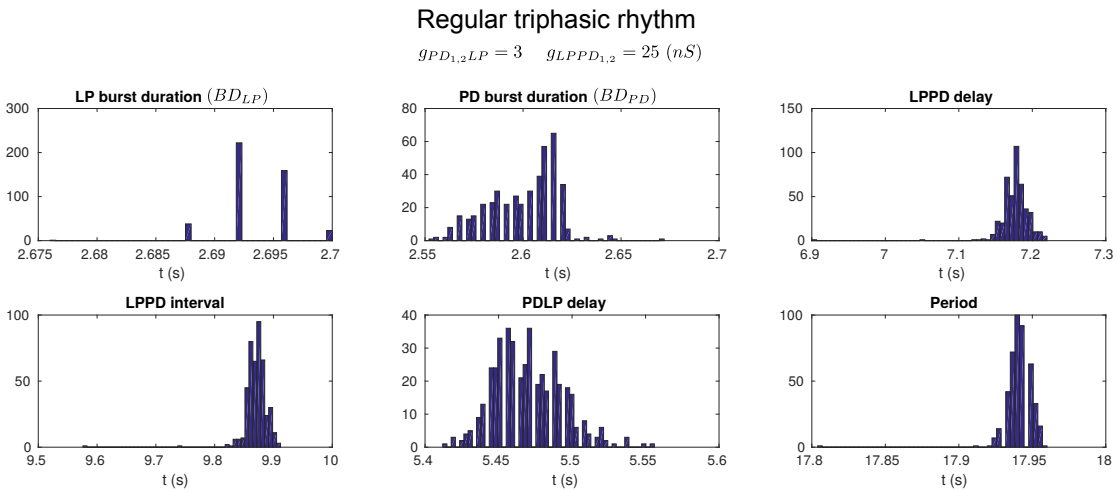

Figure 9.4: Histograms of the interval duration distributions of a representative example of regular triphasic activity regime (see ***Table 9.2***). Note the lower variability present in the intervals as compared to the distributions obtained from the living system, c.f. ***Figure 5.4*** and ***Table 5.1***, and the cluster distribution of the BD_{LP}. Maximal conductances: $g_{PD_{1,2}LP} = 3\ nS$ $g_{LPPD_{1,2}} = 25\ nS$.

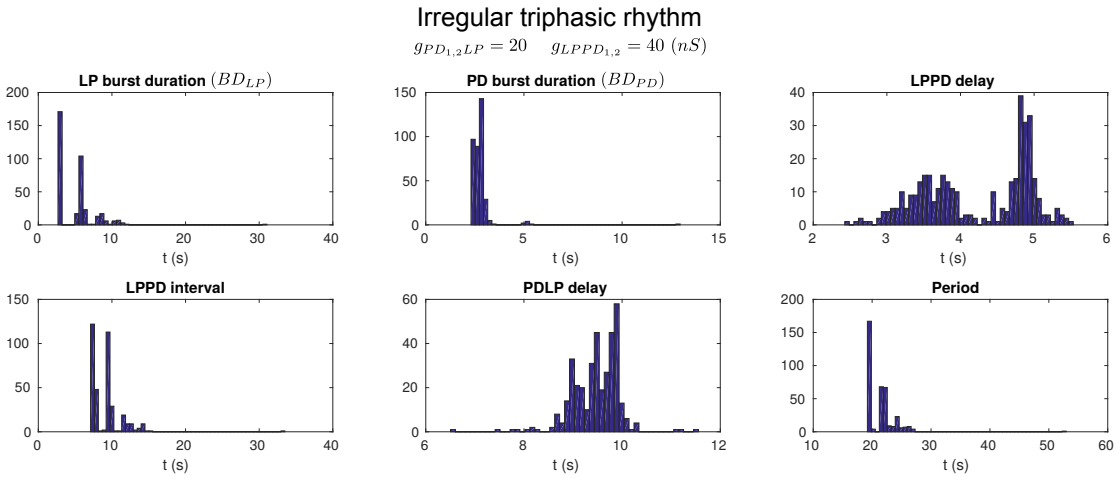

Figure 9.5: Histograms of the interval duration distributions of a representative example of irregular triphasic activity regime (see ***Table 9.2*** and ***Figure 9.4***). Note the change in the scale of the duration for the different intervals due to the higher variability of the activity. BD_{LP}, $LPPD\ interval$ and $Period$ present also cluster distribution, c.f. ***Figure 5.5***. Maximal conductances: $g_{PD_{1,2}LP} = 20\ nS$ $g_{LPPD_{1,2}} = 40\ nS$.

Table 9.2: Values of the coefficient of variation CV(%) of the considered intervals for 9 representative configurations regular and irregular triphasic regimes. Other experiments show similar results.

Triphasic regular regime CV(%)	$g_{PD_{1,2}LP} = 7$ $g_{LPPD_{1,2}} = 17.5$	$g_{PD_{1,2}LP} = 3$ $g_{LPPD_{1,2}} = 25$	$g_{PD_{1,2}LP} = 10$ $g_{LPPD_{1,2}} = 25$	$g_{PD_{1,2}LP} = 2$ $g_{LPPD_{1,2}} = 5$	$g_{PD_{1,2}LP} = 13$ $g_{LPPD_{1,2}} = 30$
BD_{LP}	18	0	19	18	45
BD_{PD}	5	1	2	27	20
$LPPD\ delay$	3	0	3	13	6
$LPPD\ inter.$	6	0	5	7	13
$PDLP\ delay$	5	0	2	11	5
$PDLP\ inter.$	4	0	2	4	6
$Period$	3	0	2	3	7

Triphasic irregular regime CV(%)	$g_{PD_{1,2}LP} = 4$ $g_{LPPD_{1,2}} = 35$	$g_{PD_{1,2}LP} = 8$ $g_{LPPD_{1,2}} = 4$	$g_{PD_{1,2}LP} = 14$ $g_{LPPD_{1,2}} = 47.5$	$g_{PD_{1,2}LP} = 18$ $g_{LPPD_{1,2}} = 30$	$g_{PD_{1,2}LP} = 20$ $g_{LPPD_{1,2}} = 40$
BD_{LP}	73	69	56	66	55
BD_{PD}	14	12	25	36	24
$LPPD\ delay$	20	21	21	17	17
$LPPD\ inter.$	18	21	20	29	24
$PDLP\ delay$	11	9	8	9	5
$PDLP\ inter.$	7	6	7	7	4
$Period$	11	12	11	14	12

9.4 Discussion

A model of the pyloric CPG was used to assess the role of the asymmetric connectivity between the neurons in shaping the rhythm and keeping the LP-PY-PD sequences even in irregular bursting regimes. We aimed to understand the intrinsic mechanisms for sustaining dynamical invariants not only during induced changes of the cycle period but, most importantly, on the transient dynamics of ongoing activity. This is the reason why we used a neuron model with intrinsic variability in the bursting activity. We also modeled realistic graded synapses with the observed asymmetry in the connections to search for dynamical invariants. By adjusting the value of the maximal conductances of the synapses of the model, four different rhythm types can be produced: regular (defined as $C_v < 5\%$); irregular triphasic (LP-PY-PD sequence) bursting activity, which can be related to the activity produced by a CPG in control conditions and with intrinsic irregularity, respectively; and regular and irregular non-triphasic bursting rhythms.

The results show that both asymmetric maximal conductances and inhibitory synaptic time scales contribute to the shaping of wide regimes of regular and irregular triphasic spiking-bursting activity. The model did not reproduce the invariants found in the experiments despite the intrinsic variability introduced by setting the individual neuron dynamics in a chaotic bursting regime. The study of the variability of the triphasic activity produced by the model with different sets of maximal conductances revealed that the model variability presented a rather different distribution as compared to the living system variability. The clustered distribution of the histograms indicates that the intrinsic variability of the model is not biologically realistic. One possible source for the model restricted variability is its bursting waveform, which is much more stereotyped than the one observed in the living system. The absence of the invariants suggests that the flexibility required to build them is not captured by commonly used conductance-based models. This result must be taken

with caution, as many biological factors were not considered in the model description. On the one hand, the model circuit was realistic but simplified. Several neurons (AB, VD and IC) were not included and the PY population was simplified as a single neuron. On the other hand, individual model neurons were not tuned to reproduce cell heterogeneity in the form of neuron-specific waveforms and spike temporal structure (Szücs et al., 2003). Other existing pyloric CPG network models that have been used to explain phase maintenance (Greenberg and Manor, 2005; Soofi et al., 2012) are unlikely to generate the observed cycle-by-cycle invariants, at least within the typical regular spiking bursting regime of the constituent individual neurons.

Part IV

Results: Propagation of dynamical invariants in Hybrid Circuits

Chapter 10

Propagation of dynamical invariants in Hybrid Circuits

In the previous chapters, we showed that the asymmetry in both maximal conductances and the inhibitory synaptic time scale contribute to shape regimes of triphasic spiking-bursting activity. However, the models could not reproduce the dynamical invariants found in the experiments. This result suggests that, despite the intrinsic variability introduced by setting the individual neuron dynamics in a chaotic bursting regime, the flexibility and variability required to build the invariants are not captured by the model.

In this chapter, we continue our study of dynamical invariants by building hybrid circuits by connecting a living neuron of the pyloric CPG to a model neuron. Hybrid circuits combine the best features of computer modeling and experimental electrophysiology. In particular, the rich dynamics of living systems and the variability of the rhythm can be incorporated into a hybrid system. Our results indicate that dynamical invariants can be propagated through artificial synapses but only under certain configurations.

10.1 Introduction

To better understand the origin and relevance of the unveiled dynamical invariants and their role in balancing flexibility and robustness in the rhythm, we have designed and implemented hybrid circuits by connecting neuron models to the living CPG circuit (Selverston et al., 2000; Prinz et al., 2004a; Amaducci et al., 2019; Reyes-Sanchez et al., 2018). Using models of fast and slow graded chemical synapses, we connected the living LP neuron to a model neuron. We show that as a function of the connectivity parameters dynamical invariants arise between living and model neurons. We discuss the conditions under which new dynamical invariants arise in the hybrid circuit.

10.2 Methods

Electrophysiology was performed following the same procedure as in section 5.2.1. For these experiments, the LP neuron was chosen to build the hybrid circuit since it does not

have electrical connections to any other cell in the circuit and is relatively easy to find in most preparations. LP neuron was previously identified by means of the waveform and the corresponding spikes in the extracellular nerve. To implement the hybrid connections, current injection was delivered using a second electrode on the same neuron. This current was implemented by a dynamic clamp protocol in which both living and model neuron voltages are adapted to the same scale in real-time, using the RThybrid software (Amaducci et al., 2019; Reyes-Sanchez et al., 2018). The neuron model (*NM*) used in the hybrid circuits was the Izhikevich model, which is detailed in section 3.2.2. The synapse models used to implement the different hybrid circuit configurations of connections were: gap junctions, fast graded and slow graded synapses, which are explained in section 3.3.

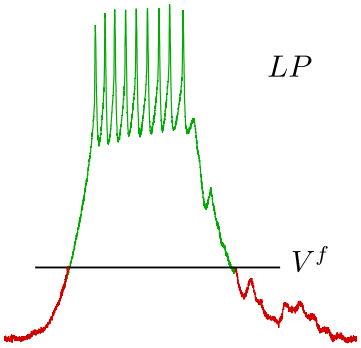

Figure 10.1: Schematic representation of the effect of the V^f parameter. V^f determines the threshold from which the graded synapse starts to act. This parameter controls the timing of the model bursts with respect to the living neuron and, thus, affects $LPNM\ interval$ and $LPNM\ delay$.

The maximal conductances between the living and model neurons were automatically calibrated to achieve an effective interaction allowing both neurons to work in their natural dynamical regime. In addition to the calibration of the maximal conductances, other parameters were used to tune the hybrid connections: the time scale constants k_1 and k_2 to control the speed and duration of the slow synaptic currents and V^f, which determines the threshold of the graded synapse. In particular, V^f is a key parameter to control the timing in which the model bursts begin, since, by changing this threshold, the plateau of the previous burst in the living neuron can delay the beginning of the model burst if it set low enough (see ***Figure 10.1***).

To perform an analogous analysis to the one used to unveil the dynamical invariants, new intervals were defined for the hybrid circuits: $LPNM\ delay$: interval defined from the LP last spike to the NM first spike; $LPNM\ interval$: interval defined from the LP first spike to the NM first spike; $Period$: interval from the LP first spike to the next LP first spike in the following burst. ***Figure 10.2*** shows an example of the activity of a hybrid circuit between the LP neuron and an Izhikevich model neuron. The newly defined intervals are also represented.

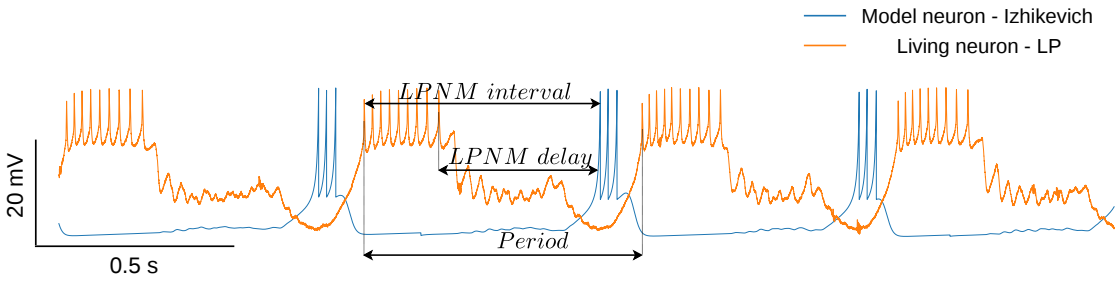

Figure 10.2: Scheme of the redefinition of the time intervals between the living and model neurons: $LPNM\ delay$: interval defined from the LP last spike to the NM first spike; $LPNM\ interval$: interval defined from the LP first spike to the NM first spike; $Period$: interval from the LP first spike to the next LP first spike in the following burst.

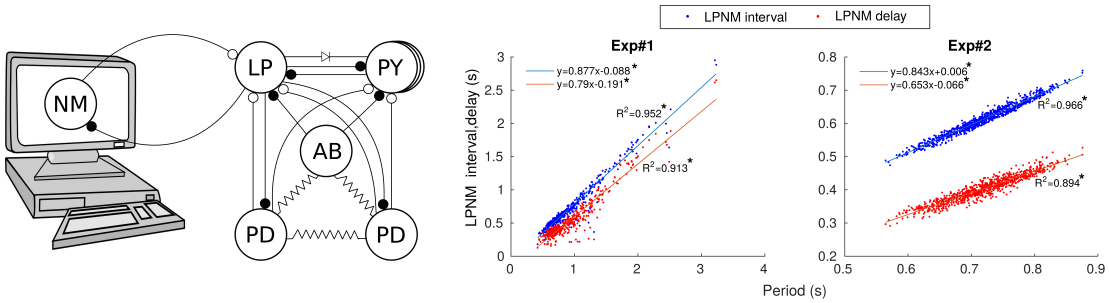

Figure 10.3: Presence of the two dynamical invariants with a bidirectional chemical synapse in two representative preparations. The correlation between $LPNM\ interval$ and $Period$ is shown in blue while the correlation between $LPNM\ delay$ and $Period$ is shown in red. Each point corresponds to one pyloric cycle of continuous recordings. Linear regressions are depicted for each experiment. Regression analysis showed that both $LPNM\ interval$ and $LPNM\ delay$ values increased with $Period$. The linear dependence is indicated by R^2 values displayed for each experiment in the corresponding panel. * Slope significantly different from 0 ($p < 8 \cdot 10^{-4}$).

10.3 Results

There are many possibilities to build hybrid circuits using different types of synapses and choosing the living neuron to build the connection. In this work, the living neuron selected to be connected to the model was the LP and the NM was the Izhikevich paradigm. Four hybrid circuits were built between the LP and Izhikevich model using different configurations of connectivity: bidirectional chemical graded synapses and inverse bidirectional electrical synapse, a monodirectional fast chemical synapse from LP to NM and a monodirectional slow chemical synapse from NM to LP.

10.3.1 Propagation of dynamical invariants with bidirectional chemical graded synapses

In this first configuration of hybrid circuit, we have connected the LP with the model neuron with a bidirectional chemical synapse that mimics the connection between the LP and PD neuron. From LP to NM we implemented a fast graded chemical synapse while for the opposite direction we used a slow graded chemical synapse (see left panel in ***Figure 10.3***). We found that the analogous relationships to ***Figure 6.1*** presented strong linear correlations in all preparations: the measured $LPNM\ delay$ and $Period$ and $LPNM\ interval$ and $Period$ (see ***Figure 10.2***). These dynamical invariants consistently remained tightly preserved with a slope close to one for many different preparations and under different conditions. Right panel in ***Figure 10.3*** illustrates these two preserved relationships for two representative experiments in control conditions with their corresponding linear regression.

10.3.2 Propagation of dynamical invariants with bidirectional inverse electrical synapse

We also tested if the invariants were present when the LP was connected to the NM with a bidirectional inverse electrical synapse. This type of synapse has been used before to achieve antiphase behavior in dynamic clamp preparations (Elson et al., 1998; Szucs et al.,

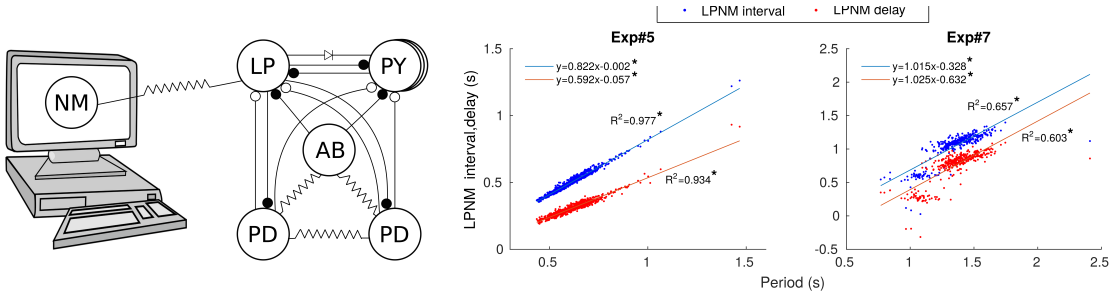

Figure 10.4: Presence of the two dynamical invariants with a bidirectional inverse electrical synapse in two representative preparations. The correlation between $LPNM\ interval$ and $Period$ is shown in blue while the correlation between $LPNM\ delay$ and $Period$ is shown in red. Each point corresponds to one pyloric cycle of continuous recordings. Linear regressions are depicted for each experiment. Regression analysis showed that both $LPNM\ interval$ and $LPNM\ delay$ values increased with $Period$. The linear dependence is indicated by R^2 values displayed for each experiment in the corresponding panel. * Slope significantly different from 0 ($p < 8 \cdot 10^{-4}$).

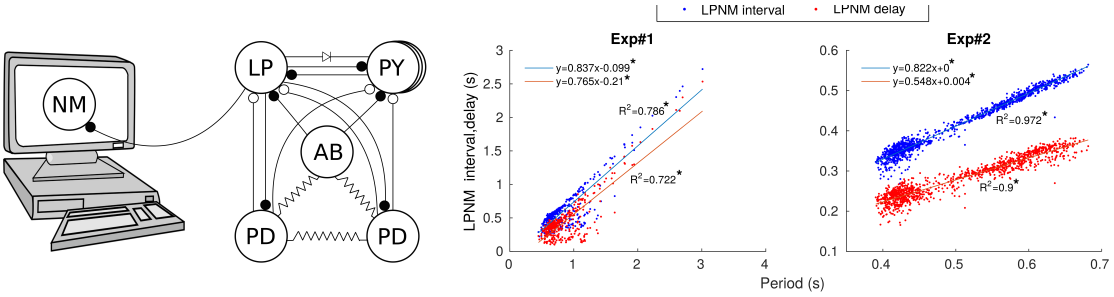

Figure 10.5: Presence of the two dynamical invariants with a monodirectional fast chemical synapse from LP to NM in two representative preparations. The correlation between $LPNM\ interval$ and $Period$ is shown in blue while the correlation between $LPNM\ delay$ and $Period$ is shown in red. Each point corresponds to one pyloric cycle of continuous recordings. Linear regressions are depicted for each experiment. Regression analysis showed that both $LPNM\ interval$ and $LPNM\ delay$ values increased with $Period$. The linear dependence is indicated by R^2 values displayed for each experiment in the corresponding panel. * Slope significantly different from 0 ($p < 8 \cdot 10^{-4}$).

2000). Right panel in ***Figure 10.4*** displays the invariants for two different representative experiments in control conditions with their corresponding linear regression. The values of the slopes and R^2 are very similar to the obtained with the chemical synapses.

10.3.3 Propagation of dynamical invariants with a monodirectional fast chemical graded synapse from LP to NM

We also explored the propagation of the invariant when the LP and the NM were only connected in one direction, from the living to the model neuron with a fast chemical synapse. As ***Figure 10.5*** shows, both invariants $LPNM\ interval$ and $Period$, and $LPNM\ delay$ and $Period$ are also present in this hybrid circuit. Again for these two representative examples, the slopes and R^2 values are similar to the other configurations.

10.3.4 Propagation of dynamical invariants with a monodirectional slow chemical graded synapse from NM to LP

In this last configuration, we connected the LP and NM in the reverse direction, from the model to the living neuron, with a slow chemical synapse. ***Figure 10.6*** shows that the lack of correlation among the $LPNM\ interval$ and $Period$, and $LPNM\ delay$, with R^2 values below 0.029.

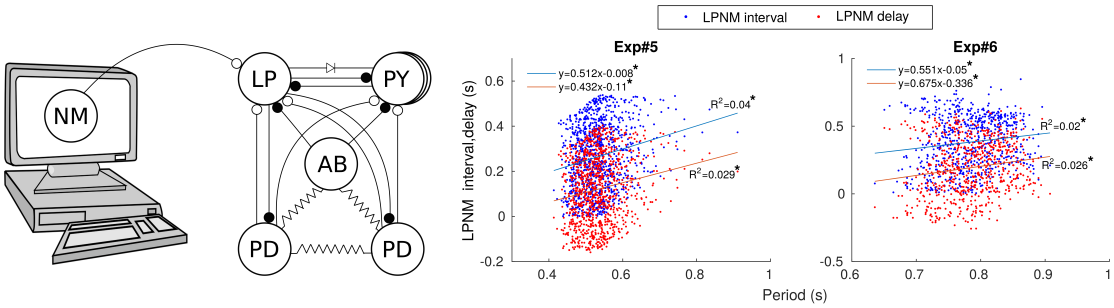

Figure 10.6: Presence of the two dynamical invariants with a monodirectional slow chemical synapse from NM to LP in two representative preparations. The correlation between $LPNM\ interval$ and $Period$ is shown in blue while the correlation between $LPNM\ delay$ and $Period$ is shown in red. Each point corresponds to one pyloric cycle of continuous recordings. Linear regressions are depicted for each experiment. Regression analysis showed that both $LPNM\ interval$ and $LPNM\ delay$ values did not increase with $Period$. R^2 values are displayed for each experiment in the corresponding panel. * Slope significantly different from 0 ($p < 8 \cdot 10^{-4}$).

10.3.5 Offline mapping of dynamical invariants propagation with a monodirectional fast chemical graded synapse from LP to NM

Monodirectional connection from a recording of a living neuron to the neuron model is very effective and convenient to map offline the best configuration of the synaptic parameters with regard to the strength of the correlation between the time intervals that give rise to the invariants. In particular, we have observed that the parameters V_f together with the maximal conductance g_{LPNM} are essential to produce robust dynamical invariants as shown in ***Figure 10.7***. The case of the parameter V_f is especially interesting since it acts as a threshold to control the input of information from the rest of the living circuit, in particular, the PY group (see ***Figure 10.1***). The lower V_f is, the more information is transmitted to the model, and thus, the stronger the correlation is between the interval and the period.

10.4 Discussion

When connectivity is asymmetric, the selection of the living neuron used to build the hybrid circuit is crucial to study dynamical invariants. LP neuron receives fewer connections than other neurons in the pyloric circuit and more important, LP does not receive any electrical synapse. Therefore, it has more flexibility to adapt and coordinate its activity with the model and the rest of the circuit elements on a cycle-by-cycle basis, making this neuron a better candidate to connect to the model neuron.

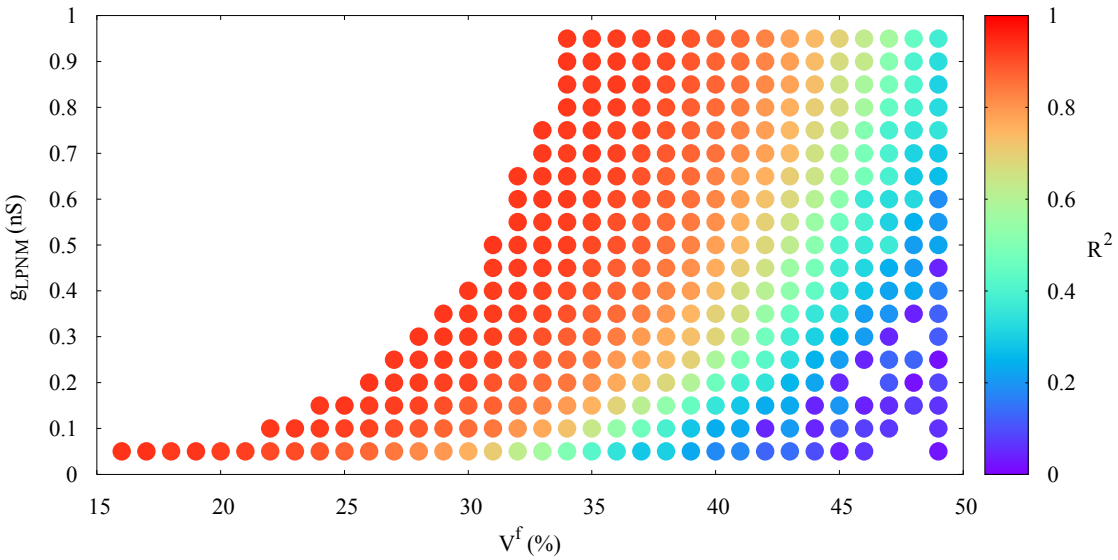

Figure 10.7: Offline map of the dynamical invariant propagation with a monodirectional fast chemical graded synapse from LP to NM. Dots represent pairs of values of the maximal conductances g_{LPNM} and V_f that generated the dynamical invariant $LPNM\ interval[Period]$. Color palette represents the strength of the correlation between the intervals that give rise the invariants calculated as R^2. White areas correspond to configurations where antiphase between the living neuron and the model neuron was not achieved. V_f is calculated as a percentage from the minimum value of the membrane potential of the living neuron.

The dynamical invariants between $Period$ and the analogous intervals $LPNM\ interval$ and $LPNM\ delay$ are propagated through bidirectional chemical and electrical synapses and through a monodirectional chemical synapse from the LP to the neuron model. These invariants arise as a function of the connectivity parameters. Monodirectional chemical synapse from the neuron model to the LP neuron was not effective in propagating the invariants in any configuration that we tested. Monodirectional synapses from the living circuit to the model are particularly convenient to map the configurations of parameters for optimal propagation of the dynamical invariants. Parameters that control the input of information towards the model such as g_{LPNM} and V_f are critical to achieve strong correlations between the intervals that give rise to the invariants.

Hybrid circuits are a powerful tool to study the origin and role of the dynamical invariants. The analysis presented in this chapter regarding the propagation of the dynamical invariants could be expanded in future experiments to address the origin and role of dynamical invariants. In particular, hybrid circuits can be useful to determine which are the key properties in the neuron dynamics and in the connectivity that give rise to the invariants to reproduce them in a model.

Part V

Conclusions

Chapter 11

Conclusions

11.1 Lessons from the experimental and computational studies

11.1.1 Restricted variability in sequential activations and dynamical invariants

In this thesis, we have studied the flexibility and robustness of pyloric CPG activity. In the first part of the thesis, we have characterized experimentally intrinsic and induced variability in CPG rhythms. Induced irregularity was obtained by biophysical disruption with ethanol. Ethanol proved to be very effective in revealing the rich dynamics of neurons and connections and also presents the advantage of being reversible, thus the neurons return to the original rhythm after washing out.

Our results showed that intrinsic irregular rhythms presented high variability in hyperpolarization intervals (corresponding to PY bursts) and in PD and LP waveforms. In particular, LP neurons showed larger plateaus and higher variability in burst duration while PD activity remained more constant. Under the influence of ethanol, the robustness of the sequence was preserved while large variability in both PD and LP neurons was induced as shown in ***Figure 5.3*** and ***Figure 5.5***.

Despite the variability seen in the pyloric activity, we found two strong linear correlations between pivotal time intervals building the sequence, which we have denominated dynamical invariants. These dynamical invariants were present both in regular and irregular activity. Our results show that $LPPD\ interval$ and $LPPD\ delay$ closely followed the changes in $Period$ cycle-by-cycle. Other explored relationships among the remaining intervals that build the sequence did not lead to any correlations. After removing the fast synapses (glutamatergic) by applying PTX, the correlation $LPPD\ delay[Period]$ was lost while $LPPD\ interval[Period]$ was still preserved.

11.1.2 Effect of the asymmetry on shaping rhythm and sequential activity in minimal circuit configurations and in CPG model networks

In the second part of this thesis, we have studied the connectivity of the pyloric CPG from a computational point of view. We observed that closed-loop algorithms were effective in controlling irregular activity in half-center oscillators by modifying adaptively one of the synaptic maximum conductances. We also studied the effect of external stimulation. We observed that such stimulation was more effective in regularizing the circuit activity when taking into account the state of the circuit.

Furthermore, we have studied the role of asymmetric connectivity in shaping robust sequential rhythms. In particular, the analysis was focused on the asymmetry in synaptic maximal conductances and time constants in half center oscillators as well as modulation by gap-junctions. We showed that the asymmetry in both synaptic strength and temporal synaptic dynamics contributed synergistically to shape large regions of regular and smaller regions of irregular spiking-bursting regimes. The use of closed-loop algorithms allowed to map and characterize the coordination properties arising from the asymmetric connections and the dynamics of the individual neurons in the circuit.

As a continuation of the study of asymmetric connectivity, a simplified model of the pyloric CPG was built based on mutual inhibition. This work allowed to assess the effect of the asymmetry on the shape of the rhythm and its constituent sequence. This circuit produced four different rhythm types as a function of the maximal conductances of the synapses, depending on the regularity and the maintenance of the sequence LP-PY-PD (triphasic or non triphasic). Mapping the activity produced by the circuit in terms of synaptic strength (maximal synaptic conductances) and temporal scale of the synapses (fast or slow graded synapses) showed that the asymmetry in both scales produced a wider range for the combinations of parameters leading to triphasic rhythms. However, this model circuit did not reproduce the invariants observed in experiments.

11.1.3 Propagation of dynamical invariants in hybrid circuits

Finally, in the last part of this thesis, we have studied sequential activity and the presence of the dynamical invariants in hybrid circuits. We connected the LP neuron of a living circuit to a neuron model (NM) by means of a fast graded model synapse while in the opposite direction we implemented a slow graded synapse. Analogous time intervals were defined between the LP neuron and the neuron model $LPNM\ interval$ and $LPNM\ delay$. The results showed that dynamical invariants can be present between the $Period$ and $LPNM\ interval$ and $LPNM\ delay$ as a function of the connectivity parameters. In particular, with a bidirectional chemical synapse, the invariants consistently remained tightly preserved with a slope close to one for many different preparations and under different conditions. Bidirectional inverse electrical synapses proved to be also effective in producing the invariants with correlation coefficients similar to those obtained with chemical synapses. In the case of monodirectional chemical synapses, we observed that if the connection was established from the LP to the NM both invariants were present, while in the opposite direction, the connection was not effective in producing dynamical invariants.

11.2 Discussion and conclusions

Although typically characterized by frequency, most brain rhythms throughout the nervous system are built from sequential activations of groups of neurons (Buzsaki, 2006; Rajan et al., 2016; Rabinovich and Varona, 2017; Ma and Zhang, 2018). Some of these sequences are often very robust and directly related to the execution of motor commands, cognitive decisions, and behavioral actions (Varona and Rabinovich, 2016; Rabinovich and Varona, 2018). When generating robust sequential activations, cycle-by-cycle flexibility and fine-tuning of instantaneous periods, phases and event timings can be crucial for the optimization and the achievement of effective functions. In this thesis, we have addressed this issue in the pyloric CPG, a well-known experimental model where these questions can be more easily examined.

Our characterization of cycle-by-cycle variability in CPG circuits has revealed the presence of dynamical invariants in neural sequences in the form of linear correlations between pivotal time intervals that build the sequence. An adequate time reference frame and experimental conditions were used to expose transient dynamics. Taking into account the experiments analyzed in this thesis, these invariants seem to arise from the rich intrinsic cell dynamics and the asymmetric connectivity balancing robustness and flexibility in the transients that build functional neural rhythms. Both invariants, $LPPD\ interval[Period]$ and $LPPD\ delay[Period]$, can be found in regular and irregular control conditions and also under extreme conditions induced by ethanol. Particularly, the presence of the invariants in control conditions was a very robust result, since they were found in all experiments. Our results show that even outside the steady state $LPPD\ delay$ and $LPPD\ interval$ closely follow the changes in $Period$ despite the variability present in intrinsic transient dynamics and induced by ethanol. The cycle-by-cycle analysis showed that the intervals BD_{LP}, BD_{PD} and $PDLP\ delay$ tend to compensate their variability and, as a consequence, contribute to maintain dynamical invariants. Cycle-by-cycle temporal relationships between CPG neurons are preserved even under extreme conditions, which underlies the highly effective negotiating properties of this circuit to produce a motor rhythm that balances robustness and flexibility. The reported invariants and other possible preserved relationships could act as rules to program their function to adapt to distinct circumstances, which reflects the remarkable adaptability and functional efficiency of the CPG.

Other relationships between time intervals and the period were also studied but did not lead to invariants, which might reflect they are not related to rhythm negotiation and fulfill another role. It is important to note, that the approximate phase maintenance reported in previous studies (Hooper, 1997a,b; Bucher et al., 2005; Rabbah and Nadim, 2005; Soofi et al., 2014) is also reproduced; when interval averages are calculated within preparations, linear relationships were always found between all intervals and the period due to all sources of interval variability canceling each other.

The asymmetric connectivity of the pyloric circuit can play a key role in shaping the dynamical invariants. We have observed that one of the invariants, $LPPD\ delay[Period]$, disappeared when glutamatergic synaptic inputs were removed (PTX). However, the invariant $LPPD\ interval[Period]$ was preserved probably due to the variability compensation between the LP and PD burst duration, even under the effect of ethanol.

As was explained in section 2.4, in most CPGs the building block of the network is reciprocal inhibition between pairs of neurons, i.e., the so-called half-center oscillator. Moreover, they present a non-open topology (Huerta et al., 2001; Stiesberg et al., 2007), since all neurons receive input from other cells in the circuit in a closed-loop connection. However, there are very few studies on the closed-loop control of the irregular activity in this

minimal CPG circuit. Thus, in this thesis we have explored a simple closed-loop protocol to regularize the activity of a minimal CPG circuit model by changing one of its inhibitory conductances. We adaptively modified synaptic maximum conductances using a closed-loop algorithm to find regular and irregular activity regimes.

The asymmetry in the CPG connectivity, whose role in the preservation of the reported dynamical invariants was discussed above, played a fundamental role in shaping the rhythm of a half-center oscillator. We have shown that a closed-loop protocol adapting online the synaptic parameters under a regularization goal is an effective methodology in mapping and characterizing the coordination properties that arise both from the connection topology and from the individual neuronal dynamics in these circuits.

Departing from these results, a model of the pyloric CPG was used to continue the study of asymmetry in the connectivity, to assess its role in shaping the rhythm and keeping the triphasic rhythm (LP-PY-PD sequences) even in irregular bursting regimes. With this study, we aimed to understand the intrinsic mechanisms that sustain dynamical invariants on the transient dynamics of ongoing activity. Our results show that the asymmetry in strength and time scales of the inhibitory synapse contribute to shape wide regimes of regular and irregular triphasic spiking-bursting activity. However, the invariants were not found in the model despite the intrinsic variability derived from setting the individual neuron dynamics in a chaotic bursting regime. The absence of the invariants suggests that the most commonly used conductance-based models do not capture the flexibility and variability required to reproduce them. As many biological factors could not be considered in the model description, this result must be taken with caution. Even though the model circuit was realistic, the network was simplified; several neurons (AB, VD and IC) were not included and the PY population was simplified as a single neuron. Additionally, cell heterogeneity such as neuron-specific waveforms and spike temporal structure were not included in the individual model neurons (Szücs et al., 2003).

Finally, to improve our understanding of the origin and role of the dynamical invariants, we designed and implemented hybrid circuits (Selverston et al., 2000; Prinz et al., 2004a; Amaducci et al., 2019; Reyes-Sanchez et al., 2018). Results showed that the dynamical invariants between period and the analogous intervals $LPNM\ interval$ and $LPNM\ delay$ can be propagated and they arise as a function of the connectivity parameters. We assessed the conditions under which the neuron and synapse models provide the minimum elements to generate robust invariants in the hybrid circuits. Hybrid circuits are a powerful tool to study which are the key properties in the neuron dynamics and connectivity that give rise to the invariants in order to reproduce them in a model.

Most neural functions are supported by neuronal oscillatory activity, often simply referred to as a rhythm (Buzsaki, 2006; Steriade, 2006). Rhythms are recorded in specific brain circuits, such as in CPGs, or observed in recordings spanning distinct frequencies and anatomical regions, such as the cerebellum, the hippocampus, the basal ganglia, and cortical areas. In most cases, brain rhythms are characterized and quantified with regard to only their frequencies and synchronization properties. However, a wide variety of experimental works show that robust sequential activations of different neuron types participate or are recruited at different phases of the oscillations that define brain rhythms (e.g. (O'Keefe and Recce, 1993; Sakai et al., 2004; Klausberger and Somogyi, 2008; Jacobson et al., 2009; Bienvenu et al., 2012; Zheng et al., 2016; Buzsáki and Tingley, 2018)).

Typically, neural rhythms such as pyloric neural oscillations are based on inhibition as the main mechanism shaping not only the rhythmic activity (Buzsáki and Watson, 2012), but also most importantly, the sequential activation of its constituent elements. Inhibition based mechanisms offer specific time windows where neurons can express their excitabil-

ity, balancing the robustness of the sequence and the flexibility to tune activation timings. The actual execution of a sequential neural command, e.g., in the performance of a movement, is determined not only by the serial order of individual participants but also by their timing. This is the case for the pyloric CPG, as most likely fine timing adaptations are required to optimize the function of the motor plant beyond keeping the sequence needed to move food from one side to the other.

The unveiling of dynamical invariants in the spatio-temporal patterns of neural activity may have an important impact on robotics. Traditional robotic locomotion control paradigms are based on ad-hoc rules to deal with different scenarios (e.g. obstacle avoidance, uneven terrain, etc). The concept of dynamical invariants provides an alternative way to autonomously build constraints to drive behavior in all situations. In this context, a dynamical invariant based CPG control arising from the connectivity and rich intrinsic neuron dynamics (Herrero-Carrón et al., 2011) can provide autonomous solutions to different situations informed by sensory feedback. Modern rehabilitation protocols that characterize neural sequential activations are another field of active research where the results of this thesis could be applied (Latorre et al., 2019).

Beyond spiking-bursting activity and CPG function, dynamical invariants in other brain rhythms can underlie the creation of cyclic windows within oscillations when synaptic input can be most efficiently integrated for the effective execution of sequences generated in a given informational context (Klausberger and Somogyi, 2008; Krook-Magnuson et al., 2012). We foresee that the study of specific time references and dynamical invariants in different neural systems will provide insights into the functional role of brain rhythms and their constituent sequences.

11.3 Future work

Part of the work presented in this thesis can be extended. Firstly, we believe that the results presented about the dynamical invariants in the pyloric CPG of crustaceans can be generalized to other systems. In particular, a first step in this direction would be analyzing similar triphasic rhythms in other invertebrates CPG such as the feeding CPG in *Lymnaea* stagnalis, vertebrate breathing CPGs and the robust sequential activations observed in the hippocampus, cerebellar and cortical circuits, etc.

Additionally, the study of the presence of invariants in the models can be continued by assessing the effect of the introduction of noise as a source of variability, and also additional intrinsic dynamics into the neurons. This would shed light on the question of whether there are missing key dynamical elements in the theoretical paradigms.

Finally, regarding hybrid circuits, there is a wide variety of possibilities that can be implemented for further dynamical invariant characterization. For instance, different models of neurons can be used to assess which ones allow the propagation of invariants and which fail to do so. An additional possibility is changing the connectivity in the living system by adding PTX as it was done in the experiments presented in this work. Another bottom-up approach would be to connect an isolated living neuron to a model circuit with increasing complexity to analyze whether the source of the dynamical invariant resides in the single neuron dynamics.

Parte VI

Conclusiones

Capítulo 12

Conclusiones

12.1 Resultados de los estudios experimentales y computacionales

12.1.1 La variabilidad de la actividad de los CPGs está restringida por la activación secuencial y los invariantes dinámicos

En esta tesis hemos estudiado la flexibilidad y robustez en la actividad del CPG pilórico. En la primera parte, hemos caracterizado experimentalmente la variabilidad intrínseca e inducida en el ritmo producido por el CPG. La irregularidad inducida se ha implementado mediante la alteración biológica del sistema con etanol. El uso de etanol ha resultado ser muy efectivo para revelar la riqueza de la dinámica de las neuronas y conexiones y además presenta la ventaja de ser reversible. Por tanto, las neuronas vuelven a su ritmo original tras la eliminación del etanol.

Los resultados de los experimentos realizados en esta tesis han demostrado que los ritmos con irregularidad intrínseca presentan una alta variabilidad en los intervalos de hiperpolarización (correspondientes a las ráfagas de las neuronas PYs) y en la estructura de las ráfagas de las neuronas PD y LP. En particular, la neurona LP presenta en esta condición *plateaus* largos y una alta variabilidad en la duración de la ráfaga, mientras que la actividad de la PD se mantiene más constante. Bajo la acción del etanol, la secuencia del ritmo se preserva de forma robusta induciendo al mismo tiempo una gran variabilidad en las neuronas PD y LP como muestran las figuras ***Figura 5.3*** y ***Figura 5.5***.

A pesar de la variabilidad observada en la actividad del circuito pilórico, hemos encontrado dos correlaciones lineales muy estables entre intervalos de tiempo claves que componen la secuencia. A estas correlaciones las hemos denominado invariantes dinámicos. Los invariantes dinámicos se identificaron tanto en actividad regular como en irregular. Los resultados del análisis muestran que los intervalos $LPPD\ interval$ y $LPPD\ delay$ varían ciclo-a-ciclo siguiendo a los cambios en el $Period$. Otras combinaciones entre el resto de intervalos no han presentado correlación lineal. Al eliminar las sinapsis rápidas (glutamatérgicas) mediante el uso de PTX, la correlación lineal $LPPD\ delay[Period]$ desaparece mientras que la correlación $LPPD\ interval[Period]$ se mantiene presente.

12.1.2 Efecto de la asimetría en la caracterización del ritmo y la actividad secuencial en configuraciones de circuito mínimas y en modelos de CPG

En la segunda parte de la tesis, hemos estudiado la conectividad del CPG pilórico desde una perspectiva computacional. Hemos observado que los algoritmos de ciclo cerrado son efectivos para controlar la actividad irregular en un *half-center oscillator* cuando se modifica una de las conductancias sinápticas máximas. Se ha estudiado también el efecto de la estimulación externa, observando que es mucho más efectivo para regularizar la actividad del circuito al tener en cuenta el propio estado del circuito.

Además, hemos estudiado el papel de la conectividad asimétrica en la caracterización de la actividad secuencial robusta. En particular, el análisis se centró en la asimetría en la conductancia sináptica máxima y las constantes de tiempo del *half-center oscillator*, así como también la modulación mediante *gap-junctions*. Se ha demostrado que la asimetría en la fuerza sináptica y la dinámica temporal de la sinapsis contribuyen conjuntamente en la configuración de regiones amplias de regímenes de actividad en ráfagas regular y más reducidas de actividad en ráfagas irregular. Los algoritmos en ciclo cerrado han permitido mapear y caracterizar las propiedades de coordinación que surgen de la conectividad asimétrica y de la dinámica neuronal en el circuito.

Continuando con el estudio de la asimetría en la conectividad, se ha diseñado un modelo del CPG pilórico simplificado basado en la inhibición mutua. Este trabajo ha permitido evaluar el efecto de la asimetría sobre la forma del ritmo y su secuencia. Este circuito ha generado cuatro tipos diferentes de ritmo en función de la conductancia máxima de las sinapsis que han podido ser clasificados según la regularidad y del mantenimiento de la secuencia LP-PY-PD (trifásico o no trifásico). La actividad generada por el circuito ha sido mapeada en función de la conductancia máxima y la escala temporal de las sinapsis (sinapsis gradual rápida o lenta) demostrando que la asimetría en ambas produce un rango mayor de combinaciones de parámetros con ritmo trifásico. Sin embargo, con este modelo no se ha podido reproducir los invariantes dinámicos observados en los experimentos.

12.1.3 Propagación de los invariantes dinámicos en circuitos híbridos

Finalmente, en la última parte de la tesis, hemos estudiado la actividad secuencial y la presencia de los invariantes dinámicos en circuitos híbridos. Para ello, hemos conectado la neurona LP de un circuito vivo a un modelo de neurona (NM) mediante una sinapsis gradual rápida y en la dirección contraria una sinapsis gradual lenta. De forma análoga se han definido intervalos de tiempo entre la neurona LP y el modelo, $LPNM\ interval$ y $LPNM\ delay$. Según los resultados, los invariantes dinámicos pueden estar presentes entre el $Period$ y los intervalos $LPNM\ interval$ y $LPNM\ delay$ dependiendo de los parámetros de conexión. En particular, con la sinapsis química bidireccional ambos invariantes se mantienen presentes con una pendiente cercana a uno en diferentes preparaciones y condiciones. La sinapsis bidireccional eléctrica inversa también resulta ser efectiva para reproducir los invariantes con unos coeficientes de correlación similares a los obtenidos con la sinapsis química bidireccional. En el caso de sinapsis química monodirecional, hemos observado que si la conexión se establece desde la LP a la NM ambos invariantes están presentes. Sin embargo, si la conexión se implementa en la dirección opuesta, la sinapsis no es efectiva para propagar los invariantes dinámicos.

12.2 Discusión y conclusiones

A pesar de que es típico caracterizar los ritmos producidos por el sistema nervioso en función de su frecuencia, muchos de ellos se basan en la activación secuencial de grupos de neuronas (Buzsaki, 2006; Rajan et al., 2016; Rabinovich and Varona, 2017; Ma and Zhang, 2018). Algunas de estas secuencias son muy robustas y se relacionan directamente con la ejecución de señales motoras, la toma de decisiones cognitivas y características de comportamiento (Varona and Rabinovich, 2016; Rabinovich and Varona, 2018). Cuando se generan activaciones secuenciales de forma robusta, la flexibilidad ciclo-a-ciclo y el ajuste fino de los periodos, fases y eventos temporales pueden ser cruciales para la optimización del sistema y obtener una funcionalidad efectiva. En esta tesis, hemos abordado esta cuestión en el CPG pilórico, ya que es un buen modelo experimental en el que estudiar estas preguntas de forma relativamente fácil.

Con nuestra caracterización de la variabilidad del CPG ciclo-a-ciclo, se ha revelado la presencia de invariantes dinámicos en secuencias neuronales en forma de correlaciones lineales entre intervalos de tiempo claves que forman parte de la secuencia. Para ello, se han empleado una serie de referencias temporales y condiciones experimentales que han permitido exponer una dinámica transitoria del circuito. Según los experimentos analizados en esta tesis, los invariantes surgen de la dinámica rica intrínseca de las células y de la conectividad asimétrica que equilibran la robustez y la flexibilidad durante la actividad transitoria de los ritmos neuronales asociados a una función específica. Ambos invariantes, $LPPD\ interval[Period]$ y $LPPD\ delay[Period]$ se pueden observar en condiciones de control con ritmos tanto regulares como irregulares e incluso en condiciones extremas inducidas por etanol. En particular, la aparición de los invariantes en condiciones de control es un resultado muy robusto, ya que se han encontrado en todos los experimentos realizados. Nuestros resultados muestran que incluso fuera del estado estacionario los intervalos $LPPD\ delay$ y $LPPD\ interval$ evolucionan siguiendo al $Period$ a pesar de la variabilidad presente en la dinámica transitoria y la producida por el etanol. El análisis ciclo-a-ciclo muestra que los intervalos BD_{LP}, BD_{PD} y $PDLP\ delay$ tienden a compensar su variabilidad, y como consecuencia, contribuyen a mantener los invariantes dinámicos. Las relaciones temporales entre las neuronas del CPG se mantienen ciclo-a-ciclo incluso en condiciones extremas, lo que subyace a las propiedades de negociación altamente efectivas de este circuito para producir un ritmo motor que equilibra robustez y flexibilidad. Es posible que los invariantes reportados aquí, junto con otras posibles relaciones temporales, lineales o no lineales, que también se puedan mantener, actúen como reglas de programación para desempeñar su función adaptándose a las distintas circunstancias, lo que reflejaría la notable adaptabilidad y la eficiencia funcional de este circuito.

Se han estudiado también otras relaciones entre otros intervalos de tiempo y el período que no han dado lugar a invariantes, lo que podría reflejar que no están relacionadas con la negociación del ritmo y, por tanto, que cumplen otro rol. Es importante recalcar, que el mantenimiento de fase reportado en anteriores estudios (Hooper, 1997a,b; Bucher et al., 2005; Rabbah and Nadim, 2005; Soofi et al., 2014) también ha sido reproducido; se ha observado que, al calcular el promedio de los intervalos de tiempo para cada preparación, siempre existe correlación lineal entre todos los intervalos y el periodo, ya que todas las fuentes de variabilidad se cancelan mutuamente.

La conectividad asimétrica del circuito pilórico puede jugar también un papel crucial en la configuración de los invariantes dinámicos. Hemos observado que uno de los invariantes, $LPPD\ delay[Period]$, se pierde cuando las señales sinápticas de tipo glutamatérgico se eliminan (PTX). Sin embargo, el otro invariante $LPPD\ interval[Period]$ se mantiene probablemente debido a que la duración de las ráfagas de la LP y la PD compensan entre sí su

variabilidad, incluso bajo el efecto del etanol.

Como ya se explicó en la sección 2.4, la mayoría de CPGs se construyen en base a la inhibición mutua entre pares de neuronas, los llamados *half-center oscillators*. Además, estos circuitos presentan una topología no-abierta (Huerta et al., 2001; Stiesberg et al., 2007), ya que todas las neuronas reciben la señalización de otras células del circuito formando una conexión en ciclo cerrado. Sin embargo, existen pocos estudios centrados en el control mediante ciclo-cerrado de la actividad irregular producida por este tipo de circuitos CPG mínimo. Por ello, en esta tesis hemos explorado un protocolo simple de ciclo cerrado para regularizar la actividad de un modelo de circuito de CPG mínimo cambiando una de sus conductancias inhibitorias. Para ello, se ha modificado adaptativamente las conductancias sinápticas máximas utilizando un algoritmo de ciclo cerrado para encontrar regímenes de actividad regular e irregular.

La asimetría en la conectividad del CPG, cuyo papel en la preservación de los invariantes dinámicos reportados ya hemos discutido, desempeña además una función fundamental en la configuración del ritmo en un *half-center oscillator*. Hemos demostrado que un protocolo de bucle cerrado que adapta *online* los parámetros sinápticos siguiendo un objetivo de regularización es una metodología efectiva para mapear y caracterizar las propiedades de coordinación que surgen tanto de la topología de conexión como de la dinámica neuronal individual en estos circuitos.

Partiendo de los resultados anteriores, se desarrolló un modelo del CPG pilórico para continuar el estudio de la asimetría en la conectividad, y evaluar su papel en la configuración del ritmo y mantenimiento del ritmo trifásico (secuencia LP-PY-PD) incluso en regímenes de ráfagas irregulares. Con este estudio, hemos buscado comprender los mecanismos intrínsecos que sustentan los invariantes en las dinámicas transitorias de la actividad en curso. Nuestros resultados muestran que la asimetría en la intensidad de conexión y en la escala temporal de la sinapsis inhibitoria contribuye a dar forma a amplios regímenes de actividad en ráfagas regular e irregular que presentan ritmo trifásico. Sin embargo, los invariantes no se han podido observar en el modelo a pesar de la variabilidad intrínseca derivada de la configuración de las neuronas del circuito en un régimen caótico. Su ausencia sugiere que los modelos basados en conductancias usuales no capturan propiedades como la flexibilidad y variabilidad, que son requeridas para reproducir los invariantes dinámicos. Sin embargo, este resultado debe tomarse con precaución, puesto que no se han podido considerar en la descripción del modelo muchos factores biológicos del CPG. A pesar de que el modelo de circuito es altamente realista, la red se ha tenido que simplificar; varias neuronas (AB, VD y IC) no se han incluido y la población de PYs ha sido simulada como una sola neurona. Además, la heterogeneidad de las células, las formas de onda específicas de cada neurona y la estructura temporal de los *spikes* no se han considerado en los modelos de neuronas individuales (Szücs et al., 2003).

Finalmente, para mejorar nuestra comprensión del origen y el papel de los invariantes dinámicos, hemos diseñado e implementado circuitos híbridos, muy útiles para los estudios de dinámica neuronal(Selverston et al., 2000; Prinz et al., 2004a; Amaducci et al., 2019; Reyes-Sanchez et al., 2018). Los resultados muestran que los invariantes dinámicos encontrados entre el período y los intervalos $LPNM\ interval$ y $LPNM\ delay$ se pueden propagar y surgen en función de los parámetros de conectividad. Hemos evaluado también las condiciones bajo las cuales los modelos de neurona y sinapsis proporcionan los elementos básicos para construir invariantes robustos en circuitos híbridos. Los circuitos híbridos constituyen una herramienta muy potente para estudiar las propiedades clave en la dinámica neuronal y la conectividad que dan lugar a los invariantes para reproducirlos en los modelos.

La mayoría de las funciones neuronales están basadas actividad oscilatoria neuronal, que a menudo se denomina simplemente ritmo (Buzsaki, 2006; Steriade, 2006). Los ritmos se pueden registrar en circuitos cerebrales específicos, como los CPG, u observar en grabaciones que abarcan distintas frecuencias y regiones anatómicas, como el cerebelo, el hipocampo, los ganglios basales y las áreas corticales. En la mayoría de los casos, los ritmos cerebrales se caracterizan y cuantifican solo en relación con sus frecuencias y propiedades de sincronización. Sin embargo, una amplia variedad de trabajos experimentales ha mostrado que las secuencias de activación robustas de diferentes tipos de neuronas participan en diferentes fases de las oscilaciones que definen los ritmos cerebrales, ver por ejemplo (O'Keefe and Recce, 1993; Sakai et al., 2004; Klausberger and Somogyi, 2008; Jacobson et al., 2009; Bienvenu et al., 2012; Zheng et al., 2016; Buzsáki and Tingley, 2018).

Normalmente, los ritmos neuronales, como las oscilaciones neuronales pilóricas, se basan en la inhibición como mecanismo principal que da forma no solo a la actividad rítmica (Buzsáki and Watson, 2012), sino de forma más importante, a la activación secuencial de sus elementos constituyentes. Los mecanismos basados en la inhibición hacen que las neuronas solo pueden expresar su excitabilidad en determinadas ventanas de tiempo específicas, equilibrando la robustez de la secuencia y la flexibilidad para calibrar los tiempos de activación. La ejecución de una secuencia neuronal, por ejemplo, la ejecución de un movimiento, está determinada no solo por el orden en serie de los participantes individuales, sino también por los tiempos específicos de activación. Este es el caso de CPG pilórico, pues es muy probable que sean necesarias adaptaciones de tiempo muy refinadas para optimizar la función de la planta motora más allá de mantener la secuencia y mover los alimentos de un lado al otro de forma efectiva.

El descubrimiento de los invariantes dinámicos en los patrones espacio-temporales de la actividad neuronal puede tener un impacto importante en la robótica. Los paradigmas de control de locomoción en robótica tradicional se basan en reglas *ad hoc* para tratar diferentes escenarios (por ejemplo, evitar obstáculos, terrenos desiguales, etc.). El concepto de invariantes dinámicos proporciona una forma alternativa de crear restricciones de forma autónoma para dirigir y controlar el comportamiento en todas las situaciones. En este contexto, un control mediante CPGs basado en invariantes dinámicos que surgen de la conectividad y la dinámica intrínseca de las neuronas (Herrero-Carrón et al., 2011) puede proporcionar soluciones de forma autónoma para diferentes situaciones en función del *feedback* sensorial. Los protocolos de rehabilitación modernos basados en secuencias de activación neuronal son también otro campo de investigación activa en el que se podrían aplicar los resultados obtenidos en esta tesis (Latorre et al., 2019).

Los invariantes dinámicos, además de aparecer en la actividad *spiking* en ráfagas y de su papel en la funcionalidad de CPG, pueden ser la base en otros ritmos cerebrales para la creación de ventanas cíclicas dentro de las oscilaciones cuando las señales sinápticas pueden ser integradas de manera más eficiente para la ejecución efectiva de secuencias generadas en un contexto informativo dado (Klausberger and Somogyi, 2008; Krook-Magnuson et al., 2012). Prevemos que el estudio de referencias temporales específicas e invariantes dinámicos en diferentes sistemas neuronales proporcionará puntos de vista novedosos sobre el papel funcional de los ritmos cerebrales y las secuencias que los constituyen.

12.3 Trabajo futuro

Parte del trabajo presentado en esta tesis se puede extender. En primer lugar, creemos que el resultado presentado sobre los invariantes dinámicos en el CPG pilórico en crustá-

ceos puede generalizarse a otros sistemas. En particular, un primer paso en esta dirección sería analizar ritmos trifásicos similares en otros CPGs en invertebrados, como el CPG que controla alimentación en *Lymnaea* stagnalis, los CPGs que controlan la respiración en vertebrados y las activaciones secuenciales robustas observadas en el hipocampo, los circuitos del cerebelo, etc.

Además, el estudio de la presencia de invariantes en los modelos también se puede continuar mediante la evaluación del efecto de la introducción de ruido como una fuente de variabilidad, así como también de la introducción de dinámica intrínseca adicional en las neuronas. Esto arrojaría luz sobre la cuestión de la falta de elementos dinámicos clave en los paradigmas teóricos.

Finalmente, con respecto a los circuitos híbridos, existe una amplia variedad de posibilidades que pueden implementarse para ampliar la caracterización de los invariantes dinámicos. Por ejemplo, se pueden emplear diferentes modelos de neuronas para estudiar cuáles permiten la propagación de invariantes y cuáles no. Otra posibilidad es cambiar la conectividad en el sistema vivo agregando PTX como se hizo en los experimentos presentados en este trabajo. Finalmente, un enfoque alternativo sería conectar una neurona viva aislada a un circuito modelo aumentando la complejidad gradualmente para analizar si la fuente de los invariantes dinámicos reside en la dinámica individual de las neuronas.

Part VII

Appendices

Appendix A

Models parameters

A.1 Komendantov-Kononenko model parameters

Table A.1: Parameters used in our simulations for the different regimes in which Komendantov-Kononenko model can be tuned: beating-mode (tonic spiking activity), chaotic-mode (irregular spiking activity), regular bursting activity and chaotic bursting activity. See section 3.2.1 and appendix of (Komendantov and Kononenko, 1996)

	$V_{Na}\ (mV)$	$V_K\ (mV)$	$V_B\ (mV)$	$V_{Ca}(mV)$	$C_m\ (\mu F)$	$R\ (mm)$	$K_s\ (1/s)$	ρ	$K_\beta\ (1/mM)$
All regimes	40	-70	-58	150	0.02	0.1	50	0.002	15000

Regime	$\beta\ (mM)$	$g^*_K\ (\mu S)$	$g^*_{Na}\ (\mu S)$	$g^*_{Na}(V)\ (\mu S)$	$g^*_B\ (\mu S)$	$g^*_{Na(TTX)}\ (\mu S)$	$g^*_{K(TEA)}\ (\mu S)$	$g^*_{Ca}\ (\mu S)$	$g^*_{Ca-Ca}\ (\mu S)$
Beating	0.00004	0.25	0.02	0.13	0.1	400	10	1	0.01
Chaotic	0.00004	0.25	0.0231	0.11	0.1372	400	10	1.5	0.02
Regular b.	0.00004	0.25	0.0231	0.11	0.165	400	10	1.5	0.02
Chaotic b.	0.00004	0.25	0.02	0.13	0.18	400	10	1	0.01

A.2 Izhikevich model parameters

Table A.2: Parameters used in our simulations for two examples of regimes in which Izhikevich model can be tuned. Initial conditions: $V^0 = 70$, $u = b \cdot V$. See section 3.2.2.

Regime	**a**	**b**	**c**	**d**
Tonic spiking	0.02	0.2	-65	6
Tonic bursting	0.02	0.2	-50	2

Appendix B

Time references and interval measures

Table B.1: Percentage of dismissed bursts of the total number of burst of LP and PD neurons in all experiments because of missing time references (see figure B.1).

# Experiment	Dismissed LP bursts	Dismissed PD bursts
1	2%	6%
2	3%	2%
3	4%	11%
4	12%	13%
5	5%	4%
6	2%	1%
7	17%	26%
8	10%	27%
9	10%	12%
10	2%	3%
11	2%	4%
12	7%	4%
13	1%	1%
14	6%	16%
15	3%	1%
16	2%	2%

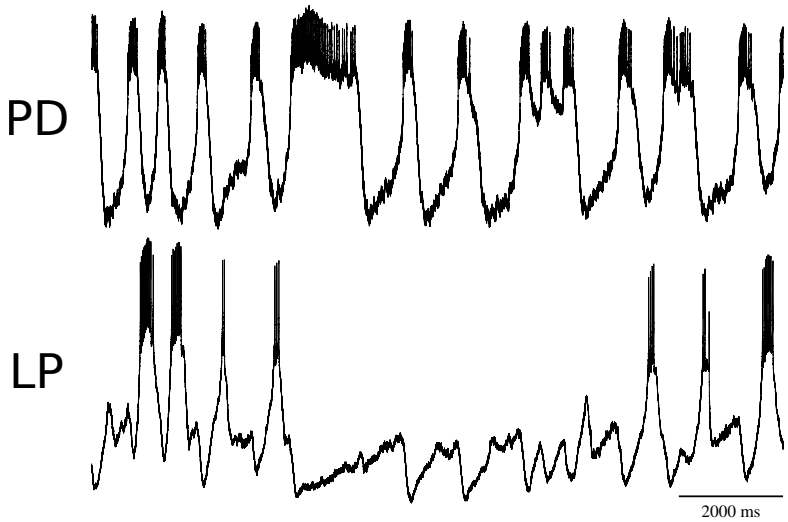

Figure B.1: Example of highly irregular rhythms in which the measures used to characterize the rhythm and its variability (LP, PD burst durations, LPPD last-first period and first-first LP period) could not be defined. The corresponding activity had to be dismissed in those analyses because the time references used were lost. LP neuron stops bursting while PD sustains its activity.

Appendix C

Matlab scripts for the analysis of neural sequential activity

These Matlab scripts calculate the intervals defined in the text from the recording spike-times and plot the invariants and barplots of the coefficient of variation. They can be used for further validation in other CPG circuits and, in fact, in any other candidate neural sequence.

C.1 Main script

```
1
2  %% Dynamical invariant characterization scripts
3  %%  If you use these scripts please cite:
4  %%  I. Elices, R. Levi, D. Arroyo, F. B. Rodriguez, and P. Varona.
       Robust dynamical invariants in sequential neural activity
5
6
7
8  %%%%%%%%%%%%%%%%%%%%%%%%%%%%%%%%%%%%%%%%%%%%%%%%%%%%%%%%%%%%%%%%%%%%%%%
9  %%%%%%%%%%%%%%% Main script %%%%%%%%%%%%%%%%%%%%%%%%%%%%%%%%%%%%%%%%%%%
10 %%%%%%%%%%%%%%%%%%%%%%%%%%%%%%%%%%%%%%%%%%%%%%%%%%%%%%%%%%%%%%%%%%%%%%%
11
12 %%% The script requires to provide in two separate files the spike-
       times of
13 %%% the PD and LP neurons in a single column in ms.
14 %%% Burst windows should be adjusted according to the period of the
       recording in ms
15 %%%
16
17 clc
18 clear all
19 close all
20
21 flag=1;
22 proporcion=0;
```

```
23
24 %%flag 1
25 perc_a=0.4;
26 perc_b=0.2;
27
28 %%flag 0
29 x_R = 0.66;
30 y_R = 0.4;
31
32
33 %It is important to maintain the asignation of the LP and PD spike-
       times files
34
35 folder = '';
36 file = '16h44m42s-06-Feb-2018_short';
37 disp(file);
38 PD_file = strcat(folder,'Control_PD_', file, '.txt'); %%%%%% name PD
       spike-times file
39 LP_file  = strcat(folder,'Control_LP_', file, '.txt'); %%%%%% name LP
        spike-times file
40 csvwrite_text = strcat(folder, 'data_', file, '.txt');
41 fig_bar = strcat(folder, file, '_bar');
42 fig_invariant = strcat (folder, file);
43 disp(PD_file);
44
45
46 PDspk_tm=importdata(PD_file);          %%%%%% read PD spike detection
        file
47 auxmeanPD=PDspk_tm(:,1);
48
49 PD_FL=findperi(auxmeanPD, 100);    %%% burst window in ms
50
51 LPspk_tm=importdata(LP_file);          %%%%%% read LP spike detection
        file
52 auxmeanLP=LPspk_tm(:,1);
53
54 LP_FL=findperi(auxmeanLP, 150);    %%% burst window in ms
55 n=1;
56 for m=1:length(LP_FL)-1
57     fLP=LP_FL(m,1);
58     nLP=LP_FL(m+1,1);
59     fPD_I=find(PD_FL(:,1)>fLP&PD_FL(:,1)<nLP);
60     if length(fPD_I)==1
61         brst(n)=fPD_I;
62         firstPD(n)=PD_FL(fPD_I,1);
63         lastPD(n)=PD_FL(fPD_I,2);
64         burstPDd(n)=PD_FL(fPD_I,2)-PD_FL(fPD_I,1);
65         firstLP(n)=LP_FL(m,1);
66         lastLP(n)=LP_FL(m,2);
67         burstLPd(n)=LP_FL(m,2)-LP_FL(m,1);
68         fst2fst(n)=LP_FL(m+1,1)-fLP;
69         latenc(n)=PD_FL(fPD_I,1)-LP_FL(m,2);
70         LPPDfst2fst(n)=PD_FL(fPD_I,1)-LP_FL(m,1);
```

```
71          PDLP(n)=LP_FL(m+1,1)-PD_FL(fPD_I,2);
72          n=n+1;
73      end
74      if m==1
75          firstPDtiempo=PD_FL(fPD_I,1);
76      end
77      if m==length(LP_FL)-1
78          lastPDtiempo=PD_FL(fPD_I,2);
79      end
80  end
81
82  auxarray1=[(1:n-1)' firstLP' lastLP' firstPD' lastPD' burstLPd'
        burstPDd' fst2fst' latenc' LPPDfst2fst' PDLP'];
83  dlmwrite(csvwrite_text, auxarray1,'delimiter', ',', 'precision', 9);
84
85  %%%Parameters%%%
86  Periodo=mean(fst2fst);
87  stdPeriodo=std(fst2fst);
88  Plateau=mean(latenc);
89  stdPlateau=std(latenc);
90  LPPDfstinterval=mean(LPPDfst2fst);
91  stdLPPDfstinterval=std(LPPDfst2fst);
92  phase= mean(LPPDfst2fst./fst2fst);
93  stdphase=std(LPPDfst2fst./fst2fst);
94  tiempo=lastPDtiempo-firstPDtiempo;
95  velocidad=m/(tiempo/1000);
96  bdurationPD=mean(burstPDd);
97  stdbdurationPD=std(burstPDd);
98  bdurationLP=mean(burstLPd);
99  stdbdurationLP=std(burstLPd);
100 PDLPmean=mean(PDLP);
101 PDLPstd=std(PDLP);
102
103 %%% Coefficient of variation bar figure
104 figure
105 bar([100*stdbdurationLP/bdurationLP 100*stdbdurationPD/bdurationPD
        100*stdPlateau/Plateau 100*stdLPPDfstinterval/LPPDfstinterval 100*
        PDLPstd/PDLPmean  100*stdPeriodo/Periodo; 0 0 0 0 0 0]);
106 saveas(gcf,fig_bar,'epsc');
107 table=[100*stdbdurationLP/bdurationLP 100*stdbdurationPD/bdurationPD
         100*stdPlateau/Plateau 100*stdLPPDfstinterval/LPPDfstinterval
        100*PDLPstd/PDLPmean 100*stdPeriodo/Periodo];
108
109 %%%Figure of invariant
110 figure
111 p(1)=scatter(fst2fst/1000,LPPDfst2fst/1000,100,brst,'.');
112 colorbar;
113 hold on
114 p(2)=plot(fst2fst/1000,latenc/1000,'r.');
115
116 lmc= LinearModel.fit(fst2fst/1000,LPPDfst2fst/1000,'linear');
117 yrc=lmc.Coefficients.Estimate(2)*fst2fst/1000+lmc.Coefficients.
        Estimate(1);
```

```
118 p(3)=plot(fst2fst/1000,yrc);
119
120 lm2= LinearModel.fit(fst2fst/1000,latenc/1000,'linear');
121 yr2=lm2.Coefficients.Estimate(2)*fst2fst/1000+lm2.Coefficients.
        Estimate(1);
122 p(4)=plot(fst2fst/1000,yr2);
123
124 legend(p,{'LPPDfst2fst','latenc',['y=',num2str(lmc.Coefficients.
        Estimate(2)),'x',num2str(lmc.Coefficients.Estimate(1))],['y=',
        num2str(lm2.Coefficients.Estimate(2)),'x',num2str(lm2.Coefficients
        .Estimate(1))]},'Location','northwest')
125
126 if proporcion==1
127     lim_x = xlim;
128     lim_y = ylim;
129     if lim_x(1)<lim_y(1)
130         min = lim_x(1);
131     else
132         min = lim_y(1);
133     end
134     if lim_x(2)>lim_y(2)
135         max = lim_x(2);
136     else
137         max = lim_y(2);
138     end
139     xlim([min max])
140     ylim([min max])
141 end
142
143 if flag==1
144     lim_x = xlim;
145     lim_y = ylim;
146
147     x_R = sum(lim_x)/2;
148     y_Ra = sum(lim_y)/2 + perc_a*(lim_y(2)-lim_y(1));
149     y_Rb = sum(lim_y)/2 - perc_b*(lim_y(2)-lim_y(1));
150 end
151
152 text(x_R,y_Ra,['R^2=',num2str(lmc.Rsquared.Ordinary)])
153 text(x_R,y_Rb,['R^2=',num2str(lm2.Rsquared.Ordinary)])
154 xlabel('Period (s)');
155 ylabel('LPPD interval, Delay (s)');
156 saveas(gcf,fig_invariant,'epsc');
157 %%%
```

C.2 Auxiliary script

```
1 function FL=findperi(spiketime, interval)
2 % FINDPERI detects bursts in spike time data.
3 % Detects a burst when an interval occurs.
4
5 firstspike = -1;
```

```
lastspike = spiketime(1);
S=size(spiketime,1); % get number of rows
i=0;
max=1; % there must be max +1 spikes in a burst for it to be
    recognized as a burst
tag=0;

%FL=0
for n = 1:S-max
    if (spiketime(n)-lastspike) >= interval
        tag=1;
        for j=1:max
            if spiketime(n+j) - spiketime(n+j-1) >= interval
                tag=0;
            end
        end
        if tag == 1
            if (firstspike ~= -1)
                i=i+1;
                FL(i,1) = firstspike;
                FL(i,2) = lastspike;
            end
            firstspike = spiketime(n);
        end
    end
    if tag ==1 || firstspike == -1
        lastspike = spiketime(n);
    end
end
```

Appendix D

Publications

Publications in indexed JCR journals

In this appendix, we present the list of publications that have been accomplished throughout the thesis in indexed JCR journals and international congresses, and relate them to the corresponding chapters:

1. **I. Elices, P. Varona. 2015. Closed-loop control of a minimal central pattern generator network, *Neurocomputing* 170: 55-62.**
   JIF: 2.392 (COMPUTER SCIENCE, ARTIFICIAL INTELLIGENCE, 2015)
   QUARTILE: Q1 (31/130)
   EDITORIAL: ELSEVIER SCIENCE
   ISSN: 0925-2312
   DOI: 10.1016/j.neucom.2015.04.097
   Methods and results described in **chapter 7**

2. **I. Elices, P. Varona. 2017. Asymmetry Factors Shaping Regular and Irregular Bursting Rhythms in Central Pattern Generators, *Front. Comput. Neurosci.* 11:9.**
   JIF: 2.073 (MATHEMATICAL AND COMPUTATIONAL BIOLOGY, 2017)
   QUARTILE: Q2 (16/59)
   EDITORIAL: FRONTIERS MEDIA SA
   ISSN: 1662-5188
   DOI: 10.3389/fncom.2017.00009
   Methods and results described in **chapter 8**

3. **R. Amaducci, M. Reyes-Sanchez, I. Elices, F.B. Rodriguez, P. Varona. 2019. RTHybrid: a standardized and open-source real-time software model library for experimental neuroscience, *Frontiers in Neuroinformatics* 13:11.**
   JIF: 3.074 (MATHEMATICAL AND COMPUTATIONAL BIOLOGY, 2017)
   QUARTILE: Q1 (8/59)
   EDITORIAL: FRONTIERS MEDIA SA
   ISSN: 1662-5196
   DOI: 10.3389/fninf.2019.00011
   Related with **chapter 10**

4. **I. Elices, R. Levi, D. Arroyo, F. B. Rodriguez, P. Varona. 2018. Robust dynamical invariants in sequential neural activity, *Scientific Reports*, in press.**
   JIF: 4.122 (MULTIDISCIPLINARY SCIENCES, 2017)
   QUARTILE: Q1 (12/64)
   EDITORIAL: NATURE PUBLISHING GROUP
   ISSN: 2045-2322
   DOI: 10.1038/s41598-019-44953-2
   Methods and results described in **chapters 5 y 6**

Articles under revision

1. **M. Reyes-Sanchez, R. Amaducci, I. Elices, F.B. Rodriguez, P. Varona. 2018. Automatic adaptation of model neurons and connections to build hybrid circuits with living networks, *bioRxiv*, 419622 (DOI: 10.1101/419622). Submitted to *Neuroinformatics*, second revision.**
   JIF: 3.852 (COMPUTER SCIENCE, INTERDISCIPLINARY APPLICATIONS, 2017)
   QUARTILE: Q1 (13/105)
   EDITORIAL: HUMANA PRESS INC
   ISSN: 1539-2791
   Related with **chapter 10**

Contributions to international congresses

1. I. Elices, P. Varona. Dynamics of heteroclinic networks with diffusive gap-junction coupling. AIMS 2014. Special Session 112: Nonlinear Dynamics in Neuroscience 2. Madrid, Spain. Oral presentation.

2. I. Elices, P. Varona. Regularization of a half-center oscillator network by closed-loop control. Computational Neuroscience Meeting CNS 2015 Prague, BMC Neuroscience 2015, 16 (Suppl 1): P275.

3. I. Elices, P. Varona. Closed-loop dynamics exploration in central pattern generators. Congreso de la Sociedad Española de Neurociencia SENC 2015 Granada.

4. I. Elices, D. Arroyo, R. Levi, F. B. Rodriguez, P. Varona. Assessing irregularity and coordination of spiking-bursting rhythms in central pattern generators. Computational Neuroscience Meeting CNS 2016 Jeju, Oral session I: Oscillations and rhythms 1. BMC Neuroscience 2016, 17 (Suppl 1): O1.

5. I. Elices, D. Arroyo, R. Levi, F. B. Rodriguez, P. Varona. Coordination of irregular bursting rhythms in central pattern generators. Society for Neuroscience Meeting SfN 2016 San Diego. Session 535, Rhythmic Motor Patterns: Connectivity, 535.11 / CCC1.

6. I. Elices, R. Levi, D. Arroyo, F. B. Rodriguez, P. Varona. Role of asymmetry in shaping spiking-bursting activity of Central Pattern Generators. Computational Neuroscience Meeting CNS 2017 Antwerp, Belgium, BMC Neuroscience 2017, 18 (Suppl 1):P282.

7. M. Reyes-Sanchez, I. Elices Ocon, R. Amaducci, C. Muniz, F.B. Rodriguez, P. Varona. Automatic calibration for hybrid circuits of living and artificial neurons. Computational Neuroscience Meeting CNS 2017 Antwerp, Belgium, BMC Neuroscience 2017, 18 (Suppl 1):P281.

8. I. Elices, R. Levi, D. Arroyo, F. B. Rodriguez, P. Varona. Robust rhythm coordination in asymmetric central pattern generators. Congreso de la Sociedad Española de Neurociencia SENC 2017 Alicante.

9. M. Reyes-Sanchez, I. Elices Ocon, R. Amaducci, C. Muniz, F.B. Rodriguez, P. Varona. Dynamic Adaptation for Hybrid Circuit Interactions. Congreso de la Sociedad Española de Neurociencia SENC 2017 Alicante.

10. I. Elices, M. Reyes-Sanchez, R. Amaducci, R. Levi, F.B. Rodriguez, P. Varona. Dynamical invariants in Central Pattern Generators. FENS 2018, Berlin, Germany, P-D058.

11. M. Reyes-Sanchez, R. Amaducci, I. Elices, F.B. Rodriguez, P. Varona. Auto-adaptation of neuron models to perform hybrid interactions with living neurons. FENS 2018, Berlin, Germany, P-H017.

12. R. Amaducci, M. Reyes-Sanchez, I. Elices, F.B. Rodriguez, P. Varona. Building hybrid circuits using a multiplatform real-time software model library. FENS 2018, Berlin, Germany, P-H016.

13. I. Elices, M. Reyes-Sanchez, R. Amaducci, R. Levi, F.B. Rodriguez, P. Varona. Unveiling and Characterizing Dynamical Invariants in Central Pattern Generators. Computational Neuroscience Meeting CNS 2018 Seattle, USA, BMC Neuroscience 2018, 19 (Suppl 2):P173.

14. M. Reyes-Sanchez, R. Amaducci, I. Elices, F.B. Rodriguez, P. Varona. Assisted construction of hybrid circuits: making easy the implementation and automation of interactions between living and model neurons. Computational Neuroscience Meeting CNS 2018 Seattle, USA, BMC Neuroscience 2018, 19 (Suppl 2):O19.

15. R. Amaducci, M. Reyes-Sanchez, I. Elices, F.B. Rodriguez, P. Varona. A cross-platform real-time model library to build hybrid neural circuits. Computational Neuroscience Meeting CNS 2018 Seattle, USA, BMC Neuroscience 2018 19 (Suppl 2):P172.

16. I. Elices, M. Reyes-Sanchez, R. Amaducci, R. Levi, F.B. Rodriguez, P. Varona. Dynamical invariants underlying robustness and flexibility in sequential neural dynamics. Society for Neuroscience Meeting SfN 2018 San Diego. Session 151, Rhythmic Motor Pattern Generation: Connectivity, 151.10 / PP13.

Publications in journals not related to the thesis

Finally we include two publications of works carried out before starting the PhD program:

1. **J.J. Torres, I. Elices and J. Marro. 2013. Stochastic multiresonances in complex nets of spiking neurons, *Int. J. Complex Systems in Science* 3(1), 21-25.**

2. **J.J. Torres, I. Elices and J. Marro. 2015. Efficient transmission of subthreshold signals in complex networks of spiking neurons, *PLoS ONE* 10(3), e0121156.**
JIF: 3.057 (MULTIDISCIPLINARY SCIENCES, 2015)
QUARTILE: Q1 (11/63)
EDITORIAL: PUBLIC LIBRARY SCIENCE
ISSN: 1932-6203
DOI: 10.1371/journal.pone.0121156

Bibliography

Abarbanel, H. D. I., Huerta, R., Rabinovich, M. I., Rulkov, N. F., Rowat, P. F., and Selverston, A. I. (1996). Synchronized action of synaptically coupled chaotic model neurons. *Neural Comput.*, 8:1567–1602.

Amaducci, R., Reyes-Sanchez, M., Elices, I., Rodriguez, F. B., and Varona, P. (2019). Rthybrid: A standardized and open-source real-time software model library for experimental neuroscience. *Frontiers in Neuroinformatics*, 13:11.

Amini, A. and Hosseini-Golgoo, S. M. (2012). Rapid Recognition of Airborne Combustible Molecules with an Operating Temperature-Modulated Gas Sensor. *Sensor Letters*, 10(3):821–825.

Arsiero, M., Lüscher, H. R., and Giugliano, M. (2007). Real-time closed-loop electrophysiology: towards new frontiers in in vitro investigations in the neurosciences. *Archives italiennes de biologie*, 145(3):193–209.

Bal, T., Nagy, F., and Moulins, M. (1988). The pyloric central pattern generator in crustacea: a set of conditional neuronal oscillators. *Journal of Comparative Physiology A*, 163(6):715–727.

Bartos, M., Manor, Y., Nadim, F., Marder, E., and Nusbaum, M. P. (1999). Coordination of fast and slow rhythmic neuronal circuits. *J. Neurosci.*, 19:6650–6660.

Bem, T. and Rinzel, J. (2004). Short Duty Cycle Destabilizes a Half-Center Oscillator, But Gap Junctions Can Restabilize the Anti-Phase Pattern. *Journal of Neurophysiology*, 91(2):693–703.

Benjamin, P. R., Kemenes, G., and Staras, K. (2001). *Molluscan Nervous Systems*. American Cancer Society.

Bienvenu, T. C., Busti, D., Magill, P. J., Ferraguti, F., and Capogna, M. (2012). Cell-type-specific recruitment of amygdala interneurons to hippocampal theta rhythm and noxious stimuli in vivo. *Neuron*, 74(6):1059 – 1074.

Broccard, F. D., Joshi, S., Wang, J., and Cauwenberghs, G. (2017). Neuromorphic neural interfaces: from neurophysiological inspiration to biohybrid coupling with nervous systems. *Journal of neural engineering*, 14(4):41002.

Brochini, L., Carelli, P. V., and Pinto, R. D. (2011). Single Synapse Information Coding in Intraburst Spike Patterns of Central Pattern Generator Motor Neurons. *The Journal of Neuroscience*, 31(34):12297–12306.

Brookings, T., Grashow, R., and Marder, E. (2012). Statistics of Neuronal Identification with Open- and Closed-Loop Measures of Intrinsic Excitability. *Frontiers in Neural Circuits*, 6:19.

Bucher, D., Prinz, A. A., and Marder, E. (2005). Animal-to-animal variability in motor pattern production in adults and during growth. *Journal of Neuroscience*, 25(7):1611–1619.

Buzsaki, G. (2006). *Rhythms of the brain*. Oxford University Press.

Buzsáki, G. and Watson, B. O. (2012). Brain rhythms and neural syntax: implications for efficient coding of cognitive content and neuropsychiatric disease. *Dialogues in Clinical Neuroscience*, 14(4):345–67.

Buzsáki, G. and Tingley, D. (2018). Space and time: The hippocampus as a sequence generator. *Trends in Cognitive Sciences*, 22(10):853 – 869. Special Issue: Time in the Brain.

Cajal, S. R. y. (1888). Estructura de los centros nerviosos de las aves. *Rev Trim Histol Norm Pat*, 1:1–10.

Cazelles, B., Courbage, M., and Rabinovich, M. I. (2001). Anti-phase regularization of coupled chaotic maps modelling bursting neurons. *Europhys. Lett.*, 56:504–509.

Chamorro, P., Muñiz, C., Levi, R., Arroyo, D., Rodríguez, F. B., and Varona, P. (2012). Generalization of the dynamic clamp concept in neurophysiology and behavior. *PLOS ONE*, 7(7):1–10.

Christini, D. J., Stein, K. M., Markowitz, S. M., and Lerman, B. B. (1999). Practical Real-Time Computing System for Biomedical Experiment Interface. *Annals of Biomedical Engineering*.

Clemens, S., Combes, D., Meyrand, P., and Simmers, J. (1998). Long-Term Expression of Two Interacting Motor Pattern-Generating Networks in the Stomatogastric System of Freely Behaving Lobster. *Journal of Neurophysiology*, 79(3):1396–1408.

Connors, B. W. and Long, M. A. (2004). Electrical synapses in the mammalian brain. *Annu Rev Neurosci*, 27:393–418.

Cowen, M., Südhof, T. C., and Stevens, C. F. (2001). The Structure of Synapses. In *Synapses*.

Cymbalyuk, G. S., Gaudry, Q., Masino, M. A., and Calabrese, R. L. (2002). Bursting in leech heart interneurons: Cell-autonomous and network-based mechanisms. *Journal of Neuroscience*, 22(24):10580–10592.

Denker, M., Szucs, A., Pinto, R. D., Abarbanel, H. D. I., and Selverston, A. I. (2005). A network of electronic neural oscillators reproduces the dynamics of the periodically forced pyloric pacemaker group. *IEEE Transactions on Biomedical Engineering*, 52(5):792–798.

Destexhe, A. and Bal, T., editors (2009). *Dynamic-Clamp: From Principles to Applications*. Springer, New York.

Dicaprio, R., Jordan, G., and Hampton, T. (1997). Maintenance of motor pattern phase relationships in the ventilatory system of the crab. *Journal of Experimental Biology*, 200(6):963–974.

Doloc-Mihu, A. and Calabrese, R. L. (2011). A database of computational models of a half-center oscillator for analyzing how neuronal parameters influence network activity. *Journal of Biological Physics*, 37(3):263–283.

Doloc-Mihu, A. and Calabrese, R. L. (2014). Identifying Crucial Parameter Correlations Maintaining Bursting Activity. *PLoS Computational Biology*, 10(6).

Doloc-Mihu, A. and Calabrese, R. L. (2016). Analysis of Family Structures Reveals Robustness or Sensitivity of Bursting Activity to Parameter Variations in a Half-Center Oscillator (HCO) Model. *eNeuro*, 3(4):ENEURO.0015–16.2016.

Duarte, J., Januário, C., and Martins, N. (2009). Reciprocal inhibitory coupling: Measure and control of chaos on a biophysically motivated model of bursting. *Communications in Nonlinear Science and Numerical Simulation*, 14(6):2734–2746.

Elices, I., Levi, R., Arroyo, D., Rodriguez, F. d. B. B., and Varona, P. (2019). Robust dynamical invariants in sequential neural activity. *Scientific Reports*, In press, doi:10.1038/s41598-019-44953-2.

Elices, I. and Varona, P. (2015). Closed-loop control of a minimal central pattern generator network. *Neurocomputing*, 170:55–62.

Elices, I. and Varona, P. (2017). Asymmetry factors shaping regular and irregular bursting rhythms in central pattern generators. *Frontiers in Computational Neuroscience*, 11:9.

Elson, R. C., Huerta, R., Abarbanel, H. D. I., Rabinovich, M. I., and Selverston, A. I. (1999). Dynamic control of irregular bursting in an identified neuron of an oscillatory circuit. *J. Neurophysiol.*, 82:115–122.

Elson, R. C., Selverston, A. I., Huerta, R., Rulkov, N. F., Rabinovich, M. I., and Abarbanel, H. D. I. (1998). Synchronous behavior of two coupled biological neurons. *Phys. Rev. Lett.*, 81:5692–5695.

Fischer, H., Schmidt, J., Haas, R., and Büschges, A. (2001). Pattern Generation for Walking and Searching Movements of a Stick Insect Leg. I. Coordination of Motor Activity. *Journal of Neurophysiology*, 85(1):341–353.

Gjorgjieva, J., Drion, G., and Marder, E. (2016). Computational implications of biophysical diversity and multiple timescales in neurons and synapses for circuit performance. *Current Opinion in Neurobiology*, 37:44 – 52.

Golowasch, J., Casey, M., Abbott, L. F., and Marder, E. (1999). Network stability from activity-dependent regulation of neuronal conductances. *Neural Comput.*, 11:1079–1096.

Gouwens, N. W., Berg, J., Feng, D., Sorensen, S. A., Zeng, H., Hawrylycz, M. J., Koch, C., and Arkhipov, A. (2018). Systematic generation of biophysically detailed models for diverse cortical neuron types. *Nature Communications*, 9(1):710.

Grashow, R., Brookings, T., and Marder, E. (2010). Compensation for variable intrinsic neuronal excitability by circuit-synaptic interactions. *Journal of Neuroscience*, 30(27):9145–9156.

Graubard, K., Raper, J. A., and Hartline, D. K. (1983). Graded synaptic transmission between identified spiking neurons. *Journal of Neurophysiology*, 50(2):508–521.

Greenberg, I. and Manor, Y. (2005). Synaptic depression in conjunction with a-current channels promote phase constancy in a rhythmic network. *Journal of Neurophysiology*, 93(2):656–677. PMID: 15356180.

Grillner, S. and Kashin, S. (1976). On the Generation and Performance of Swimming in Fish. In *Neural Control of Locomotion*, Advances in Behavioral Biology, pages 181–201. Springer, Boston, MA.

Harris-Warrick, R. M., Marder, E., Selverston, A. I., and Moulins, M., editors (1992). *Dynamic Biological Networks: The Stomatogastric Nervous System.* MIT Press, Cambridge, MA.

Hartline, D. K. and Maynard, D. M. (1975). Mottor patterns in the stomatogastric ganglion of the lobster Panulirus argus. *J. Exp. Biol.*, 62(2):405–420.

Herreras, O. (1990). Propagating dendritic action potential mediates synaptic transmission in ca1 pyramidal cells in situ. *Journal of Neurophysiology*, 64(5):1429–1441. PMID: 2178183.

Herrero-Carrón, F., Rodríguez, F. B., and Varona, P. (2011). Bio-inspired design strategies for central pattern generator control in modular robotics. *Bioinspir Biomim*, 6(1):16006.

Hille, B. (2001). *Ion Channels of Excitable Membranes. 3rd Edition. Sinauer Associates, Inc.*

Hodgkin, A. L. and Huxley, A. F. (1952). A quantitative description of membrane current and its application to conduction and excitation in nerve. *J. Physiol.*, 117:500–544.

Hooper, R. M., Tikidji-Hamburyan, R. A., Canavier, C. C., and Prinz, A. A. (2015). Feedback control of variability in the cycle period of a central pattern generator. *Journal of Neurophysiology*, 114(5):2741–52.

Hooper, S. L. (1997a). Phase maintenance in the pyloric pattern of the lobster (panulirus interruptus) stomatogastric ganglion. *Journal of Computational Neuroscience*, 4(3):191–205.

Hooper, S. L. (1997b). The pyloric pattern of the lobster (panulirus interruptus) stomatogastric ganglion comprises two phase-maintaining subsets. *Journal of Computational Neuroscience*, 4(3):207–219.

Hooper, S. L. (1998). Transduction of temporal patterns by single neurons. *Nature Neuroscience*, 1(8):720–726.

Hooper, S. L., Buchman, E., Weaver, A. L., Thuma, J. B., and Hobbs, K. H. (2009). Slow conductances could underlie intrinsic phase-maintaining properties of isolated lobster (Panulirus interruptus) pyloric neurons. *The Journal of Neuroscience*, 29(6):1834–45.

Huerta, R., Sanchez-Montañes, M. A., and Corbacho, F. (2000). A Central pattern generator to control a pyloric-based system. *Biol. Cybern.*, 82:85–94.

Huerta, R., Varona, P., Rabinovich, M. I., and Abarbanel, H. D. I. (2001). Topology selection by chaotic neurons of a pyloric central pattern generator. *Biological Cybernetics*, 84(1):L1–L8.

Hull, T., Enright, W., Fellen, B., and Sedgwick, A. (1972). Comparing numerical methods for ordinary differential equations. *SIAM Journal on Numerical Analysis*, 9(4):603–637.

Ijspeert, A. J. (2008). Central pattern generators for locomotion control in animals and robots: a review. *Neural Netw*, 21(4):642–653.

Izhikevich, E. M. (2003). Simple model of spiking neurons. *IEEE Transactions on Neural Networks*, 14(6):1569–1572.

Jacobson, G. A., Lev, I., Yarom, Y., and Cohen, D. (2009). Invariant phase structure of olivocerebellar oscillations and its putative role in temporal pattern generation. *Proceedings of the National Academy of Sciences*, 106(9):3579–3584.

Kandel, E. R., Schwartz, J. H., and Jessell, T. M. (2012). *Principles of Neural Science*. McGraw-Hill Education, New York, 5 edition.

Kemenes, I., Marra, V., Crossley, M., Samu, D., Staras, K., Kemenes, G., and Nowotny, T. (2011). Dynamic clamp with StdpC software. *Nat Protoc*, 6(3):405–417.

Klausberger, T. and Somogyi, P. (2008). Neuronal Diversity and Temporal Dynamics: The Unity of Hippocampal Circuit Operations. *Science*, 321(5885):53–57.

Koch, C. (1999). *Biophysics of computation: information processing in single neurons*. Oxford University Press, New York.

Komarov, M. A., Osipov, G. V., and Suykens, J. A. K. (2008). Variety of synchronous regimes in neuronal ensembles. *Chaos*, 18(3).

Komendantov, A. O. and Kononenko, N. I. (1996). Deterministic Chaos in Mathematical Model of Pacemaker Activity in Bursting Neurons of Snail, Helix Pomatia. *J. Theor. Biol.*, 183:219–230.

Krook-Magnuson, E., Varga, C., Lee, S. H., and Soltesz, I. (2012). New dimensions of interneuronal specialization unmasked by principal cell heterogeneity. 35(3):175–184.

Latorre, R., Aguirre, C., Rabinovich, M. I., and Varona, P. (2013a). Transient dynamics and rhythm coordination of inferior olive spatio-temporal patterns. *Frontiers in Neural Circuits*, 7:138.

Latorre, R., Levi, R., and Varona, P. (2013b). Transformation of context-dependent sensory dynamics into motor behavior. *PLoS Computational Biology*, 9(2):e1002908.

Latorre, R., Rodríguez, F. B., and Varona, P. (2002). Characterization of Triphasic Rhythms in Central Pattern Generators (I): Interspike Interval Analysis. *Lect. Notes Comput. Sci.*, 2415:167–173.

Latorre, R., Rodríguez, F. B., and Varona, P. (2006). Neural signatures: multiple coding in spiking-bursting cells. *Biol Cybern*, 95(2):169–183.

Latorre, R., Varona, P., and Rabinovich, M. I. (2019). Rhythmic control of oscillatory sequential dynamics in heteroclinic motifs. *Neurocomputing*, 331:108–120.

LeMasson, G., Masson, S. R.-L., Debay, D., and Bal, T. (2002). Feedback inhibition controls spike transfer in hybrid thalamic circuits. *Nature*, 417:854.

Linaro, D., Couto, J., and Giugliano, M. (2015). Real-time Electrophysiology: Using Closed-loop Protocols to Probe Neuronal Dynamics and Beyond. *Journal of Visualized Experiments*, 100:e52320.

Ma, Z. and Zhang, N. (2018). Temporal transitions of spontaneous brain activity. *eLife*, 7:e33562.

Marder, E. and Bucher, D. (2001). Central pattern generators and the control of rhythmic movements. *Curr. Biol.*, 11:R986–R996.

Marder, E. and Calabrese, R. L. (1996). Principles of rhythmic motor pattern generation. *Physiol. Rev.*, 76:687–717.

Marder, E. and Eisen, J. S. (1984). Transmitter identification of pyloric neurons: electrically coupled neurons use different transmitters. *Journal of Neurophysiology*, 51(6):1345–1361.

Maze, I. S., Wright, G. A., and Mustard, J. A. (2006). Acute ethanol ingestion produces dose-dependent effects on motor behavior in the honey bee (apis mellifera). *Journal of Insect Physiology*, 52(11):1243 – 1253.

Miller, J. P. and Selverston, A. I. (1982). Mechanisms underlying pattern generation in lobster stomatogastric ganglion as determined by selective inactivation of identified neurons. IV. Network properties of pyloric system. *Journal of Neurophysiology*, 48(6):1416–1432.

Mulloney, B. (1977). Organization of the stomatogastric ganglion of the spiny lobster.v. *Journal of comparative physiology*, 122(2):227–240.

Mulloney, B. and Selverston, A. I. (1974a). Organization of the stomatogastric ganglion of the spiny lobster.i. *Journal of comparative physiology*, 91(1):1–32.

Mulloney, B. and Selverston, A. I. (1974b). Organization of the stomatogastric ganglion of the spiny lobster.iii. *Journal of comparative physiology*, 91(1):53–78.

Muñiz, C., Arganda, S., Rodriguez, F. D., and de Polavieja, G. G. (2005). Realistic stimulation through advanced dynamic-clamp protocols. *Mechanisms, Symbols and Models Underlying Cognition, Pt 1, Proceedings*, 3561:95–105.

Muñiz, C., Rodríguez, F. B., and Varona, P. (2009). RTBiomanager: a software platform to expand the applications of real-time technology in neuroscience. *BMC Neurosci*, 10(Suppl 1):P49.

Nadim, F., Olsen, O. H., DeSchutter, E., and Calabrese, R. L. (1995). Modeling the leech heartbeat elemental oscillator. I. Interactions of intrinsic and synaptic currents. *Journal of Computational Neuroscience*, 2(3):215–235.

Nadim, F., Zhao, S., Zhou, L., and Bose, A. (2011). Inhibitory feedback promotes stability in an oscillatory network. *Journal of Neural Engineering*, 8(6):065001.

Nagornov, R., Osipov, G., Komarov, M., Pikovsky, A., and Shilnikov, A. (2016). Mixed-mode synchronization between two inhibitory neurons with post-inhibitory rebound. *Communications in Nonlinear Science and Numerical Simulation*, 36:175–191.

Norman, S. E., Butera, R. J., and Canavier, C. C. (2016). Stochastic slowly adapting ionic currents may provide a decorrelation mechanism for neural oscillators by causing wander in the intrinsic period. *Journal of Neurophysiology*.

Nowotny, T., Szücs, A., Levi, R., and Selverston, A. I. (2007). Models wagging the dog: are circuits constructed with disparate parameters? *Neural Computation*, 19(8):1985–2003.

Nowotny, T. and Varona, P. (2012). Dynamic Clamp. *Encyclopedia of Nanotechnology*, pages 613–621.

Nowotny, T., Zhigulin, V. P., Selverston, A. I., Abarbanel, H. D. I., and Rabinovich, M. I. (2003). Enhancement of synchronization in a hybrid neural circuit by spike timing dependent plasticity. *J. Neurosci.*, 23:9776–9785.

O'Keefe, J. and Recce, M. L. (1993). Phase relationship between hippocampal place units and the EEG theta rhythm. *Hippocampus*, 3:317–330.

Oprisan, S. A., Prinz, A. A., and Canavier, C. C. (2004). Phase resetting and phase locking in hybrid circuits of one model and one biological neuron. *Biophysical journal*, 87(4):2283–2298.

Patel, Y. A., George, A., Dorval, A. D., White, J. A., Christini, D. J., and Butera, R. J. (2017). Hard real-time closed-loop electrophysiology with the Real-Time eXperiment Interface (RTXI). *PLoS Computational Biology*, 13(5).

Pinto, R. D., Elson, R. C., Szücs, A., Rabinovich, M. I., Selverston, A. I., and Abarbanel, H. D. (2001). Extended dynamic clamp: controlling up to four neurons using a single desktop computer and interface. *J Neurosci Methods*, 108(1):39–48.

Pinto, R. D., Varona, P., Volkovskii, A. R., Szücs, A., Abarbanel, H. D. I., and Rabinovich, M. I. (2000). Synchronous behavior of two coupled electronic neurons. *Physical Review E*, 62(2):2644–2656.

Prinz, A. A., Abbott, L. F., and Marder, E. (2004a). The dynamic clamp comes of age. *Trends in Neurosciences*, 27:218–224.

Prinz, A. A., Bucher, D., and Marder, E. (2004b). Similar network activity from disparate circuit parameters. *Nature Neuroscience*, 7(12):1345–1352.

Rabbah, P. and Nadim, F. (2005). Synaptic dynamics do not determine proper phase of activity in a central pattern generator. *Journal of Neuroscience*, 25(49):11269–11278.

Rabinovich, M., Abarbanel, H., Huerta, R., Elson, R., and Selverston, A. (1997). Self-regularization of chaos in neural systems: experimental and theoretical results. *IEEE Transactions on Circuits and Systems I: Fundamental Theory and Applications*, 44(10).

Rabinovich, M. I., Torres, J. J., Varona, P., Huerta, R., and Weidman, P. (1999). Origin of coherent structures in a discrete chaotic medium. *Phys Rev E Stat Phys Plasmas Fluids Relat Interdiscip Topics*, 60(2 Pt A):R1130—-R1133.

Rabinovich, M. I. and Varona, P. (2017). Consciousness as sequential dynamics, robustness, and mental disorders. *JAMA Psychiatry*, 74(8):771–772.

Rabinovich, M. I. and Varona, P. (2018). Discrete Sequential Information Coding: Heteroclinic Cognitive Dynamics. *Frontiers in Computational Neuroscience*, 12:73.

Rajan, K., Harvey, C. D., and Tank, D. W. (2016). Recurrent Network Models of Sequence Generation and Memory. *Neuron*, 90:128–142.

Reyes, M. B., Carelli, P. V., Sartorelli, J. C., and Pinto, R. D. (2015). A modeling approach on why simple central pattern generators are built of irregular neurons. *PLoS ONE*, 10(3).

Reyes, M. B., Huerta, R., Rabinovich, M. I., and Selverston, A. I. (2008). Artificial synaptic modification reveals a dynamical invariant in the pyloric CPG. *European Journal of Applied Physiology*, 102(6):667–675.

Reyes-Sanchez, M., Amaducci, R., Elices, I., Rodriguez, F. B., and Varona, P. (2018). Automatic adaptation of model neurons and connections to build hybrid circuits with living networks. *bioRxiv*.

Rezer, E. and Moulins, M. (1983). Expression of the crustacean pyloric pattern generator in the intact animal. *Journal of Comparative Physiology*, 153(1):17–28.

Robinson, H. P. and Kawai, N. (1993a). Single channel properties at the synaptic site. *EXS*, 63:250–265.

Robinson, H. P. C. and Kawai, N. (1993b). Injection of digitally synthesized synaptic conductance transients to measure the integrative properties of neurons. *Journal of Neuroscience Methods*.

Rolston, J. D., Gross, R. E., and Potter, S. M. (2010). Closed-loop, open-source electrophysiology. *Frontiers in Neuroscience*, 4(31):1–8.

Rulkov, N. F. (2001). Regularization of synchronized chaotic bursts. *Physical Review Letters*, 86(1):183–186.

Sakai, K., Hikosaka, O., and Nakamura, K. (2004). Emergence of rhythm during motor learning. *Trends in Cognitive Sciences*, 8(12):547 – 553.

Sakurai, A., Gunaratne, C. a., and Katz, P. S. (2014). Two interconnected kernels of reciprocally inhibitory interneurons underlie alternating left-right swim motor pattern generation in the mollusc Melibe leonina. *Journal of Neurophysiology*.

Sakurai, A. and Katz, P. S. (2017). Artificial synaptic rewiring demonstrates that distinct neural circuit configurations underlie homologous behaviors. *Current Biology*, 27(12):1721 – 1734.e3.

Schiff, S. J. (2012). *Neural Control Engineering*. The MIT Press, Cambridge, MA.

Selverston, A. (2005). A neural infrastructure for rhythmic motor patterns. *Cell and Mol Neurobiol*, 25:223–244.

Selverston, A. I. (2010). Invertebrate central pattern generator circuits. *Philosophical transactions of the Royal Society of London B*, 365(1551):2329–2345.

Selverston, A. I. and Moulins, M., editors (1987). *The Crustacean Stomatogastric System: a Model for the Study of Central Nervous System.* Springer-Verlag, Berlin Heidelberg New York London Paris Tokyo.

Selverston, A. I. and Mulloney, B. (1974). Organization of the stomatogastric ganglion of the spiny lobster.ii. *Journal of comparative physiology*, 91(1):33–51.

Selverston, A. I., Rabinovich, M. I., Abarbanel, H. D. I., Elson, R., Szücs, A., Pinto, R. D., Huerta, R., and Varona, P. (2000). Reliable circuits from irregular neurons: a dynamical approach to understanding central pattern generators. *Journal of Physiology-Paris*, 94(5-6):357–374.

Selverston, A. I., Russell, D. F., Miller, J. P., and King, D. G. (1976). The stomatogastric nervous system: Structure and function of a small neural network. *Progress in Neurobiology*, 7:215 – 289.

Sharp, A. A., O'Neil, M. B., Abbott, L. F., and Marder, E. (1993a). Dynamic clamp: computer-generated conductances in real neurons. *Journal of Neurophysiology*, 69(3):992–995.

Sharp, A. A., O'Neil, M. B., Abbott, L. F., and Marder, E. (1993b). The dynamic clamp: artificial conductances in biological neurons. *Trends in Neurosciences*, 16:389.

Sharp, A. A., Skinner, F. K., and Marder, E. (1996). Mechanisms of oscillation in dynamic clamp constructed two-cell half-center circuits. *Journal of Neurophysiology*, 76(2):867–883.

Simoni, M. F. and DeWeerth, S. P. (2007). Sensory feedback in a half-center oscillator model. *IEEE Transactions on Biomedical Engineering*, 54(2):193–204.

Soofi, W., Archila, S., and Prinz, A. A. (2012). Co-variation of ionic conductances supports phase maintenance in stomatogastric neurons. *Journal of Computational Neuroscience*, 33(1):77–95.

Soofi, W., Goeritz, M. L., Kispersky, T. J., Prinz, A. A., Marder, E., and Stein, W. (2014). Phase maintenance in a rhythmic motor pattern during temperature changes in vivo. *Journal of Neurophysiology*, 111(12):2603–2613. PMID: 24671541.

Steriade, M. (2006). Grouping of brain rhythms in corticothalamic systems. *Neuroscience*, 137(4):1087 – 1106.

Stiesberg, G. R., Reyes, M. B., Varona, P., Pinto, R. D., and Huerta, R. (2007). Connection topology selection in central pattern generators by maximizing the gain of information. *Neural Comput*, 19(4):974–993.

Sulzer, J., Haller, S., Scharnowski, F., Weiskopf, N., Birbaumer, N., Blefari, M. L., Bruehl, A. B., Cohen, L. G., DeCharms, R. C., Gassert, R., Goebel, R., Herwig, U., LaConte, S., Linden, D., Luft, A., Seifritz, E., and Sitaram, R. (2013). Real-time fMRI neurofeedback: progress and challenges. *NeuroImage*, 76:386–399.

Szücs, A., Elson, R. C., Rabinovich, M. I., Abarbanel, H. D. I., and Selverston, A. I. (2001). Nonlinear behavior of sinusoidally forced pyloric pacemaker neurons. *Journal of Neurophysiology*, 85(4):1623–1638. PMID: 11287486.

Szücs, A., Huerta, R., Rabinovich, M. I., and Selverston, A. I. (2009). Robust microcircuit synchronization by inhibitory connections. *Neuron*, 61(3):439 – 453.

Szücs, A., Pinto, R. D., Rabinovich, M. I., Abarbanel, H. D. I., and Selverston, A. I. (2003). Synaptic modulation of the interspike interval signatures of bursting pyloric neurons. *J. Neurophysiol.*, 89(3):1363–1377.

Szucs, A., Varona, P., Volkovskii, A. R., Abarbanel, H. D. I., Rabinovich, M. I., and Selverston, A. I. (2000). Interacting Biological and Electronic Neurons Generate Realistic Oscillatory Rhythms. *Neuroreport*, 11(3):563–569.

Tang, L. S., Goeritz, M. L., Caplan, J. S., Taylor, A. L., Fisek, M., and Marder, E. (2010). Precise temperature compensation of phase in a rhythmic motor pattern. *PLOS Biology*, 8(8):1–13.

Thounaojam, U. S., Cui, J., Norman, S. E., Butera, R. J., and Canavier, C. C. (2014). Slow Noise in the Period of a Biological Oscillator Underlies Gradual Trends and Abrupt Transitions in Phasic Relationships in Hybrid Neural Networks. *PLoS Computational Biology*, 10(5).

Thuma, J. B. and Hooper, S. L. (2003). Quantification of cardiac sac network effects on a movement-related parameter of pyloric network output in the lobster. *J Neurophysiol*, 89(2):745–753.

Torres, J. J. and Varona, P. (2012). Modeling Biological Neural Networks. In *Handbook of Natural Computing*, volume 1-4, pages 533–564. Springer, Berlin, Heidelberg.

Used, J., Wagemakers, A., and Sanjuán, M. A. (2012). Regularization of map-based neuron models using phase control. *Discontinuity, Nonlinearity, and Complexity*, 1(1):69–78.

van Boxtel, G. J. M. and Gruzelier, J. H. (2014). Neurofeedback: Introduction to the special issue. *Biological Psychology*, 95:1–3.

Varona, P. and Rabinovich, M. I. (2016). Hierarchical dynamics of informational patterns and decision-making. *Proceedings of the Royal Society B*, 283(1832):20160475.

Varona, P., Torres, J. J., Abarbanel, H. D. I., Rabinovich, M. I., and Elson, R. C. (2001a). Dynamics of two electrically coupled chaotic neurons: Experimental observations and model analysis. *Biological Cybernetics*, 84(2):91–101.

Varona, P., Torres, J. J., Huerta, R., Abarbanel, H. D. I., and Rabinovich, M. I. (2001b). Regularization mechanisms of spiking-bursting neurons. *Neural Networks*, 14:865–875.

Virchow, R. (1846). Über das granulierte ansehen der wandungen der gerhirnventrikel. *Allg Z Psychiatr*, 3:424–450.

Wang, S., Chandrasekaran, L., Fernandez, F. R., White, J. A., and Canavier, C. C. (2012). Short conduction delays cause inhibition rather than excitation to favor synchrony in hybrid neuronal networks of the entorhinal cortex. *PLoS computational biology*, 8(1):e1002306.

Weaver, A. L. and Hooper, S. L. (2003a). Follower neurons in lobster (Panulirus interruptus) pyloric network regulate pacemaker period in complementary ways. *Journal of Neurophysiology*, 89(3):1327–38.

Weaver, A. L. and Hooper, S. L. (2003b). Relating network synaptic connectivity and network activity in the lobster (Panulirus interruptus) pyloric network. *Journal of Neurophysiology*, 90:2378–2386.

Wojcik, J., Schwabedal, J., Clewley, R., and Shilnikov, A. L. (2014). Key bifurcations of bursting polyrhythms in 3-cell central pattern generators. *PLoS ONE*, 9(4).

Yakovenko, S., McCrea, D. a., Stecina, K., and Prochazka, A. (2005). Control of locomotor cycle durations. *Journal of Neurophysiology*, 94:1057–1065.

Yarom, Y. (1991). Rhythmogenesis in a hybrid system–interconnecting an olivary neuron to an analog network of coupled oscillators. *Neuroscience*, 44(2):263–275.

Yuste, R., MacLean, J. N., Smith, J., and Lansner, A. (2005). The cortex as a central pattern generator. *Nat Rev Neurosci*, 6(6):477–483.

Zheng, C., Bieri, K. W., Hsiao, Y. T., and Colgin, L. L. (2016). Spatial Sequence Coding Differs during Slow and Fast Gamma Rhythms in the Hippocampus. *Neuron*, 89(2):398–408.